UNIVERSITY OF CAMERINO

SCHOOL OF ADVANCED STUDIES

DOCTOR OF PHILOSOPHY IN INFORMATION SCIENCES AND COMPLEX SYSTEMS - XXVI CYCLE

SCHOOL OF SCIENCE AND TECHNOLOGY

FORMAL COMPUTATIONAL MODELLING OF BONE PHYSIOLOGY AND DISEASE PROCESSES

Advisor
Prof. Emanuela Merelli

Ph.D. Candidate
Nicola Paoletti

Examiners
Prof. Luca Bortolussi
Prof. Flavio Corradini
Prof. Guido Sanguinetti

ACADEMIC YEAR 2012-2013 - CYCLE XXVI

To the women of my life

ABSTRACT

This thesis addresses the definition and the application of formal techniques in the field of Computational Systems Biology, with particular focus on bone remodelling (BR), the cellular process of bone renewal, and on the analysis and control of disease processes.

Firstly, we study the multiscale and spatial mechanisms that connects disruptions at the molecular signalling level, to osteoporosis and other diseases characterized by low bone mass and structural weakening at the tissue level. We define a modelling framework based on a formal specification language which extends the Shape Calculus, a process algebra with spatial and geometrical primitives. The executable side is obtained by encoding the specification into an agent-based model, where agents are enriched with stochastic actions and perception. This framework is used to define a novel spatial and individual-based model of bone remodelling, parametrized in order to reproduce both healthy and osteoporotic conditions, and to analyse how the disposition of bone cells affects bone microstructure at the tissue level.

Secondly, we propose a methodological study aiming at evaluating and comparing different models of bone remodelling and different techniques for the analysis of bone diseases and of stabilization and homeostasis-related properties. We consider a non-linear ODE model, over which we perform simulation and sensitivity analysis; a stochastic model on which we employ probabilistic model checking; and a hybrid piecewise-multiaffine approximation of the ODEs, supporting model checking and LTL-based parameter synthesis. We extend the model in order to describe osteoporosis and osteomyelitis (a bone infection) and we show how quantitative verification methods could provide clinically meaningful diagnostic estimators.

Thirdly, we investigate the use of formal languages and hybrid techniques in the modelling of disease processes and in the synthesis of treatment strategies. In particular, hybrid models allow us to describe the disease dynamics in a continuous fashion, while the scheduling of multiple drugs discretely. We define a process-algebraic language for specifying general disease processes and treatments, called D-CGF (an extension to the CGF process algebra), from which multiple semantics can be derived: stochastic hybrid automata and hybrid dynamical systems. Then, hybrid non-linear control is employed to compute the optimal scheduling of multiple therapies. The approach is applied to an epidemic model of the H1N1 influenza, where we derive the optimal combination of vaccination and antiviral treatments.

ACKNOWLEDGEMENTS

Firstly, I am deeply grateful to my supervisor, Emanuela Merelli, for her extraordinary guidance and support not only on the scientific side but also on the personal side. It has been a privilege learning from and working with her, and with the other researchers/friends from Camerino, Luca, Pierluigi and Matteo above all.

A special thank to Pietro Liò, my unofficial co-supervisor, for hosting me in Cambridge and for having significantly contributed to my research with thousands ideas, advices and front line work. I also thank Moni, Claudio and all the other friends from Pietro's group in Cambridge.

I would also like to thank Ezio Bartocci for his active collaboration and valuable help, since the time he was my bachelor thesis co-advisor.

I am also grateful to Marco Viceconti, who believed in and funded this research project, besides providing the domain knowledge and expertise on bone remodelling without which this thesis would not have been possible.

Many thanks to Hillel Kugler for giving me the opportunity of an internship at Microsoft Research and to Youssef, Christoph and Boyan for having taught me so much in so short time.

I thank my family for supporting me during my bachelor, master and doctoral studies. Finally, I want to thank my partner (and colleague) Marianna, for her love, patience, for always telling me the right thing to do, and for always making me happy, even in the bluest days.

CONTENTS

LIST OF FIGURES

LIST OF TABLES

LIST OF ABBREVIATIONS

ABM Agent-Based Model

BMD Bone Mineral Density

BMU Basic Multicellular Unit

BR Bone Remodelling

CCS Calculus of Communicating Systems

CGF Chemical Ground Form

CSL Continuous Stochastic Logic

CSS Controlled Switched System

CTMC Continuous Time Markov Chain

D-CGF Disease CGF

EOCP Embedded Optimal Control Problem

ESC Extended Shape Calculus

FSCT METHOD Finite Set Control Transcription method

LTL Linear Temporal Logic

LTS Labelled Transition System

MPC Model Predictive Control

OB Osteoblast

OC Osteoclast

ODE Ordinary Differential Equation

OPG Osteoprotegerin

OY Osteocyte

PA Process Algebra

PB Pre-osteoblast

PC Pre-osteoclast

PMC Probabilistic Model Checking

RANK Receptor Activator of Nuclear factor κ-B

RANKL Receptor Activator of Nuclear factor κ-B ligand

SD Switching Drug

SHA Stochastic Hybrid Automaton

SIR MODEL Susceptible Infected Recovered model

SOCP Switched Optimal Control Problem

SOS Structural Operational Semantics

STI Structured Therapy Interruption

BIOLOGICAL abbreviations

COMPUTATIONAL abbreviations

1 INTRODUCTION

This dissertation addresses the definition and application of formal techniques in Computational Systems Biology, the study field aiming to describe, analyse and understand complex biological systems using mathematical and computational methods. From the perspective of a computer scientist, biological systems can be regarded as *reactive concurrent systems* [60], i.e. systems consisting of multiple components, each of them may change state in reaction to another component changing state (*reactivity*) and competitively access to shared resources (*concurrency*). Formal computational methods have therefore proven to be suitable tools in biology, to the same extent as classical mathematical techniques.

Specifically, we consider the case study of *bone remodelling (BR)*, the cellular process of bone renewal, with a particular focus on studying the clinically relevant pathologies arising from disorders in the BR process (e.g. osteoporosis and bone infections). BR is a multiscale process, where the molecular signalling level strongly affects the cellular level and in turn, the density and microstructure of the bone tissue.

The ultimate goal is understanding how multiscale effects contribute to the development of global disease conditions, thus making in turn BR a challenging test-bed for novel modelling techniques. In this thesis, we will show how the application of formal languages and automated analysis methods like probabilistic model checking could provide not just useful tools in biomedical research but more importantly, novel insights into the biological process under study.

Building a model able to reproduce and predict disease scenarios is just the starting point for a more systematic investigation of treatments that can be administered for recovering the desired conditions. To this purpose, we develop methods in the context of *Structured Therapy Interruption (STI)*, i.e. the programmed interruption of a medication for a period of time. STI has several advantages, like regaining effectiveness after a period of continuous use and, like in HIV, combinations of alternating therapies (HAART) are typically administered.

We consider STI problems which, given a dynamic disease model, aim to compute a dosage strategy of multiple drugs able to recover from the disease, in a way that the impact on the patient (or on the affected population) is minimized. In this case, we will show the effectiveness of process alge-

bras, hybrid systems and control-theoretic tools in specifying and solving this class of problems.

Mathematical and Computational Modelling of Bone Remodelling

In the last twenty years, a variety of mathematical models has been proposed in order to better understand the dynamics of bone remodeling (reviewed in [64, 63, 125]). Early models were focused on the organ level, and they typically describe bone as a continuum material only characterized by its density. Bone micro-structure is not taken into account, thus ignoring structural adaptation mechanisms as well as complex cellular-level dynamics. Therefore in continuum-based organ-level models the differences between cortical and trabecular bone were just in their apparent density.

In order to address the lack of micro-structural information, later models started looking at the biomechanical properties of the bone tissue that is, how mechanical loading affects the tissue structure and consequently its function. Models describing the mechanical response and adaptation of bone typically rely on *Finite Element Methods (FEM)* [151], a technique borrowed from the engineering community. In this case, bone adaptation is often modeled as a structural optimization problem: a FEM analysis computes the mechanical stresses at each location of the bone matrix; then, structural changes are driven in order to optimize the homogeneous distribution of mechanical loading, until a remodeling equilibrium is reached.

Another class of models describe the single-cellular and multi-cellular level and the interactions occurring among the different types of bone cells involved in the BR process. Most of these models analyze the continuous variations in the number of bone cells, and the bone density is usually calculated as a function of the number of osteoblasts and osteoclasts and their formation and resorption rates. These models can also incorporate intracellular signaling pathways and mechanosensing mechanisms, that is the process by which mechanical stimuli are transduced into cellular signals.

To present, the application of formal computational methods in bone remodelling has not received as much attention as mathematical ones, and to the best of our knowledge, only Petri Nets [95] and membrane-based models [36] have been considered so far.

Contrarily in this thesis, we primarily focus on the definition of novel *computational models for bone remodelling*, where formal languages and automated verification methods open to the analysis of a variety of biological and clinical properties, that go beyond the reach of classical mathematical and simulation-based methods.

1.1 STRUCTURE OF THE THESIS

This thesis is divided in four chapters:

- Chapter 2 provides some biological background on bone remodelling and on the pathological dynamics of osteoporosis and osteomyelitis. From the computational side, an introduction to the CCS process algebra, stochastic models and probabilistic model checking is given.
- In Chapter 3, we define a spatial process algebra called ESC, which extends the Shape Calculus with terms for describing cell population dynamics, and we exploit it as the formal specification language for a novel spatial model of bone remodelling. By encoding ESC specifications into stochastic agent-based models we provide a simulation platform which allowed us to reproduce the spatial patterns of the remodelling processes, and to parametrize the model for reproducing both healthy and osteoporotic conditions. Finally, we analyse how the location of signalling osteocytes (responsible for initiating the remodelling process) affects in the long run the bone microstructure at the tissue level.
- In Chapter 4, we investigate multiple models and analysis techniques over two main classes of biological properties: bone diseases and stabilization properties. We consider a non-linear ODE model, over which we perform simulation and sensitivity analysis; a stochastic model (derived from the differential equations) on which we employ probabilistic model checking; and a hybrid piecewise-multiaffine approximation of the ODEs, supporting model checking and LTL-based parameter synthesis. We finally extend the model in order to describe osteoporosis and osteomyelitis and we show how quantitative verification methods are able to provide meaningful diagnostic estimators with potentialities in medical practice.
- In Chapter 5 we investigate the use of formal languages and hybrid techniques in the modelling of disease processes and in the synthesis of treatment strategies. The approach consists in the definition of a process-algebraic language for specifying general disease processes and treatments, called D-CGF (an extension to the CGF process algebra), from which a stochastic hybrid automata semantics and a relaxation in terms of hybrid dynamical systems are provided. The key idea is describing the disease dynamics in a continuous fashion, while the dosage of multiple drugs discretely. Then, we investigate approximate

methods for the hybrid non-linear optimal control of the D-CGF semantics, in order to compute the optimal scheduling of multiple therapies. We finally apply the approach to an epidemic model of the H1N1 influenza occurred in the US in 2009, where we seek to find the optimal combination of vaccination and antiviral treatments. By considering multiple scenarios where the two treatments are given different costs, we found that a strategy of repeated pulse vaccinations is much more effective in controlling and counteracting the course of the infection than any strategy based on the antiviral treatment.

Figure 1 gives an overview of the methods developed and applied in this dissertation. The common paradigm consists in the definition of a formal specification language (specifically, of bio-inspired process algebras), from which a concrete semantics is derived that can be directly executed, simulated or analysed. Then, specific models together with the range of supported analysis techniques are employed to the study of specific biological properties.

1.2 PUBLISHED MATERIAL

The material presented in this thesis has been revised and extended from works published during my PhD studies. In particular, Chapter 3 is based on [99, 118, 119]; the methodological part of Chapter 4 appeared in [97, 97], while the osteomyelitis model was published in [100]; and the definition of the D-CGF process algebra in Chapter 5 was originally presented in [98], while the formal semantics and the control methods have been extensively revised.

Other contributions not in the scope of this dissertation include the SMT-based synthesis of genetic regulatory interactions in sea urchin development [120]; the formalization of a transition system-based model for self-adaptive systems [105, 146, 104, 106]; and the modelling of contaminated marine food webs and bacterial bioremediation [144, 142, 123, 143, 141].

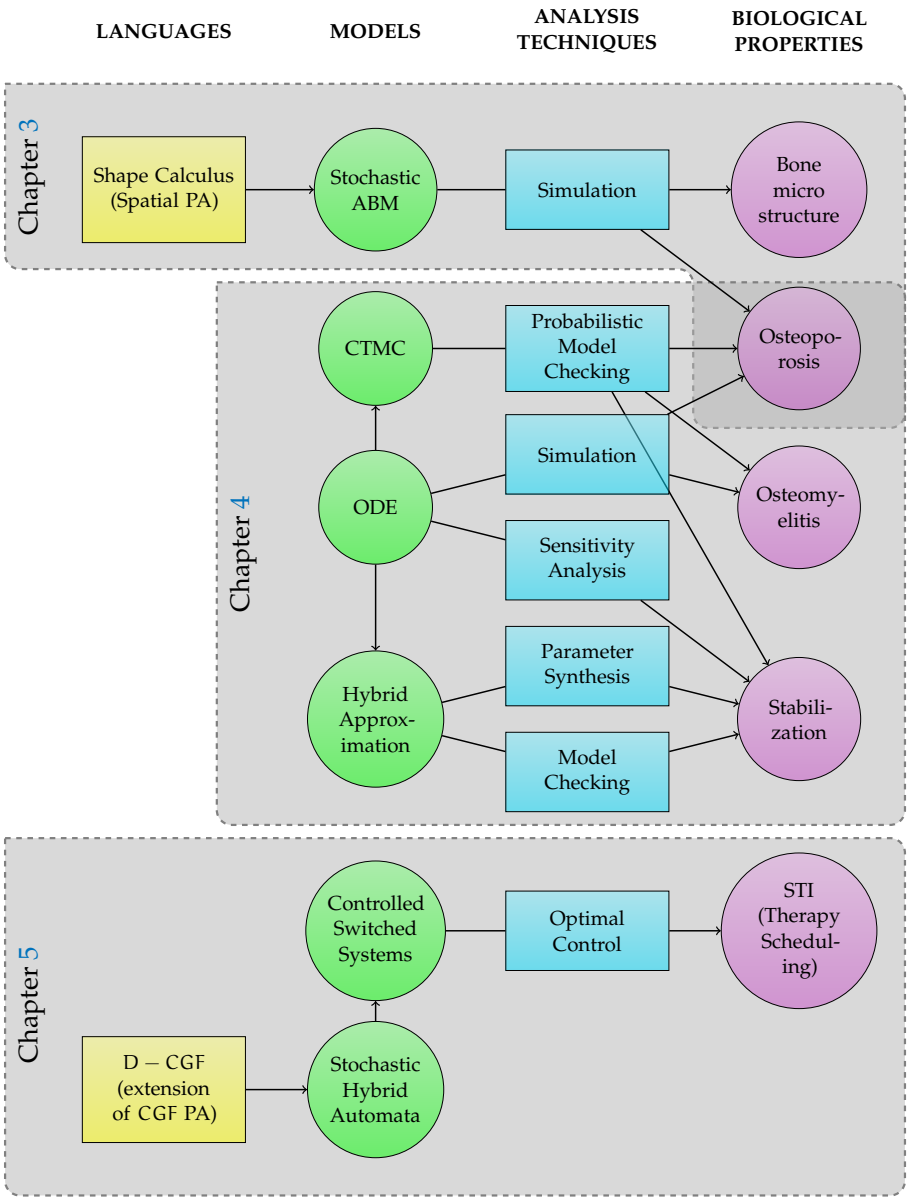

Figure 1: Methodological map. In each chapter, specific *biological properties* are investigated through the definition and application of suitable *models* (that can correspond to the semantics of formal specification *languages*), supporting specific *analysis techniques*.

2 BACKGROUND

2.1 BONE REMODELLING: A MULTISCALE PHYSIOLOGICAL SYSTEM

There are two main types of bone tissues: *cortical bone*, and *trabecular bone*. The former is a compact tissue that makes up the outer shell of bones. It consists of a very hard (virtually solid) mass of bony tissue arranged in concentric layers called Haversian systems. Trabecular (also known as cancellous or "spongy") tissue is located beneath the compact bone and consists of a meshwork of bony bars (trabeculae) with many interconnecting spaces containing bone marrow. Both bone tissues undergo a continuous remodelling dynamics where old bone is replaced by new tissue ensuring the mechanical integrity and the morphology of the bone [103, 83]. However, pathological conditions such as cancer, infection and autoimmune diseases can alter the equilibrium between bone resorption and bone formation, reducing bone density and increasing the risk of spontaneous fractures.

Bone remodelling (BR) is a process iterating throughout life, by which aged bone is continuously renewed in a balanced alternation of bone resorption (performed by cells called *osteoclasts*) and formation (performed by *osteoblasts*). It is responsible for repairing micro-damages, for maintaining mineral homeostasis and for the structural adaptation of bone in response to mechanical stress. In other words, a regular remodelling activity ensures the mechanical quality of the bone.

Osteoblasts follow osteoclasts in a highly coordinated manner, forming the so-called *Basic Multi-cellular Units (BMUs)*. While osteoblasts and osteoclasts are located in the fluid part of the BMU, another type of cells, the *osteocytes*, are trapped in the bone matrix and they play a relevant role in the remodelling process. Osteocytes serve as mechanosensors: they translate mechanical stimuli at the tissue level into biochemical signals that flow through the osteocytic canalicular network to the BMU cells. In normal bone, the number of BMUs, the bone resorption rate, and the bone formation rate are all relatively constant [131].

The *RANK/RANKL/OPG* signalling pathway plays an important role in bone metabolism. RANK is a protein expressed by osteoclasts; RANK is a receptor for RANKL, a protein produced by osteoblasts. RANK/RANKL

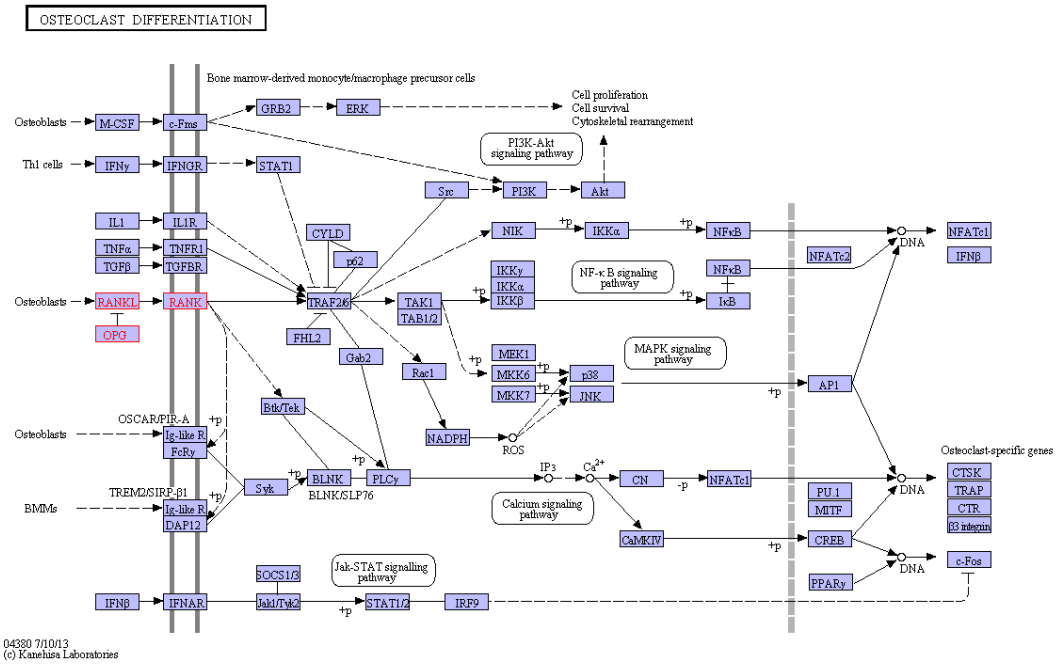

Figure 2: Osteoclast differentiation pathway, evidencing the central role of RANK, RANKL and OPG (highlighted in red) in the early stages of cell specialization.

signalling triggers osteoclast differentiation, proliferation and activation (as shown in Figure 2), thus it prominently affects the resorption phase during bone remodelling. Osteoprotegerin (OPG) is a decoy receptor for RANKL. It is expressed by mature osteoblasts and it binds to RANKL, thus inhibiting the production of osteoclasts and protecting in this way bone from excessive resorption. Figure 3 shows the key steps during the bone remodelling process, that are:

1. **Origination.** During normal turnover or after a micro-crack, or as a response to mechanical stress, the osteocytes in the bone matrix produce biochemical signals showing sufferance towards the lining cells, i.e. the surface cells around the bone. The lining cells pull away from the bone matrix, forming a canopy which merges with the blood vessels.

2. **Osteoclast recruitment.** Stromal cells divide and differentiate into osteoblasts precursors. Pre-osteoblasts start to express RANKL, inducing the differentiation of and attracting pre-osteoclasts, which have RANK receptors on their surfaces. RANKL is a homotrimeric molecule displayed on the membrane of osteoblasts that stimulates differentia-

tion in osteoclasts and is a key induction molecule involved in bone resorption leading to bone destruction.

3. **Resorption.** The pre-osteoclasts enlarge and fuse into mature osteoclasts. In cortical BMUs, osteoclasts excavate cylindrical tunnels in the predominant loading direction of the bone, while in trabecular bone they act at the bone surface, digging a trench rather than a tunnel. After the resorption process has terminated, osteoclasts undergo apoptosis.

4. **Osteoblast recruitment.** Pre-osteoblasts mature into osteoblasts and start producing osteoprotegerin (OPG). OPG inhibits the osteoclastic activity by binding to RANKL and thus preventing it from binding to RANK. When RANKL expression is high, osteoprotegerin levels are low and vice versa.

5. **Mineralization.** Osteoblasts fill the cavity by secreting layers of osteoids. Once the complete mineralization of the renewed tissue is reached, some osteoblasts can go apoptosis, other can turn into lining cells, while other can remain trapped in the bone matrix and become osteocytes.

6. **Resting.** Once the cavity has been filled by osteoblasts, the initial situation is re-established.

Bone remodelling can be seen as *a paradigm for several other physiological systems*, since similarly to the epithelium renewal process, the hematopoiesis process and many others, it is characterized by a birth-death dynamics involving different populations of cells (osteoclasts and osteoblasts) which together contribute in maintaining the stability of the tissue level and of the organ level. Furthermore, bone remodelling is a multiscale process where the molecular scale affects the cellular scale (e.g. RANKL induces osteoclasts' proliferation), and in turn the cellular scale affects the tissue scale (the number and the activity of bone cells determine tissue density and microstructure).

OSTEOPOROSIS The bone remodelling undergoes a pathological process, generally related to ageing, termed osteopenia and with more severity, osteoporosis, during which an unbalance of the RANKL/OPG signalling equilibrium is typically observed. The osteoporosis is a skeletal disease characterized by low *Bone Mineral Density (BMD)* and structural fragility, which consequently leads to frequent micro-damages and spontaneous fractures; it is a chronic disease requiring long-term treatment. This disease primar-

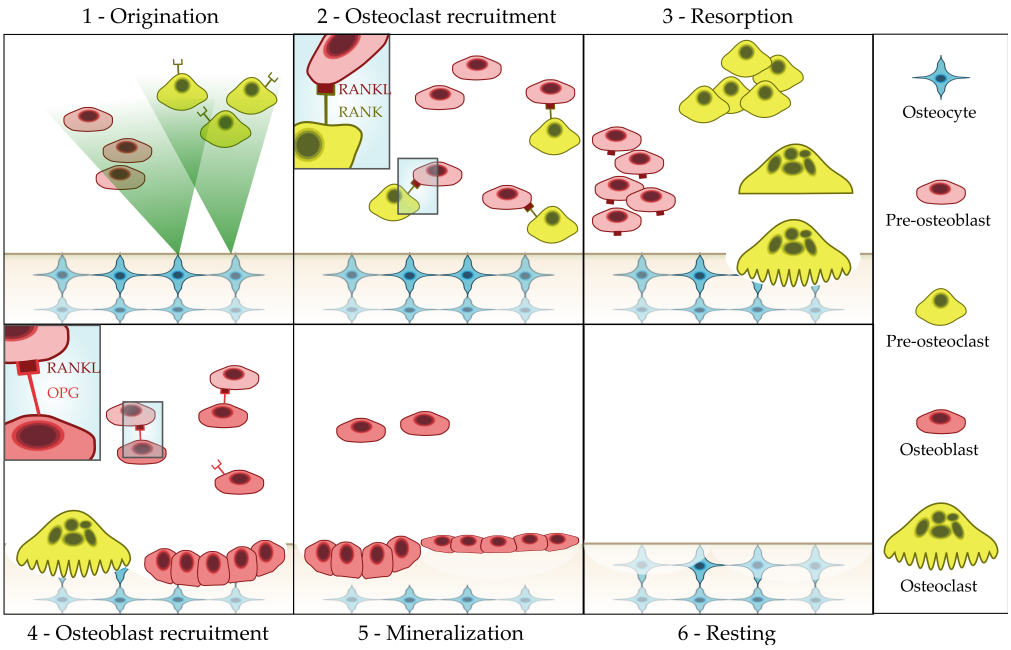

Figure 3: Illustration of the key steps in bone remodelling.

ily affects middle-aged women and elderly people and at present its social and economic impact is dramatically increasing, so much that the World Health Organization considers it to be the second-leading healthcare problem. While under normal circumstances, the ratio of RANKL/OPG is carefully balanced, the increase of RANKL plays an essential role in favouring resorption through osteoclast formation, function, and survival. With ageing and after a large number of remodelling cycles, the density of osteons increases and the cortical porosity and architectural defects of the bone increase as well. This leads to a vicious cycle where microdamages and consequently remodelling occur more and more frequently, weakening the bone structure and increasing the rate of spontaneous fractures [153]. Moreover, recent studies suggest that plasma levels OPG and RANKL are inversely related to bone mineral density and contribute to the development of osteoporosis in postmenopausal women [81], and thalassemia-induced osteoporosis [111].

OSTEOMYELITIS One of the most worrying events is the infection of the bone which causes a disease called osteomyelitis. Similarly to osteoporosis, it is characterized by severe and rapid bone loss and by an unbalance at the molecular signalling level. Osteomyelitis is caused by a bacterial infection (mostly *Staphylococcus aureus*) which alters the RANK/RANKL/OPG

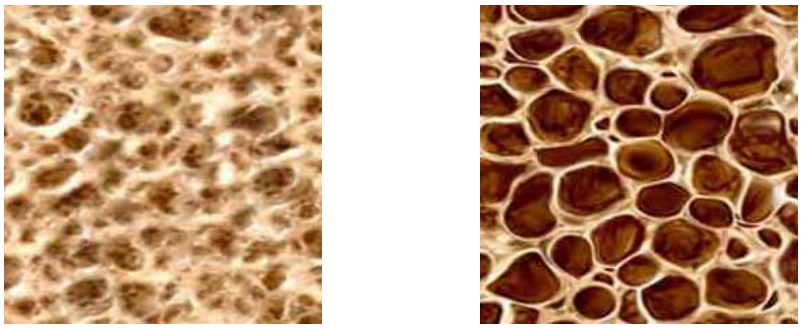

(a) Healthy **(b)** Osteoporotic

Figure 4: Differences in density and structure between healthy (a) and osteoporotic (b) trabecular bone.

signalling dynamics that regulates osteoblasts and osteoclasts behaviour in bone remodelling, i.e. the resorption and mineralization activity. The infection rapidly leads to severe bone loss, necrosis of the affected portion, and it may even spread to other parts of the body.

Upon exposure to the bone, *S. aureus* induces a severe inflammatory response followed by progressive bone destruction and loss of the vasculature, leading to a persistent chronic infection. This is further complicated by the rapid emergence of resistant strains of *S. aureus*. Experimental studies have shown that the infection prevents proliferation, induces apoptosis and inhibits mineralisation of cultured osteoblasts. The action of *S. aureus* increases RANKL expression and decreases OPG expression in osteoblasts in patients with staphylococcal osteomyelitis. Recent findings suggest that *S. aureus* SpA protein binds to osteoblasts, possibly through an interaction with the death receptor TNFR-1 which induces caspase 3 activation and apoptosis. The increase in RANKL is likely to trigger osteoclast-induced bone resorption and bone destruction, which explains why patients with osteomyelitis have significant bone loss [50]. Figure 5 illustrates the effect of the pathogen on the remodelling activity.

Although effective treatment of this disease is very difficult, one of most used drug is the fusidic acid that acts as a bacterial protein synthesis inhibitor by preventing the turnover of elongation factor G (EF-G) from the ribosome. Fusidic acid inhibits bacterial replication and does not kill the bacteria, and is therefore termed "bacteriostatic". Many strains of methicillin-resistant *S. aureus* (MRSA) remain sensitive to fusidic acid, but because there is a low genetic barrier to drug resistance (a single point mutation is all that is required), fusidic acid is usually combined with other antibiotics.

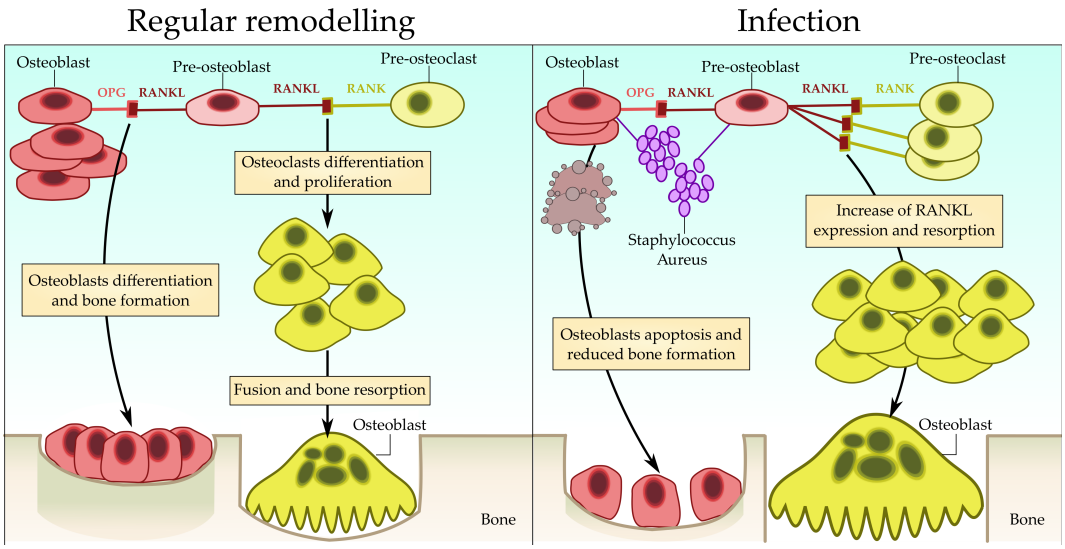

Figure 5: Osteomyelitis effect on bone remodelling. Differently from a regular remodelling cycle (left), the bone infection by *S. aureus* (right) induces the proliferation of osteoclasts and the apoptosis of osteoblasts, leading to a severe bone density loss.

2.2 THE CCS PROCESS ALGEBRA

Process algebras (PAs) are formal languages for the specification of *reactive concurrent systems*, i.e. systems that consists of multiple processes where each process may change state in reaction to another process changing state (*reactivity*), and competitively access to shared resources (*concurrency*).

A brief history of the main developments in process algebra in the last 30 years is reviewed in [6]. This established field of research stems from the works by Milner [109], Hoare [79] and Bergstra and Klop [18], who were the first to describe concurrent processes by means of algebraic structures.

In the last decade, process algebras have emerged as a suitable tool to provide formal foundations to Systems Biology, under the perspective of *biological systems as reactive concurrent systems* [60, 59]: the abstraction metaphor is to see biological components as concurrent processes and their interaction as process communication. The application of PAs in biological modelling brings several advantages, among which its compositionality, allowing the whole system to be defined starting from the definition of its subcomponents; and a toolkit of formal analysis methods for reasoning on biological properties, including the study of behavioural equivalences (e.g. strong/weak, probabilistic bisimulation) and preorders (e.g. simulation refinement), as well as model checking.

The application to the biological domain has favoured the introduction of novel bio-inspired languages and the definition of a wide variety of quantitative extensions to classical qualitative PAs, like stochastic process algebras [32, 75, 20, 76, 128, 52, 25] and spatial process algebras (reviewed in Chapter 3).

In this section we give the formal syntax and semantics of Milner's *Calculus of Communicating Systems (CCS)* [109, 1]. Firstly, we need to introduce the notion of *labelled transition systems*, i.e. the structure through which the semantics of CCS (and of many other process algebras) is defined.

2.2.1 Labelled Transition Systems

Generally speaking, a *Labelled Transition System (LTS)* is a labelled directed graph, able to describe the evolution of processes (the vertices) that change state by performing actions (edge labels). Formally, a LTS is defined as follows.

Definition 2.2.1 (Labelled Transition System)**.** *A* Labelled Transition System (LTS) *is a triple* $(\mathcal{P}, \mathsf{Act}, \rightarrow)$*, where*

- $\mathcal{P}$ *is a set of* states *(or processes);*
- Act *is a set of* actions *(or labels); and*
- $\rightarrow \subseteq \mathcal{P} \times \mathsf{Act} \times \mathcal{P}$ *is a* transition relation.

As usual, we use the notation $p \xrightarrow{a} p'$ to indicate that $(p, a, p') \in \rightarrow$ and we say that p performs an action a and becomes p'. $p \xrightarrow{a}$ (read p can perform an action a) is used in place of $\exists p' \in \mathcal{P}.\ p \xrightarrow{a} p'$, and $p \not\xrightarrow{a}$ indicate that p cannot perform an action a. Moreover, an LTS possibly admits an *initial state*; in this case, the LTS is called *rooted*.

EXAMPLE In the following we describe an example taken from [1], of a simplified vending machine supplying tea and coffee at the price of 1 € and 2 €, respectively.

Let p be the initial state, which models the situation where the machine is waiting for the customer to choose a beverage. From p two possible transitions are enabled: $p \xrightarrow{tea} p_1$ and $p \xrightarrow{coffee} p_2$. In the former case, the tea button is pressed and the machine enters state p_1.

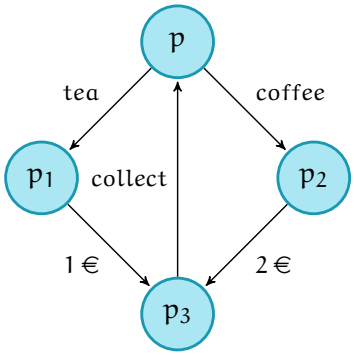

In the latter case, the `coffee` button is pressed and the machine enters state p_2.

In states p_1 and p_2, the machine is waiting for the amount of money needed for the chosen drink. By performing the transitions $p_1 \xrightarrow{1€} p_3$ and $p_2 \xrightarrow{2€} p_3$, the machine reaches the state p_3, recording that the selected drink has been paid. Finally, the drink is collected and the machine returns to its initial state p (transition $p_3 \xrightarrow{collect} p$).

2.2.2 CCS Syntax

CHANNELS, ACTIONS AND PROCESS NAMES Let us consider a countable set of *channel names* $\mathcal{A} = \{a, b, \ldots\}$ and the corresponding set of *complementary names* (or *co-names* for short) $\overline{\mathcal{A}} = \{\overline{a} \mid a \in \mathcal{A}\}$. Typically, names are interpreted as *input actions*, while co-names as *output actions*. The set $\mathcal{L}$ of *labels* and the set Act of *actions* are defined by

$$\mathcal{L} = \mathcal{A} \cup \overline{\mathcal{A}} \qquad \mathsf{Act} = \mathcal{L} \cup \{\tau\}$$

where τ is a special action called *internal* or *unobservable*. Finally, let $\mathcal{P}$ denote the set of CCS expressions and $\mathcal{K}$ denote a given countable set of *process names* or *constants*. We assume that the behaviour of each constant $K \in \mathcal{K}$ is given by a defining equation $K \stackrel{def}{=} P$, where $P \in \mathcal{P}$.

P ::=		**CCS process**
	0	Null Process
	$\alpha.P$	Sequential Composition
	$P + P$	Choice
	$P \parallel P$	Parallel Composition
	K	Process Name
	$P\backslash L$	Restriction
	$P[f]$	Renaming

Table 1: CSS syntax ($\alpha \in \mathsf{Act}$, $K \in \mathcal{K}$, $L \subseteq \mathcal{L}$, $f : \mathsf{Act} \to \mathsf{Act}$).

CCS processes are formally defined by the grammar in Table 1, where **0** denotes the *null process*, that cannot perform any action. $\alpha.P$ is the process that can perform action α and then behave as P. $P_i + P_j$ is the process that non-deterministically behaves as either P_i or P_j. $P_i \| P_j$ denotes the parallel execution of P_i and P_j; in this case, the two processes may run independently or *synchronize* via complementary channels; in the latter case, the τ action is exhibited. The restriction (or *hiding*) operator $P\backslash L$ is used to restrict the scope of process P to

$$\textsc{Act}\ \frac{}{\alpha.P \xrightarrow{\alpha} P} \qquad \textsc{Choice}_1\ \frac{P \xrightarrow{\alpha} P'}{P + Q \xrightarrow{\alpha} P' + Q} \qquad \textsc{Choice}_2\ \frac{Q \xrightarrow{\alpha} Q'}{P + Q \xrightarrow{\alpha} P + Q'}$$

$$\textsc{Com}_1\ \frac{P \xrightarrow{\alpha} P'}{P \| Q \xrightarrow{\alpha} P' \| Q} \qquad \textsc{Com}_2\ \frac{Q \xrightarrow{\alpha} Q'}{P \| Q \xrightarrow{\alpha} P \| Q'} \qquad \textsc{Com}_3\ \frac{P \xrightarrow{a} P' \; Q \xrightarrow{\overline{a}} Q'}{P \| Q \xrightarrow{\tau} P' \| Q'}$$

$$\textsc{Res}\ \frac{P \xrightarrow{\alpha} P'}{P \backslash L \xrightarrow{\alpha} P' \backslash L} \text{ where } \alpha, \overline{\alpha} \notin L \qquad \textsc{Ren}\ \frac{P \xrightarrow{\alpha} P'}{P[f] \xrightarrow{f(\alpha)} P'[f]}$$

$$\textsc{Def}\ \frac{P \xrightarrow{\alpha} P'}{K \xrightarrow{\alpha} P'} \text{ where } K \stackrel{def}{=} P$$

Table 2: SOS rules for CCS terms ($\alpha \in \mathsf{Act}, a \in \mathcal{L}$).

exclude actions in L. Finally, P[f] applies a renaming function $f : \mathsf{Act} \to \mathsf{Act}$ to actions occurring in P. The renaming function f must be such that:

$$f(\tau) = \tau \quad \text{and} \quad f(\overline{a}) = \overline{f(a)}, \ \forall a \in \mathcal{A}$$

2.2.3 CCS Semantics

The semantics of CCS is given by a set of *Structural Operational Semantics* (*SOS*) rules [126]. It is a common way to establish a correspondence between a process definition and its underlying transition system, where each operator has associated inference rules of the form $\frac{\text{premises}}{\text{conclusion}}$. In this way, the states of the resulting LTS correspond to CCS expressions.

Formally, the semantics of CCS is a labelled transition system $(\mathcal{P}, \mathsf{Act}, \to)$, where $\to \subseteq \mathcal{P} \times \mathsf{Act} \times \mathcal{P}$ is the minimal relation satisfying the SOS rules in Table 2.

Rule Act has no premises and simply yields the transition $\alpha.P \xrightarrow{\alpha} P$. Rules $\textsc{Choice}_1$ and $\textsc{Choice}_2$ regulate the non-deterministic choice $P + Q$ between processes P and Q. According to $\textsc{Com}_1$, $\textsc{Com}_2$ and $\textsc{Com}_3$, processes put in parallel can evolve independently or synchronize on complementary channels, respectively. Rule Res constraints a process $P\backslash L$ to perform transitions labelled with actions $\alpha \notin L$. Rule Ren applies when a renaming function is applied. Finally, rule Def tells that a process constant $K \stackrel{def}{=} P$ can reduce to process P.

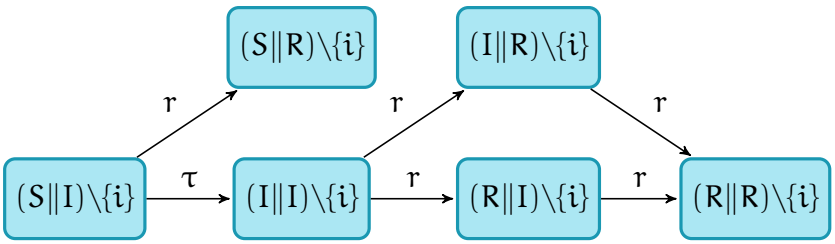

Figure 6: Possible evolutions of a SIR epidemic model described in CCS. The LTS is generated starting from the process $(S\|I)\backslash\{i\}$ (a population with one susceptible and one infected).

2.2.4 Running Example: SIR Epidemic Model

In this section, we present a qualitative variant of the SIR epidemic model [84], suitable to be described through the CCS language. The SIR model was originally formulated for studying the temporal evolution of an epidemics, via a set of coupled ODEs, in a population divided in three compartments: susceptible, exposed and individuals. A broader view on epidemic modelling and on its several variants will be given in Chapter 5. To our purposes, in the qualitative SIR model we study the evolution of an illness characterized by the following events:

- a susceptible individual (process S) can come into contact with an infected individual (input action i) and become infected;
- an infected individual (process I) can either infect a susceptible one (output action $\bar{i}$) or recover (action r); and
- a recovered individual (process R) cannot be infected anymore (basically, it performs no actions).

In process-algebraic language,

$$S \stackrel{\text{def}}{=} i.I \qquad I \stackrel{\text{def}}{=} \bar{i}.I + r.R \qquad R \stackrel{\text{def}}{=} \mathbf{0}$$

We can study the dynamics of a simple population consisting of a susceptible and an infected individual, by deriving the LTS of the CSS expression $(S\|I)\backslash\{i\}$. In this case, the use of the restriction operator prevents processes S and I to independently perform actions i and $\bar{i}$ respectively, without synchronization. The resulting LTS is illustrated in Figure 6.

2.3 PROBABILISTIC MODEL CHECKING

In this section we introduce stochastic models and probabilistic model checking, focusing on Continuous Time Markov Chains and CSL model checking. For a more comprehensive treatment of the topic, we address the interested reader to the tutorial papers [88, 91], where a number of case studies are illustrated through the use of the probabilistic model checker PRISM [90].

Probabilistic model checking (PMC) is a formal verification technique for the analysis of systems exhibiting probabilistic and stochastic dynamics. In classical model checking, given a model of the system $\mathcal{M}$ specified as a state transition system, and a property to verify (the specification) ϕ, typically described in terms of a temporal logic formula, the problem consists in computing $\mathcal{M} \models \phi$, i.e. a truth value indicating whether or not the model satisfies the specification. PMC extends conventional model checking for reasoning on the probability that a formula ϕ is satisfied by a probabilistic model $\mathcal{M}$. This enables the formal analysis of quantitative properties over the probabilistic model, and to present PMC has been successfully applied to a variety of biological systems like signalling pathways [72], stochastic population models [100], or molecular computing devices [92, 149].

Continuous Time Markov Chains (CTMCs) is a stochastic model able to express both continuous real time and probabilistic choice, formally defined as follows.

Definition 2.3.1 (CTMC)**.** *A* Continuous Time Markov Chain (CTMC) *is a tuple* $(S, \mathbf{R}, L, AP)$ *where*

- S *is a finite set of states;*
- $\mathbf{R} : S \times S \to \mathbb{R}_{\geqslant 0}$ *is a rate transition matrix, assigning a non-negative real-valued rate to each pair of states; and*
- $L : S \to 2^{AP}$ *is a labelling function that associates each state with a set of atomic propositions.*

A transition rate $\mathbf{R}(s, s')$ models the propensity of moving to state s' from state s. In particular the transition is enabled if $\mathbf{R}(s, s') > 0$. The rate determines an exponentially distributed transition duration: the probability that transition $s \to s'$ is enabled in the time interval $[0, t]$ is $1 - e^{-\mathbf{R}(s,s')t}$. In other words, higher rates determine faster transitions. The probability of moving to s' from s is given by $\mathbf{R}(s, s')/E(s)$, where $E(s) = \sum_{s' \in S} \mathbf{R}(s, s')$ is called the *exit rate* of s (the sum of the rates of all the outgoing transitions). Therefore, higher transition rates (and so faster transitions) have a higher probability of being taken before those with a lower rate.

PATHS A path ω of a CTMC $C = (S, \mathbf{R}, L, AP)$ is a non-empty sequence $\omega = s_0 t_0 s_1 t_1 \ldots$, where for all i, $s_i \in S$ and $t_i \in \mathbb{R}_{\geqslant 0}$ is the time spent in state s_i. ω is infinite when $\mathbf{R}(s_i, s_{i+1}) > 0$ for all i, and finite of length n when $\mathbf{R}(s_i, s_{i+1}) > 0$ for all $i < n-1$ and $E(s_{n-1}) = 0$. We denote by $\mathtt{Path}(s)$ the set of all paths of the CTMC C starting in state s. $\omega@t$ denotes the state of path ω at time t, i.e. the j-th state such that $\sum_{i=0}^{j} t_i \geqslant t$ and $\sum_{i=0}^{j-1} t_i < t$.

TRANSIENT AND STEADY-STATE DISTRIBUTIONS Properties of a CTMC can be conveniently studied at a given instant (transient behaviour), or in the long-run (steady-state behaviour). The *transient probability* of being in state s' at time t, from the initial state s is denoted by $\pi_{s,t}(s')$, while the *steady-state probability* of being in s' having started from s, $\pi_s(s')$, can be used for instance to compute the percentage of time, in the long-run, that the CTMC spends in each state.

REWARDS CTMCs appear often extended with reward structures, i.e. non-negative real-valued costs associated to states and/or transitions. Rewards provide additional quantitative information in the model (without increasing the state space), and according to the property to verify, they can be computed at a particular instant, called *instantaneous rewards*, or can be cumulated along the execution of the model, called *cumulative rewards*.

State rewards are defined by a function $\sigma : S \to \mathbb{R}_{\geqslant 0}$, associating a cost to each state, and can be used for instance to calculate the expected value of a state variable at a particular time. Transition rewards are used to map the transitions of a CTMC with a cost, by a function $\tau : S \times S \to \mathbb{R}_{\geqslant 0}$, and they are often employed to count the number of times a particular transition has been fired.

2.3.1 Continuous Stochastic Logic

In order to reason about the properties of stochastic models, temporal logic languages have been defined for dealing with probabilistic and quantitative aspects. In the following, we consider a version of *Continuous Stochastic Logic (CSL)* [5] extended with reward operators.

Definition 2.3.2 (CSL Syntax)**.** *The syntax of CSL is given by the following grammar:*

$$\phi ::= \mathsf{true} \mid a \mid \phi \wedge \phi \mid \neg\phi \mid \mathcal{P}_{\sim p}[\psi] \mid \mathcal{S}_{\sim p}[\psi]$$
$$\psi ::= X\phi \mid \phi \,\mathcal{U}\, \phi \mid \phi \,\mathcal{U}^{I} \phi$$

where $a \in AP$ *is an atomic proposition;* $\sim \in \{<, \leqslant, \geqslant, >\}$*;* $p \in [0,1]$ *and* I *is an interval of* $\mathbb{R}$*.*

State formulas are given by the standard operators from propositional logic: true, a (that holds in the states labelled with a), conjunction and negation; and by the probabilistic operators $\mathcal{P}$ and $\mathcal{S}$. The formula $\mathcal{P}_{\sim p}[\psi]$ is true in a state s if the probability p' of the path formula ψ being satisfied is such that $p' \sim p$. More technically, p' is a probability measure over the paths $\omega \in Path(s)$, s.t. $\omega \models \psi$.

The formula $\mathcal{S}_{\sim p}[\psi]$ is true if the steady-state probability p' of the path formula ψ being satisfied is such that $p' \sim p$. It corresponds to computing the sum of probability densities in the long run of the states s' that satisfy ψ: $p' = \sum_{s' \models \phi} \pi_s(s')$.

Path formulas are built over the next state operator X, the until operator $\mathcal{U}$ and the bounded until operator $\mathcal{U}^I$. From a state s, $X\phi$ is true if in the next state ϕ holds. Formula $\phi_1 \mathcal{U} \phi_2$ is true if ϕ_2 holds at some point from s, and ϕ_1 holds until ϕ_2 holds. Formula $\phi_1 \mathcal{U}^I \phi_2$ is true if ϕ_2 holds in the time interval I, and ϕ_1 holds until ϕ_2 holds. The future operator, $\mathcal{F}$, and globally operator, $\mathcal{G}$, and their bounded variants are derived from $\mathcal{U}$ as follows:

$$\mathcal{P}_{\sim p}[\mathcal{F}\phi] \equiv \mathcal{P}_{\sim p}[\text{true } \mathcal{U}\ \phi]$$
$$\mathcal{P}_{\sim p}[\mathcal{G}\phi] \equiv \mathcal{P}_{\tilde{\sim} 1-p}[\mathcal{F}\ \neg\phi]$$

where $\tilde{<} \equiv >$, $\tilde{\leqslant} \equiv \geqslant$, $\tilde{\geqslant} \equiv \leqslant$ and $\tilde{>} \equiv <$.

In addition, the expressions $\mathcal{P}_{=?}[\psi]$ and $\mathcal{S}_{=?}[\psi]$ can be used as functions for computing the actual probability of the formula ψ being satisfied. Rewards operators are defined by

$$\mathcal{R}_{\sim r}[\mathcal{I}^{=t}] \mid \mathcal{R}_{\sim r}[\mathcal{C}^{\leqslant t}] \mid \mathcal{R}_{\sim r}[F\phi] \mid \mathcal{R}_{\sim r}[\mathcal{S}]$$

where $p, t \in \mathbb{R}$, and ϕ is a CSL formula. From a state s, $\mathcal{R}_{\sim r}[\mathcal{I}^{=t}]$ is true if the expected instantaneous reward at time t satisfies $\sim r$. This expected value is that of the random variable $\sigma(\omega@t)$ computed w.r.t. the probability measure defined over all the paths $\omega \in Paths(s)$.

$\mathcal{R}_{\sim r}[\mathcal{C}^{\leqslant t}]$ holds if the expected (state and transition) reward cumulated up to time t, c, satisfies $\sim r$. Also in this case c is a random variable, and for any path $s_0 t_0 s_1 t_1 \ldots$, is defined by:

$$c = \sum_{i=0}^{j_t - 1} (t_i \cdot \sigma(s_i) + \tau(s_i, s_{i+1})) + (t - \sum_{i=0}^{j_t - 1} t_i) \times \tau(s_{j_t})$$

where j_t is the minimum index s.t. $\sum_{i=0}^{j_t} t_i \geqslant t$. In practice, for distinguishing among multiple reward structures, the operator $\mathcal{R}^{id}$ is used to indicate the (state or transition) reward identified by id.

$\mathcal{R}_{\sim r}[\mathcal{F}\phi]$ holds if the expected reward cumulated before ϕ becomes true meets $\sim r$, and is computed in a similar way to $\mathcal{R}_{\sim r}[\mathcal{C}^{\leqslant t}]$, except that rewards are summed up to the minimum index of the path s.t. ϕ holds (if ϕ never holds the value of the cumulated reward is ∞).

Finally, $\mathcal{R}_{\sim r}[\mathcal{S}]$ is true if the long-run instantaneous expected reward meets $\sim r$. Similarly to $\mathcal{P}_{=?}$ and $\mathcal{S}_{=?}$, quantitative reward properties can be specified with the expression $\mathcal{R}_{=?}$.

3 SPATIAL CELL BIOLOGY: FORMAL MODELLING AND SIMULATION OF BONE REMODELLING

Chapter Outline

Location and space are crucial aspects to consider in order to fully understand the dynamics of biological systems at the molecular and cellular level. In this chapter, we aim to grasp the multiscale and spatial mechanisms that connects disorders in RANKL molecular signalling, to osteoporosis and other diseases originating from defective bone remodelling dynamics and characterized by a lower bone mass and disruptions at the tissue level.
Procedurally, we provide a minimal extension (called ESC) to the *Shape Calculus*, a process algebra with spatial and geometrical primitives, and we exploit it as the formal specification language for a novel spatial model of bone remodelling. The executable side of the model is obtained by encoding the formal specification into an agent-based model (*ABM*), where Shape Calculus-based agents are enriched with *stochastic actions* and with the ability to sense the neighbourhood (*perception*).
The parametrization of ageing factors that negatively affect the activity of bone cells and of the RANKL production rate, a major regulator of the remodelling process, allowed reproducing both healthy and osteoporotic conditions. Finally, we demonstrate how the location of signalling osteocytes (responsible for initiating the remodelling process) in the long run considerably influence the bone microstructure at the tissue level.

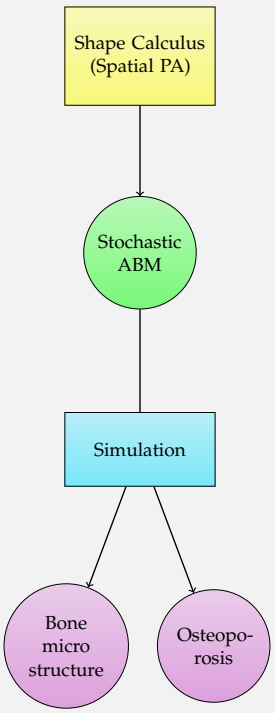

"LOCATION, location, location". In the context of property management, this turn of phrase highlights how location is the most important factor to consider when buying or selling a house. Similarly in biology, ad-

vances in experimental techniques, e.g. high content screening or high resolution microscopy, have revealed the importance of space and location also at the cellular and molecular signalling level.

Spatial organization and *location* prominently affect the behaviour, the development and the evolution of biological entities: they occupy a certain space; they move and interact with their spatial neighbours; they express signals which propagate within a particular distance; and their internal spatial organization and their shape regulates their functionalities.

For instance, cells have intrinsic mechanisms for the spatial relocation of proteins and enzymes to the cellular membrane (a process more generally called subcellular translocation), in order to activate signalling pathways that are crucial to accomplish specific processes like division, motility and migration. A typical example is the control of the *Ras/MAPK* cascade by membrane recruitment of *SOS* and *RasGAP* [85]); or, recalling the *RANK/RANKL* pathway introduced in Sect. 2.1, *RANKL* stimulation induces the translocation of important proteins from the cytoplasm to the nucleus inside bone cells [132]. In addition, different subcellular localization of signalling molecules can lead to considerably different signalling patterns [70], and spatial aspects becomes extremely meaningful in presence of crosstalk [55], i.e. when multiple signalling pathways share more than one component.

Another classical example is given by *molecular gradients*, that play a key role not only at the intra-cellular level to organize signalling between subcellular structures [85, 124]; but also at the inter-cellular level, e.g. in *chemotaxis*, the process by which cellular organisms direct their movements towards higher (positive chemotaxis), or lower (negative chemotaxis) concentration of a particular chemical, such as nutrients.

Returning to the main case study of this thesis, the dynamics of bone remodelling exhibits spatial and geometrical properties at multiple levels. For instance, the amount of resorbed bone depends on the surface extension of osteoclasts, which have ruffled borders functional to resorption; osteocytes sense micro-fractures due to the apoptosis of the cells that are closely located to it; and abnormalities in bone size and shape may underlie pathological conditions.

SPATIAL (FORMAL) METHODS FOR BIOLOGICAL MODELLING The modern computational biologist can rely on a variety of modelling techniques able to explicitly represent spatial features, ranging from the more established ones (e.g. partial differential equations, cellular automata, Brownian dynamics and Cellular Potts model) to the more recently introduced formal languages equipped with spatial capabilities. Here we will not provide a

detailed review of the available spatial techniques, but we will focus mostly on formal languages and in particular process algebras for spatial modelling in biology. For a more comprehensive introduction to the topic, we refer the interested reader to the reviews [21, 85, 145].

In the field of process algebras, *compartmentalization* is a common way to represent the localization of biological entities (or processes). In this context, (possibly nested) compartments are used to restrict the scope of the interactions among processes, so that a process can communicate only with compatible processes in the same compartment, unless the transport of processes between compartments is supported. This class of languages includes *BioAmbients* [134], a process calculus inspired by the ambient calculus [43] which supports the movement of entities between compartments and their reconfiguration; *Beta Binders* [129], that wraps π-calculus [110] processes inside boxes, the compartments, able to communicate through a set of binders, i.e. different sites of interaction; the *Brane Calculus* [39], where dynamic membranes (together with actions able to change their topology) are the only unit of computation; and simple extensions of stochastic process algebras with static compartments/locations [48, 138].

The development of languages that explicitly include spatial features (like position, space occupancy, velocity), just abstractly represented in compartment and membrane-based approaches, has received less attention in the computational biology community. Indeed *their expressive power is counterbalanced by non-trivial modelling issues*: their operational semantics needs to be tightly and unusually integrated with simulation algorithms, thus losing the appealing theoretical properties of a process-algebraic language, like behavioural equivalences and preorders. Moreover, detailed and precise spatial parameters are generally hard to retrieve, and in many cases the modeller just needs to include simpler and higher-level features (e.g. reaction rates), emerging from more complex spatial and geometrical interactions.

Some notable attempts to join formal languages, geometry and physical features are: 3π [42], which extends the π calculus with three - dimensional affine transformations in order to describe the evolution of biological entities, modelled as geometrical structures; *Space* π [82], where π calculus processes are equipped with coordinates in a two- or three-dimensional space, movement and an interaction radius that limit the range of communication; and the *Shape Calculus*, a CCS-based language [109] able to express features like mass, position, velocity, shape, collisions, binding and splitting of processes.

OSTEOPOROSIS AND DEFECTIVE BONE DYNAMICS In this chapter, we want to probe the usefulness and the effectiveness of spatial process algebras in bi-

ological modelling. We will focus on the application of the Shape Calculus as a formal language to specify stochastic agent-based models, by testing the approach with a novel spatial and agent-based model of bone remodelling. In particular, we focus on studying and reproducing defective bone remodelling dynamics that lead to pathologies like osteoporosis, and on understanding the multiscale dynamics that generate severe disruptions at the tissue level from small variations of molecular concentration.

Indeed, several important findings provide clear evidence of the multiscale properties of bone formation and of the links between RANK/RANKL and bone density in healthy and disease conditions. However, there is a lack of knowledge of the genetic and environmental factors responsible for age and gender specific differences in bone fragility and fracture rates. Recent studies indicate that the circulating levels of RANKL are inversely related to bone turnover and *Bone Mineral Density (BMD)* and contribute to the development of osteoporosis in postmenopausal women [81], and of thalassemia-induced osteoporosis [111].

In particular, we are interested in assessing the emergence of osteoporosis in older patients, that are typically characterized by a reduced cellular activity, in terms of lower bone formation and resorption rates; lower growth rates; and higher death rates. The main objective of this study is to characterize and compare two different classes of patients (corresponding to two different parameter configurations):

- *control patients*, with regular RANKL levels and cellular activity, and
- *osteoporotic patients*, with an overproduction of RANKL and a reduced cellular activity,

Structure of the chapter

SECTION 3.1 We introduce the syntax and the semantics of the Shape Calculus in its original version, and we show an application of the language to the RANKL/OPG signalling in bone remodelling.

SECTION 3.2 We present ESC, a language that extends the Shape Calculus with three additional behavioural terms: *Iteration*, for expressing repeating behaviours; *Thanatos*, for modelling the removal of a 3D shape; and *Duration*, for defining time-bounded behaviours.

SECTION 3.3 The encoding of ESC processes into agent-based models enriched with stochastic actions and perception is illustrated.

SECTION 3.4 A spatial model of bone remodelling is defined in the ESC language and details are provided on the agent-based implementation in the *Repast* simulation environment.

SECTION 3.5 Simulation results are presented and validated against statistical data from population-wide surveys. Finally, we analyse how the location of signalling osteocytes is able to affect the bone microstructure after multiple remodelling cycles.

3.1 SHAPE CALCULUS

In this section we introduce the *Shape Calculus* [9, 11, 33], a timed and spatial process calculus conceived for modelling biological systems, but also suitable to describe cyberphysical systems, i.e. systems characterized by a strong interplay between computation/communication and physical features like mass, position, velocity and geometrical form.

3.1.1 Shape and Behaviour of 3D Processes

The building blocks of the Shape Calculus are the so-called 3D processes which move, collide and interact in the 3D space. A 3D process is characterized by an *internal behaviour* B specified in a timed variant of the *CCS* process algebra (introduced in Section 2.2); and by a *3D shape* S, that defines the geometry and the physical properties of the process. $S[B]$ denotes a 3D process with behaviour B and shape S.

Collisions represent the basic mechanism of interaction between 3D processes. In particular, colliding shapes can bind (inelastic collision), indicating a successful communication between compatible processes; or repulse (elastic collision), when the corresponding processes are not able to interact. Additionally, the calculus supports the decomplexation of bounded shapes, by the so-called *split* operators.

3D SHAPES The set $\mathbb{S}$ of *3D shapes* is composed of *basic shapes* $\sigma = \langle V, m, \mathbf{p}, \mathbf{v} \rangle$, that are characterized by:

- a geometry $V \subseteq \mathbb{R}^3$, described as a *convex set* of 3D points;
- a mass $m \in \mathbb{R}$;
- a position vector $\mathbf{p} \in \mathbb{R}^3$; and

- a velocity vector $\mathbf{v} \in \mathbb{R}^3$;

and by compound shapes of the form $S_1\langle X\rangle S_2$, resulting from the binding of two 3D shapes $S_1, S_2 \in \mathbb{S}$ on a common surface X. Naturally, X cannot be empty (otherwise there would be no contact between S_1 and S_2), and can only include points at the boundary of S_1 and S_2, respectively denoted by the sets $\mathcal{B}(S_1)$ and $\mathcal{B}(S_2)$. More compactly, $\emptyset \neq X \subseteq \mathcal{B}(S_1) \cap \mathcal{B}(S_2)$.

TRAJECTORIES AND COLLISIONS Following the particular motion law chosen by the modeller, the spatial components of a 3D shape, i.e. velocity, position and geometry, are updated at discrete time-steps $t_i \in \mathbb{T}$, where $\mathbb{T} \subseteq \mathbb{R}^{\geqslant 0}$ denotes the time domain. The maximum amount of time Δ between two consecutive time steps is called *movement time step* and is such that $t_i \leqslant t_{i+1} \leqslant t_i + \Delta$. The occurrence of a collision or a split event makes necessary to update the velocities of all the shapes in the system, even before that the full movement time step Δ has passed.

At this level, the calculus has to rely on collision detection algorithms for computing the first time of contact between any two shapes. This remarks the close integration that needs to be achieved between formal aspects and simulation algorithms in spatial process algebras.

BEHAVIOUR The internal *behaviour* of a 3D process supports *bind* actions, with which processes can bind together forming a compound new process; and *split* actions for breaking bonds. The binding between 3D processes is modelled in a similar way to CCS communication on complementary channels; in the Shape Calculus, channels act as binding sites and are of the form $\langle \alpha, X\rangle$, where α is a channel name, and X is the active surface exposed for binding. The set of channels is denoted with $\mathcal{C}$. Binding between two processes occurs if they expose *compatible* channels. Two channels $c_1 = \langle \alpha, X\rangle, c_2 = \langle \beta, Y\rangle \in \mathcal{C}$ are said compatible (written $c_1 \sim c_2$), if they have complementary channel names: $\alpha = \overline{\beta}$; and they share a common surface of contact: $X \cap Y \neq \emptyset$.

The language supports two basic actions for splitting an established bond: Let $\langle \alpha, X\rangle$ be a channel and $L \subseteq \mathcal{C}$ be a subset of channels. We distinguish the *weak-split* action, $\omega(\alpha, X)$, a non-urgent split that can be postponed of an unspecified time (used for instance to model loose bonds); and the *strong-split*, $\rho(L)$, a urgent action that must be performed as soon as it is enabled, that is when all the involved components can release all the involved bonds by performing in turn split actions. The sets of weak-split actions and strong-split actions are denoted with $\omega(\mathcal{C}) = \{\omega(\alpha, X) | \langle \alpha, X\rangle \in \mathcal{C}\}$, and

$\rho(\mathcal{C}) = \{\rho(\alpha, X) | \langle \alpha, X \rangle \in \mathcal{C}\}$, respectively. In the following, we denote the set of behavioural terms of the calculus with $\mathbb{B}$.

3D PROCESSES AND NETWORKS The set 3DP of is composed of basic processes of the form $S[B]$, which are characterized by a behaviour $B \in \mathbb{B}$ encapsulated in a 3D shape $S \in \mathbb{S}$; and by composed processes $P_1 \langle a, X \rangle P_2$, where $P_1, P_2 \in$ 3DP, a is the name of the two compatible channels, and X is the common surface of contact.

Finally, we define a *network of 3D processes* (3D network, for short) as the parallel composition of zero or more 3D processes. Given a finite set of indexes $I = \{1, \ldots, n\}$, we can alternatively write $(\|P_i)_{i \in I}$ or $(\|P_i)_{i=1}^{n}$, with $P_i \in$ 3DP, to denote the network that consists of all P_i with $i \in I$: $P_1 \| \ldots \| P_n$. The set of 3D networks is denoted by $\mathbb{N}$. The full syntax of the calculus is presented in Table 3.

Example 3.1.1. *Figure 7 shows a possible evolution of a 3D network consisting of processes* $P_0 \stackrel{def}{=} S_0[B_0]$ *(blue shape) and* $P_1 \stackrel{def}{=} S_1[B_1]$ *(green shape). Behaviours are defined as*

$$
\begin{array}{llll}
B_0 \stackrel{def}{=} & \ldots + \langle \overline{a}, X_0 \rangle . B_0' + \ldots & B_1 \stackrel{def}{=} & \ldots + \langle a, X_1 \rangle . B_1' + \ldots \\
B_0' \stackrel{def}{=} & \ldots + \rho(\{\langle \overline{a}, X_0 \rangle\}) . B_0'' + \ldots & B_1' \stackrel{def}{=} & \ldots + \rho(\{\langle a, X_1 \rangle\}) . B_1'' + \ldots \\
B_0'' \stackrel{def}{=} & \ldots + \langle c, X_0' \rangle . \ldots + \ldots & B_1'' \stackrel{def}{=} & \ldots + \langle \overline{b}, X_1' \rangle . \ldots + \ldots
\end{array}
$$

P_0 *exposes an output channel* $\langle \overline{a}, X_0 \rangle$ *and* P_1 *has an input channel of the same type* $\langle a, X_1 \rangle$*. After some time* $t \leqslant \Delta$*, a collision occurs between* P_0 *and* P_1*, which consequently can bind on the channel* $\langle a, Y \rangle$*, where* $Y = X_0 \cap X_1 \neq \emptyset$ *is the surface of contact. The passage of an amount* t *of time is denoted by the temporal transition* $\xrightarrow{t}$*, while the execution of a bind synchronization between* P_0 *and* P_1 *on the surface* Y *by the functional transition* $\xrightarrow{\langle P_0, P_1, Y \rangle}$ *(transition semantics is covered in the next section). Note that the collision has required to break the timeline and update velocities before the full time step* Δ *has elapsed. Then, the compound process* $S_0[B_0'] \langle a, Y \rangle S_1[B_1']$ *is formed.*

At this point both P_0 *and* P_1 *can perform a split, by actions* $\rho(\{\langle a, X_0 \rangle\})$ *and* $\rho(\{\langle a, X_1 \rangle\})$*, respectively, and release all the channels involved in the bond. The strong split is fired after the full time step has passed (transition* $\xrightarrow{\Delta}$*) and, at the network level, is denoted by the functional transition* $\xrightarrow{\rho}$*. Finally,* P_0 *and* P_1 *evolve exposing the non-compatible channels* $\langle c, X_0' \rangle$ *and* $\langle \overline{b}, X_1' \rangle$*, respectively.*

$S ::=$		**3D shape** ($\mathbb{S}$-term)
	$\sigma = \langle V, m, \mathbf{p}, \mathbf{v} \rangle$	Basic shape
	$S\langle X \rangle S$	Composed shape
$B ::=$		**Behaviour** ($\mathbb{B}$-term)
	nil	Null behaviour
	$\langle \alpha, X \rangle.B$	Bind
	$\omega(\alpha, X).B$	Weak split
	$\rho(L).B$	Strong split
	$\epsilon(t).B$	Delay
	$B + B$	Choice
	K	Process name
$P ::=$		**3D process** (3DP-term)
	$S[B]$	$S \in \mathbb{S}, B \in \mathbb{B}$
	$P\langle a, X \rangle P$	Composed 3D process
$N ::=$		**3D network** ($\mathbb{N}$-term)
	nil	Empty network
	P	$P \in 3DP$
	$N \| N$	Parallel 3D processes

Table 3: Shape Calculus syntax.

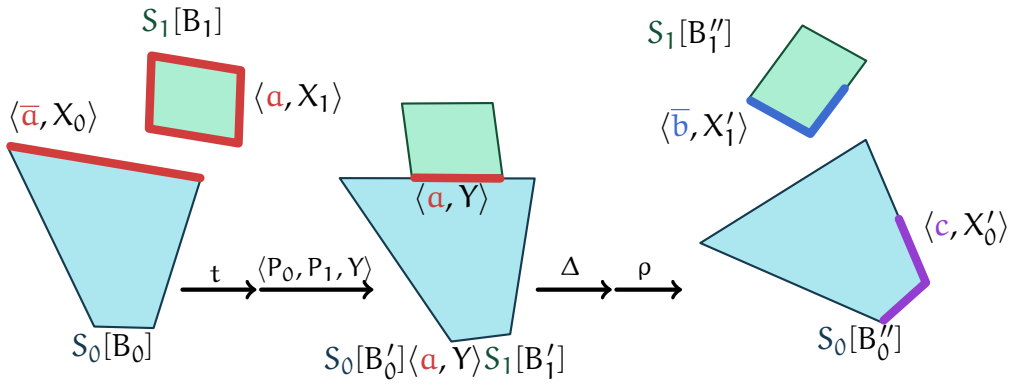

Figure 7: Evolution of 3D processes in the Shape Calculus. Processes $S_0[B_0]$ and $S_1[B_1]$ are involved in a bind on the channel $\langle a, Y \rangle$ and in a subsequent strong split.

3.1.2 Semantics

Similarly to the CCS semantics presented in Section 2.2, the semantics of the Shape Calculus is given by a set of SOS rules, listed in Table 4. The following operational rules are presented in a reduced form as in [9]. For a more comprehensive version including the semantics of split actions and collisions we refer the reader to [11] and to the technical report [10].

The evolution of Shape Calculus terms is determined by *functional* and *temporal transitions*. The former describe how processes evolve by the execution of bind and split actions; the latter describe their temporal evolution.

FUNCTIONAL TRANSITIONS Functional transitions are given by the following two relations:

- $\xrightarrow{\mu} \subseteq (\mathbb{B} \times \mathbb{B} \cup 3DP \times 3DP)$, with $\mu \in Act$; and
- $\xrightarrow{\nu} \subseteq (\mathbb{N} \times \mathbb{N})$, with $\nu \in \{\omega, \rho\}$.

where $Act = \mathcal{C} \cup \omega(\mathcal{C}) \cup \rho(\mathcal{C})$ is the set of basic actions (bind, weak-split and strong-split). For instance, a transition $B \xrightarrow{\langle \alpha, X \rangle} B'$ denotes the evolution of behavioural term B into B' after the bind action $\langle \alpha, X \rangle$; or a 3D process P evolving into P' after performing the split $\omega(\alpha, X)$ is denoted with $P \xrightarrow{\omega(\alpha,X)} P'$. ω- and ρ-labelled transitions between 3D network terms denote, respectively, a weak- and a strong-split of process bonds, seen as a unique action. We distinguish them from bind and split synchronizations, that, at the network level, are seen as internal actions.

TEMPORAL TRANSITIONS Additionally, two kinds of temporal transitions are defined:

- $\overset{t}{\rightsquigarrow} \subseteq (\mathbb{B} \times \mathbb{B} \cup 3DP \times 3DP)$, with $t \in \mathbb{T}$; $\overset{t}{\rightsquigarrow}$ is called *weak* transition, because it lets time pass even if a strong-split event is enabled.
- $\xrightarrow{t} \subseteq (\mathbb{N} \times \mathbb{N})$ with $t \in \mathbb{T}$. $\xrightarrow{t}$ restricts $\overset{t}{\rightsquigarrow}$ so that enabled strong-split events prevent the passage of time, unless all its bonds can be split simultaneously (written $P \searrow$). In other words, $P \xrightarrow{t} Q$ iff $P \overset{t}{\rightsquigarrow} Q$ and either $P \not\xrightarrow{\rho}$ or $P \searrow$.

$\mathbb{B}$-TERMS As regards the weak-temporal rules of behavioural terms, rules PREF_t and STR_t state that processes of the form $\langle \alpha, X \rangle.B$, $\omega(\alpha, X).B$ and $\rho(L).B$ can be arbitrarily delayed. Rules for non-deterministic choice (SUM_t)

$$\textsc{Nil}_t\frac{}{\mathsf{nil} \overset{t}{\rightsquigarrow} \mathsf{nil}} \qquad \textsc{Pref}_t\frac{\mu \in \mathsf{Act} \setminus \rho(\mathcal{C})}{\mu.B \overset{t}{\rightsquigarrow} \mu.B} \qquad \textsc{Sum}_t\frac{B_1 \overset{t}{\rightsquigarrow} B_1' \quad B_2 \overset{t}{\rightsquigarrow} B_2'}{B_1 + B_2 \overset{t}{\rightsquigarrow} B_1' + B_2'} \qquad \textsc{Del}_t\frac{t' \geqslant t}{\epsilon(t').B \overset{t}{\rightsquigarrow} \epsilon(t'-t).B} \qquad \textsc{Del}_{t=0}\frac{B \overset{t}{\rightsquigarrow} B'}{\epsilon(0).B \overset{t}{\rightsquigarrow} B'}$$

$$\textsc{Str}_t\frac{}{\rho(L).B \overset{t}{\rightsquigarrow} \rho(L).B} \qquad \textsc{Def}_t\frac{B \overset{t}{\rightsquigarrow} B'}{K \overset{t}{\rightsquigarrow} B'} \quad \text{if } K \overset{\text{def}}{=} B \qquad \textsc{Def}_a\frac{B \xrightarrow{\mu} B'}{K \xrightarrow{\mu} B'} \quad \text{if } K \overset{\text{def}}{=} B$$

$$\textsc{Pref}_a\frac{\mu \in \mathsf{Act} \setminus \rho(\mathcal{C})}{\mu.B \xrightarrow{\mu} B} \qquad \textsc{Del}_a\frac{B \xrightarrow{\mu} B'}{\epsilon(0).B \xrightarrow{\mu} B'} \qquad \textsc{Sum}_{a1}\frac{B_1 \xrightarrow{\mu} B'}{B_1 + B_2 \xrightarrow{\mu} B'} \qquad \textsc{Sum}_{a2}\frac{B_2 \xrightarrow{\mu} B'}{B_1 + B_2 \xrightarrow{\mu} B'}$$

$$\textsc{Str}_{a1}\frac{L = \{\langle \alpha, X\rangle\}}{\rho(L).B \xrightarrow{\rho(\alpha,X)} B} \qquad \textsc{Str}_{a2}\frac{L = \{\langle \alpha, X\rangle\} \cup L' \quad L' \neq \emptyset}{\rho(L).B \xrightarrow{\rho(\alpha,X)} \rho(L').B} \qquad \textsc{Str}_{a3}\frac{B \xrightarrow{\rho(\alpha,X)} B'}{\rho(L).B \xrightarrow{\rho(\alpha,X)} \rho(L).B'}$$

$$\textsc{Basic}_t\frac{B \overset{t}{\rightsquigarrow} B'}{S[B] \overset{t}{\rightsquigarrow} (S+t)[B']} \qquad \textsc{Com}_t\frac{P \overset{t}{\rightsquigarrow} P' \quad Q \overset{t}{\rightsquigarrow} Q' \quad X' = X + (t \cdot \mathbf{v}(P))}{P\langle a, X\rangle Q \overset{t}{\rightsquigarrow} P'\langle a, X'\rangle Q'} \qquad \textsc{Basic}_c\frac{B \xrightarrow{\langle \alpha, X\rangle} B' \quad Y = \mathsf{global}(X, \mathcal{R}(S))}{S[B] \xrightarrow{\langle \alpha, Y\rangle} S[B']}$$

$$\textsc{Basic}_w\frac{B \xrightarrow{\omega(\alpha,X)} B' \quad Y = \mathsf{global}(X, \mathcal{R}(S))}{S[B] \xrightarrow{\omega(\alpha,Y)} S[B']} \qquad \textsc{Basic}_s\frac{B \xrightarrow{\rho(\alpha,X)} B' \quad Y = \mathsf{global}(X, \mathcal{R}(S))}{S[B] \xrightarrow{\rho(\alpha,Y)} S[B']} \qquad \textsc{Comp}_{a1}\frac{P \xrightarrow{\mu} P' \; \mu \in \mathsf{Act} \setminus \mathcal{C}}{P\langle a, X\rangle Q \xrightarrow{\mu} P'\langle a, X\rangle Q}$$

$$\textsc{Comp}_{a2}\frac{P \xrightarrow{\langle \alpha, Y\rangle} P' \quad Y \subseteq \mathcal{B}(P\langle a, X\rangle Q)}{P\langle a, X\rangle Q \xrightarrow{\langle \alpha, Y\rangle} P'\langle a, X\rangle Q}$$

$$\textsc{Empty}_t\frac{}{\mathsf{Nil} \xrightarrow{t} \mathsf{Nil}} \qquad \textsc{Par}_t\frac{N \xrightarrow{t} N' \quad M \xrightarrow{t} M'}{N \parallel M \xrightarrow{t} N' \parallel M'} \qquad \textsc{Par}_{a1}\frac{N \xrightarrow{\nu} N'}{N \parallel M \xrightarrow{\nu} N' \parallel M} \qquad \textsc{Par}_{a2}\frac{M \xrightarrow{\nu} M'}{N \parallel M \xrightarrow{\nu} N \parallel M'}$$

Table 4: SOS rules for the functional and temporal semantics of Shape Calculus.

and prefixing delay (DEL_t and $\text{DEL}_{t=0}$) are defined as in the semantics of Timed CCS [152]. Functional transitions between $\mathbb{B}$-terms are determined by the PREF_a rule, describing process prefixing by bind and weak split actions; DEL_a handles process terms prefixed by a 0-delay; and rules SUM_{a1} and SUM_{a2} give the classic non-deterministic choice. On the other hand, the strong-split operator needs a slightly different treatment. Rules STR_{a1} and STR_{a2} describe the evolution of a behavioural term $\rho(L).B$ after the release of one of the channels $\langle \alpha, X \rangle \in L$ involved in the strong split action. STR_{a3} is needed to handle arbitrarily nested terms, e.g. $\rho(\{\langle a, X\rangle\}).\rho(\{\langle \overline{b}, Y\rangle\}).B$.

3DP-TERMS The semantics of 3D processes is inherited from that of their internal behaviour ($\mathbb{B}$-terms). In this case, the temporal transitions take into account the shape changes due to the motion of 3D processes. Indeed in the rule BASIC_t, the 3D shape S evolves in $(S + t)$ after a time t, and in rule COM_t the surface X is updated according to the velocity of the process. The functional behaviour of basic 3D processes, i.e. those of the form $S[B]$, is described by the rules BASIC_c (bind), BASIC_w (weak-split) and BASIC_s (strong-split). In this case the observed actions are expressed w.r.t. a *global* coordinate system: $\mathsf{global}(X, \mathcal{R}(S))$ denotes the surface X being referred to the global coordinate system by the reference point $\mathcal{R}(S)$, i.e. the global position of shape S. The functional behaviour of a generic composed 3D process $P \langle a, X\rangle Q$ is given by the rules COMP_{a1} and COMP_{a2} (their symmetric equivalent have been omitted). According to rule COMP_{a2}, a bind action $\langle \alpha, Y\rangle$ enabled in P (or in Q) can fire only if the exposed surface Y is completely contained in the boundary of the composed shape $\mathcal{B}(P \langle a, X\rangle Q)$.

$\mathbb{N}$-TERMS Finally, rules EMPTY_t and PAR_t ensure that (strong) temporal transitions are executed simultaneously by all the processes P_i composing the 3D network $(\|P_i)$. Thus, if a process P_i cannot let time pass, so the 3D network it is embedded in. In fact, $P_i \not\xrightarrow{t}$ implies $(\|P_i) \not\xrightarrow{t}$. Rules PAR_{a1} and its symmetric PAR_{a2} state that a network can perform an action $\nu \in \{\omega, \rho\}$ only if one of its subcomponent can perform ν.

3.1.3 Example: RANKL/OPG Signalling in Bone Remodelling

In this part we give an idea of the semantics of the Shape Calculus through the example depicted in Fig. 8: the OPG inhibition of RANKL, also discussed in Section 2.1. Briefly explained, this example describes a reaction from a pair *(pre-osteoblast, mature osteoblast)* to a pair *(mature osteoblast, active osteoblast)*.

Consider the following 3D processes:

$$
\begin{aligned}
N &\stackrel{\text{def}}{=} \ldots \parallel Pb \parallel Ob \parallel \ldots && \text{(3D Network)}\\
Pb &\stackrel{\text{def}}{=} S_{Ob}[B_{Pb}] && \text{(Pre-osteoblast)}\\
Ob &\stackrel{\text{def}}{=} S_{Ob}[B_{OPG}] && \text{(Mature osteoblast)}\\
B_{Pb} &\stackrel{\text{def}}{=} \langle \overline{rankl}, X_1 \rangle . \rho(\overline{rankl}, X_1) . B_{OPG}\\
B_{OPG} &\stackrel{\text{def}}{=} \langle rankl, X_2 \rangle . \rho(rankl, X_2) . B_{Ob}
\end{aligned}
$$

where B_{Ob} is left unspecified and models the behaviour of an active osteoblast which forms new bone; and S_{Ob} denotes the generic shape of an osteoblast. Note that processes Pb and Ob can be in different positions and have different velocities, so technically we should have specialized S_{Ob} in two different shapes. For the sake of simplicity, we uniquely refer to S_{Ob}. In addition, when a strong split involves a single channel as in the above example, we simplify the notation by writing $\rho(rankl, X_2)$ instead of $\rho(\{rankl, X_2\})$.

Pb expresses RANKL by exposing the output channel $\langle \overline{rankl}, X_1 \rangle$; Ob expresses the decoy receptor OPG, here implemented as the input channel $\langle rankl, X_2 \rangle$. We assume that $X_1 = \mathcal{B}(Pb)$ and $X_2 = \mathcal{B}(Ob)$, meaning that the exposed surface X_1 and X_2 corresponds to the whole surface of Pb and Ob, respectively. If X_1 and X_2 come into contact, i.e. $X_1 \cap X_2 \neq \emptyset$, the channels $\langle \overline{rankl}, X_1 \rangle$ and $\langle rankl, X_2 \rangle$ will become compatible. Consequently, the two processes bind together mimicking the RANKL/OPG binding, and the resulting compound process is

$$S_{Ob}[\rho(\overline{rankl}, X_1) . B_{OPG}] \langle rankl, Y \rangle S_{Ob}[\rho(rankl, X_2) . B_{Ob}], \quad Y = X_1 \cap X_2$$

At this point, both processes can perform a split on the established bond, written $Pb \xrightarrow{\rho(\overline{rankl}, X_1)}$ and $Ob \xrightarrow{\rho(rankl, X_2)}$. Finally, when the split is fired, the resulting 3D network will be $\ldots \parallel S_{Ob}[B_{OPG}] \parallel S_{Ob}[B_{Ob}] \parallel \ldots$.

3.2 A MINIMAL SHAPE CALCULUS EXTENSION

The price to pay for the richness and the expressiveness of the Shape Calculus is the need for a large amount of spatial parameters, that are both difficult to retrieve and often too detailed for the biological system under study.

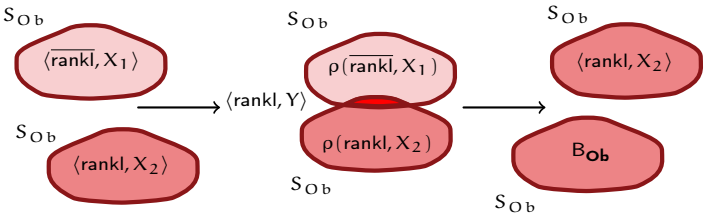

$$S_{Ob}[\langle\overline{\text{rankl}}, X_1\rangle.\rho(\overline{\text{rankl}}, X_1).B_{OPG}] \quad \| \quad S_{Ob}[\langle\text{rankl}, X_2\rangle.\rho(\text{rankl}, X_2).B_{Ob}]$$
$$\downarrow^{\langle Pb,Ob,Y\rangle}$$
$$S_{Ob}[\rho(\overline{\text{rankl}}, X_1).B_{OPG}]\langle\text{rankl}, Y\rangle S_{Ob}[\rho(\text{rankl}, X_2).B_{Ob}]$$
$$\downarrow^{\rho}$$
$$S_{Ob}[B_{OPG}] \quad \| \quad S_{Ob}[B_{Ob}]$$

Figure 8: RANKL/OPG signalling in the Shape Calculus. The pre-osteoblast expresses RANKL ($\langle\overline{\text{rankl}}, X_1\rangle$) and the mature osteoblast expresses OPG ($\langle\text{rankl}, X_2\rangle$). By binding and splitting on $\langle\text{rankl}, \cdot\rangle$, the mature osteoblast inhibits the pre-osteoclast which subsequently starts producing OPG as well. The example models a reaction *(pre-osteoblast, mature osteoblast)* $\rightarrow$ *(mature osteoblast, active osteoblast)*.

Such a richness combined with the high genericity of the calculus (e.g. geometrical space, timed behaviours, freedom in defining motion laws and non-determinism) typically lead to infinite transition system models, that therefore need to be abstracted like in [34], in order to perform any kind of formal analysis. Moreover, restrictions to the original syntax were necessary in [35] for using the Shape Calculus as an input language for concrete 3D simulations.

Rather, in this section we present a minimal extension to the calculus that introduces three new behavioural terms and improves its biological expressiveness. In the remainder of the chapter, we will refer to this extended version as ESC (extended Shape Calculus). The syntax of ESC (Table 5) includes additional terms for expressing repeating behaviours (*Iteration*), removal of a 3D shape (*Thanatos*), and time-bounded behaviours (*Duration*).

BEHAVIOURAL TERMS The term $(B)^k$ (*iteration*) is a syntactical construct for expressing behaviours repeating for a finite ($k \in \mathbb{N}$) or infinite ($k = \infty$) number of iterations.

The behavioural term Θ removes a 3D shape (*thanatos*) from the network. The introduction of Θ resolves a crucial issue in the original Shape Calculus language: the inability to remove or destroy shapes within a 3D network, a desirable features for a bio-modeller to model basic processes like cell death. Indeed, even when the behaviour B of a 3D process $S[B]$ reaches the termi-

nation state nil, the associated shape S would keep existing, moving and (elastically) colliding. By performing a Θ before the behaviour termination (e.g. $B \stackrel{\text{def}}{=} B_1.\Theta.B_2,\ B_2 \neq \text{nil}$), we ensure that the associated 3D shape will not affect the other processes that are concurrently executing.

$B ::=$	nil	Null behaviour
	$\langle \alpha, X \rangle.B$	Bind
	$\omega(\alpha, X).B$	Weak split
	$\rho(L).B$	Strong split
	$\epsilon(t).B$	Delay
	$B + B$	Choice
	K	Process name
	$(B)^k.B$	Iteration
	$\Theta.B$	Thanatos
	$\delta(t, B).B$	Duration

Table 5: Syntax of behavioural terms in ESC. Highlighted terms constitute the behaviours added to the original Shape Calculus language.

Finally, $\delta(t, B)$ (*duration*) allows us to express time-bounded behaviours, for instance an osteoblast that continuously mineralizes bone until its life time has passed. Intuitively, while $t > 0$, the $\delta(t, B)$ behaves as B; once $t = 0$, $\delta(t, B)$ corresponds to nil.

SEMANTICS From the semantics side, Θ is treated as a basic action, and therefore labels functional transitions between $\mathbb{B}$-terms and between 3DP-terms. Table 6 shows the additional SOS rules in ESC. Rules DELTA_t and $\text{DELTA}_{t=0}$ define the temporal semantics of the duration operator $\delta(t, B)$ when $t > 0$ and when $t = 0$, respectively. $\delta(t, B)$ imposes a limit t on the duration of behaviour B, which consequently can let time pass. The functional behaviour of $\delta(t, B)$ is regulated by rules DELTA_{a1} and DELTA_{a2}: B can perform any enabled action if $t > 0$, while $\delta(0, B)$ behaves like a 0-delay $\epsilon(0)$. Finally, rule THETA_a describes the semantics of the thanatos operator. Given a 3D shape $S = \langle V, m, \mathbf{p}, \mathbf{v} \rangle$, a Θ-action "removes" the shape S, by replacing it with a void 3D shape $S' = \langle \{\mathbf{p}\}, 0, \mathbf{p}, \mathbf{o} \rangle$.

3.3 FROM SHAPE CALCULUS TO STOCHASTIC AGENT-BASED MODELS

In this section we present a method to simulate Shape Calculus specifications through agent-based models featuring *stochastic actions* and *perception*. As usual, the former are used to model the propensity/probability of agents' actions; the latter refers to the capability of communicating at distance and sense the neighbourhood.

$$\textsc{Delta}_t \frac{B \overset{t'}{\rightsquigarrow} B' \quad t \geqslant t'}{\delta(t, B) \overset{t'}{\rightsquigarrow} \delta(t - t', B')} \qquad \textsc{Delta}_{t=0} \frac{B' \overset{t}{\rightsquigarrow} B''}{\delta(0, B).B' \overset{t}{\rightsquigarrow} B''}$$

$$\textsc{Delta}_1 \frac{B \xrightarrow{\mu} B' \quad t > 0}{\delta(t, B) \xrightarrow{\mu} \delta(t, B')} \qquad \textsc{Delta}_2 \frac{B' \xrightarrow{\mu} B''}{\delta(0, B).B' \xrightarrow{\mu} B''}$$

$$\textsc{Theta}_a \frac{B \xrightarrow{\Theta} B' \;\; S = \langle V, m, \mathbf{p}, \mathbf{v} \rangle \;\; S' = \langle \{\mathbf{p}\}, 0, \mathbf{p}, \mathbf{o} \rangle}{S[B] \xrightarrow{\Theta} S'[B']}$$

Table 6: Semantics of additional terms in ESC.

Biochemical and cellular processes are indeed intrinsically stochastic, and thus spatial cellular and multicellular models need to take into account stochasticity and uncertainty in order to reproduce and explain the behaviour of such systems. For instance in the bone remodelling process, important sources of variability are related to the time and space organization of the BMU. This prominently affects the number of cells involved in the process and in turn, bone density and micro-structure. Variability at the tissue level cyclically involves the cellular-level responses to mechanical stresses.

Further discussion on the role of randomness and stochasticity in biological models and in bone remodelling is given in Chapter 4 and particularly in Section 4.2, where a stochastic model for bone remodelling is presented and probabilistic verification techniques are employed to detect bone pathologies. Details on the formal translation of Shape Calculus models into agent code can be found in Section B.2 of the appendix.

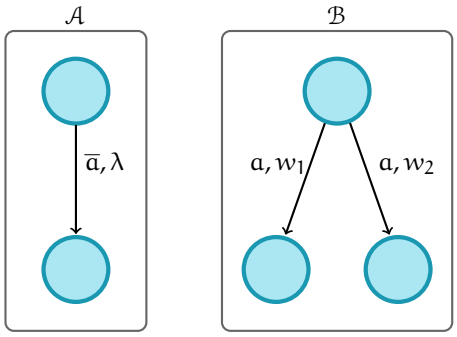

Figure 9: Stochastic agents synchronizing on compatible channels with rate λ and probability w_i.

STOCHASTICITY We follow the so-called *rated output/passive input approach* [78], where agent actions are equipped with *stochastic rates* and *weights*. In particular, *output actions* are annotated with a rate $\lambda \in \mathbb{R}^+$, while *input actions* have associated a weight $w \in \mathbb{N}^+$, representing the probability that the specific input is selected when a compatible output action is fired.

Consider the system in Figure 9, where two agents $\mathcal{A}$ and $\mathcal{B}$ are illustrated. Agent $\mathcal{A}$ can perform an output action $\overline{a}$ with rate λ; while $\mathcal{B}$ can perform the input actions (a, w_1) and (a, w_2). The relative selection probability of action (a, w_i) in agent $\mathcal{B}$, called $p(\mathcal{B}, (a, w_i))$, is calculated as the ratio between w_i and the total weight of a, that is the sum of the weights of all the enabled a-actions in $\mathcal{B}$:

$$p(\mathcal{B}, (a, w_i)) = \begin{cases} 0, & \text{if } \sum_{\mathcal{B} \xrightarrow{a, w_j}} w_j = 0 \\ \dfrac{w_i}{\sum_{\mathcal{B} \xrightarrow{a, w_j}} w_j}, & \text{otherwise} \end{cases}$$

Then, the *synchronization rate* between the actions (a, w_i) and $(\overline{a}, \lambda)$ is given by $\lambda \cdot p(a, \omega_i)$.

PERCEPTION In the Shape Calculus binding between two 3D processes can exclusively occur when they share a common surface of contact. The clear limitation is that, such an encounter based on collision is practically hard to achieve during a simulation, even if the corresponding binding has associated a high propensity.

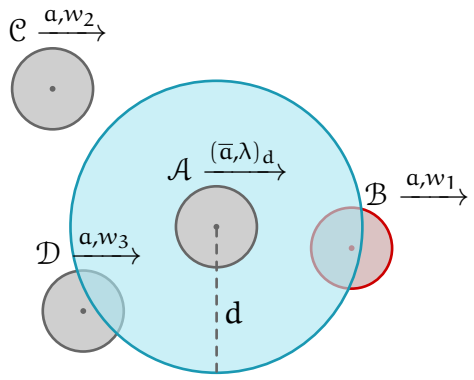

Figure 10: Stochastic agents exposing binding capabilities. The perception radius of $\mathcal{A}$ constraints its interactions with neighbour agents.

To overcome the problem of highly probable actions that are never fired due to even infinitesimal spatial discrepancies, we allow compatible agents to "bind at distance", according to a given perception radius.

More precisely, output bind actions are annotated with a parameter $d \in \mathbb{R}^+$ called *sensibility distance*, meaning that if an agent $\mathcal{A}$ can perform an action $(\overline{a}, \lambda)_d$, it can bind with any agent $\mathcal{B}$ which can perform a compatible action (a, w) and which is distant from $\mathcal{A}$ at most d. Figure 10 depicts a situation where an agent $\mathcal{A}$ is able to execute an output bind action $(\overline{a}, \lambda)_d$. Even if agents $\mathcal{C}$ and $\mathcal{D}$ expose complementary channels, they are out of the perception radius of $\mathcal{A}$, which can consequently bind only with agent $\mathcal{B}$. The actual distance between two agents affects their synchronization rate, as expected, since longer distances should lead to longer action durations and

consequently to lower rates. Therefore, we define the *binding rate* β between two bind actions $(\alpha, \lambda)_d$ and (a, w) exposed by agents $\mathcal{A}$ and $\mathcal{B}$ respectively, by:

$$\beta((\mathcal{A}, (\alpha, \lambda)_d), (\mathcal{B}, (a, w))) = \begin{cases} \dfrac{\lambda \cdot p(a, w)}{d(\mathcal{A}, \mathcal{B})} & \text{if } \alpha = \overline{a} \text{ and } d(\mathcal{A}, \mathcal{B}) \leqslant d \\ 0 & \text{otherwise} \end{cases}$$

where $d(\mathcal{A}, \mathcal{B})$ is the distance between $\mathcal{A}$ and $\mathcal{B}$.

3.3.1 Repast Simphony

The simulator is based on the *Repast Symphony Suite* [113], an agent-based modelling and simulation (ABMS) toolkit implemented in Java [1].

Repast models are based on the concept of *context*, which is a structured container serving as the agents' environment. A context may include one or more *projections*, that represent the spatial domains where agents are located (for example, continuous and discrete spaces). A projection in turn can have associated *value layers*, i.e. spatial data structures holding a numerical value for each position, and that can be accessed by agents. Simulations in Repast are based on a *discrete-event* execution model, where time proceeds by discrete steps, called *ticks* and actions are scheduled for the execution at a specific tick.

COMPUTATION MODEL Repast implements the discrete-event computation model through a scheduler holding a list of pending actions as $(\mathtt{action}, \mathtt{tick})$ couples. At each tick t all the actions (a, t) are executed. This execution model adapts well to the simulation algorithm defined for the Shape Calculus, where the time-line is divided in time-steps of duration (at most) Δt. After each Δt, the velocities and the positions of all the shapes are updated, according to their particular motion law. However in the stochastic settings we must consider actions with exponentially distributed durations that are determined by the rate of the action itself. Moreover the race condition applies so that shorter actions should be executed earlier.

The procedure implemented for scheduling stochastic actions over a discrete - event scheduler is shown in Section B.1 of the Appendix. The basic idea behind the algorithm is to keep the list of enabled actions and associated duration for each agent, at each time step. The duration can be de-

1 A prototype version is available at http://www.nicolapaoletti.com/files/research/models/Repast_BR.zip

terministic, for actions like the Shape Calculus delay operator, or custom actions fired by bone cell agents to form or consume the bone; or it can be random in the case of synchronization between stochastic actions. In the latter case, a random duration is picked from an exponential distribution with rate equals to the binding rate of the synchronization. Finally, actions with duration $d \leqslant \Delta t$ are scheduled for the execution; the remaining ones are postponed to the next tick.

3.4 BONE REMODELLING MODEL

In this section a novel model of bone remodelling is presented, where spatial features are captured at a more abstract level by a formal Shape Calculus specification (ESC extension presented in 3.2), which is instantiated into a agent-based stochastic simulation environment following the method explained in Section 3.3.

3.4.1 ESC Specification

The choice of the Shape Calculus as a specification language for biomodels and in particular, for bone remodelling has several advantages, among which its ability to *express multiple scales in a compositional way*: a BMU is defined in terms of a network of bone cells, and the bone tissue in terms of a network of BMUs. Moreover, the specification follows the paradigm of *processes as cells* and *channels as molecular signals*. As a matter of fact, cells communicate with each other via direct contact (or over short distances). Similarly in the Shape Calculus, 3D processes communicate by binding on a common surface of contact. Furthermore RANK, RANKL and OPG are surface-bound proteins and consequently can be accurately described by Shape Calculus channels of the form $\langle a, X \rangle$, where X is a portion of the surface of the associated process.

Table 7 reports the ESC specification of the bone remodelling model and quantitative parameters of the model are summarized in Table 8. In this case, we do not define particular binding surfaces for the channels exposed by the 3D processes, but we assume that their whole surface is available for binding for two main reasons. Firstly, there is no clear experimental evidence of the positioning of the RANK and RANKL molecules (implemented as Shape Calculus channels) at the cell surface. Secondly, the definition of a precise geometry for molecular channels would have restricted the binding capabilities of the bone cells, without any biological motivation. Let $\mathcal{B}(S)$

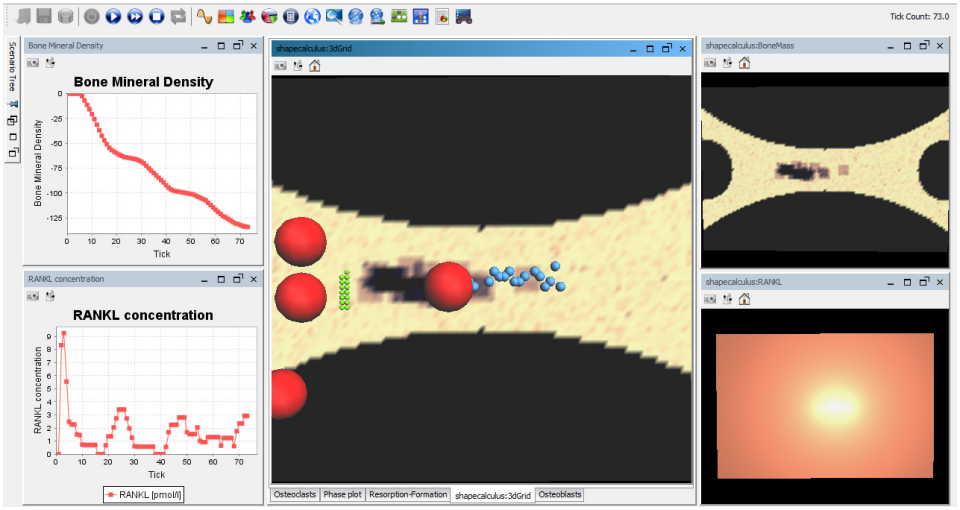

Figure 11: Screenshot of the agent-based simulator for bone remodelling. In the center panel, the location of bone cells (blue, osteocytes; green, osteoblasts; red, osteoclasts) in the BMU. On the left side, bone density and RANKL concentration plots. On the right side, bone micro-structure and RANKL diffusion (bright zones, high concentration).

be the boundaries of shape S. For the sake of succinctness, in the model we denote the channel $\langle \alpha, \mathcal{B}(S) \rangle$ with $\langle \alpha, X \rangle$.

In addition there are two particular actions not encoded as behavioural terms, **resorb** and **form**. They are timed action responsible for, respectively, decreasing and increasing the density of the part of bone which the osteoclast (osteoblast) is attached to, according to determined resorption (formation) rates. These two terms have been left unimplemented at this level in order to avoid unnecessary and inaccurate modelling artifacts. Indeed it would have been inopportune to express the bone mass as a 3D process and moreover, the activities of resorption and formation cannot be properly described by a binding operation.

3.4.2 Repast Implementation

Figure 11 shows a screenshot taken during a simulation of the bone remodelling model in Repast. The simulator allows visualizing at runtime the location of bone cells in the BMU, the bone density and micro-structure, and the spatial diffusion of RANKL. Furthermore it supports several runtime plots including bone mineral density, resorption and formation activities, RANKL concentration and number of active/total bone cells.

Tissue, BMU	Tissue	$\stackrel{\text{def}}{=}$	$(\|\mathit{ABMU}_i)_{i=1}^{a} \parallel (\|\mathit{QBMU}_j)_{j=1}^{q}$
	ABMU	$\stackrel{\text{def}}{=}$	$(\|Oy_i)_{i=1}^{n_{Oy}} \parallel (\|Oc_j)_{j=1}^{n_{Oc}} \parallel (\|Ob_k)_{k=1}^{n_{Ob}}$
	QBMU	$\stackrel{\text{def}}{=}$	$(\|Oy_i)_{i=1}^{n_{Oy}}$

Bone tissue is structured in a active BMUs (ABMU) participating in the remodelling process, and in q quiescent BMUs (QBMU). Each active BMU is in turn composed by n_{Oy} osteocytes, n_{Oc} osteoclasts and n_{Ob} osteoblasts. An inactive BMU is modelled as a network of only osteocytes.

Osteocyte	Oy	$\stackrel{\text{def}}{=}$	$S_{Oy}[(\langle can, X\rangle + \langle \overline{can}, X\rangle)^{k_{Oy}} + \langle \overline{oySig}, X\rangle.\Theta]$

An osteocyte can bind with other k_{Oy} osteocytes through the channel $\langle can, \cdot\rangle$ and form the network of canaliculi. Alternatively, if they are not near enough to communicate and bind with each other, e.g. osteocytes near the bone surface, they expose the channel $\langle \overline{oySig}, \cdot\rangle$ modelling the osteocytes' signalling that will activate the resorption phase and the remodelling process. After having performed a bind on $\langle oySig, \cdot\rangle$, the osteocyte dies since it has been consumed by the attached osteoclast.

Osteoclast	Oc	$\stackrel{\text{def}}{=}$	$S_{Oc}[B_{Oc}]$
	B_{Oc}	$\stackrel{\text{def}}{=}$	$\delta(t_{Oc}, B_{AOc}).\Theta.\langle \overline{deathF}, X\rangle^{k_{Oc}}$
	B_{AOc}	$\stackrel{\text{def}}{=}$	$(\langle oySig, X\rangle + \langle rankl, X\rangle.\rho(rankl, X)).\textbf{resorb}$

During its lifetime t_{Oc}, an osteoclast behaves as an active osteoclast (B_{AOc}): it continuously absorbs bone, induced by osteocytes' signalling (channel $\langle oySig, \cdot\rangle$) or by RANKL (channel $\langle rankl, \cdot\rangle$). Before dying, it releases death factors that will attract osteoblasts to the consumed part of bone, thus triggering the formation phase. In particular, a single "dead" osteoclast can bind with $k_{Oc} = \lfloor n_{Ob}/n_{Oc} \rfloor$ osteoblasts, so fitting the ratio between active osteoclasts and active osteoblasts.

Osteoblast	Ob	$\stackrel{\text{def}}{=}$	$S_{Ob}[\langle \overline{rankl}, X\rangle.\rho(\overline{rankl}, X).B_{OPG} + \epsilon(t_{Pb}).B_{OPG}]$
	B_{OPG}	$\stackrel{\text{def}}{=}$	$\langle rankl, X\rangle.\rho(rankl, X).B_{Ob} + B_{Ob}$
	B_{Ob}	$\stackrel{\text{def}}{=}$	$\delta(t_{Ob}, \langle deathF, X\rangle.\textbf{form}).\Theta$

An osteoblast initially behaves as a non differentiated cell: it produces RANKL, by exposing channel $\langle \overline{rankl}, \cdot\rangle$. After the effect of OPG-inhibition or after its differentiation time t_{Pb} has elapsed, it starts behaving as a mature osteoblast which produces OPG. In particular, a mature osteoblast can inhibit a single precursor, by binding on the channel $\langle rankl, \cdot\rangle$ (standing for the OPG decoy receptor) (Fig. 8). Then, the formation phase lasts a time t_{Ob}, after which the cell undergoes apoptosis.

Table 7: ESC specification and biological description of bone remodelling.

Param	Value	Description
n_{Oc}	20 [86, 135]	Expected number of Oc
n_{Ob}	2000 [86, 135]	Expected number of Ob
t_{Oc}	10 d [135]	Oc lifetime
t_{Ob}	15 d [135]	Mature Ob lifetime
t_{Pb}	5 d [135]	Ob differentiation time
$size_{BMU}$	$2.4\times1.6\times0.01$ mm^3 [135]	Size of the BMU
Δt	1 d	Time step
k_{Oc}	2.5 d^{-1}	Resorption rate
k_{Ob}	0.25 d^{-1}	Formation rate
k_{RANKL}	$\in [1, 2]$	RANKL factor
k_{ageing}	$\in [1, 2]$	Ageing factor
d_{Oc-Oy}	0.06 mm	Oc perception radius to Oy
d_{Pb-Oc}	0.01 mm	Pb perception to Oc death factor
d_{Ob-Pb}	0.01 mm	Ob/OPG perception to Pb/RANKL
D_{Oc}	10^{-2} mm^2 d^{-1}	Oc diffusion coefficent
D_{Ob}	2.15×10^{-2} mm^{2}d^{-1}	Ob diffusion coefficent

Table 8: Parameters of the agent-based bone remodelling model. Size of the BMU, lifetime and expected concentration of bone cells have been taken from literature. Other parameters have been estimated from the model.

TIME-STEP. Given that a single remodelling cycle lasts about one year and the resorption and formation processes can take months, in this model Δt is set to 1 d.

PROJECTIONS. We represent the spatial domain of the BMU through a discrete space. Space is approximated in two dimensions, and has a size of $240 \times 160 \times 10^{-4}$ mm^2 such that each cell in the grid models a portion of size 0.01×0.01 mm^2. According to the parameter $size_{BMU}$ in Table 8, we can ignore the depth of the BMU (0.01 mm) which is much smaller than its width (2.4 mm) and its height (1.6 mm).

BONE TISSUE. It is modelled as a Repast value layer, that is a real-valued matrix $Bone$. The value of a cell $Bone_{ij}$ represents the percentage of bone density at the position (i, j) of the BMU grid, and varies from 0 (void) to

100 (fully mineralized). The simulator supports both cortical and trabecular bone.

MOLECULAR SIGNALS. While at the specification level molecular signals like RANKL are modelled as communication channels, at the implementation level exposed output channels are assumed to release an amount of molecules diffusing in the space. The spatial concentration of molecules is updated at each Δt according to a *diffusion Cellular Automata* update rule [156], which corresponds to a discretization of the diffusion partial differential equation. The model considers: the RANKL signalling that affects osteoclasts' motion, in a way that osteoclasts are directed towards higher RANKL concentrations (*positive chemotaxis*); and the death factors produced by osteoclasts that attract osteoblasts towards the portions of bone previously absorbed.

CELL MOTION. In the absence of attraction factors, an agent moves according to a random walk. At time t its position $\mathbf{p}(t)$ is updated by the following law (adapted from [56]):

$$\mathbf{p}(t + \Delta t) = \mathbf{p}(t) + \xi\sqrt{2 \cdot D \cdot \Delta t}$$

where ξ is a uniformly distributed random vector ranging in $[-1, 1]$, and D is the diffusion coefficient of the agent.

In the case that a cell is also affected by attraction factors, like in the case of osteoclasts attracted by RANKL, its motion is determined by a *biased random walk*, i.e. a random walk altered by the concentration gradient of an attractant molecule u, and given by the law:

$$\mathbf{p}(t + \Delta t) = \mathbf{p}(t) + \xi_{\pm}\sqrt{2 \cdot D \cdot \Delta t}$$

Here the vector $\xi_{\pm}$ models the "molecular bias" and takes into account the concentration gradient of u. Let $\lceil \mathbf{p}(t) \rceil = (x, y) \in \mathbb{Z}^2$ be the corresponding position in the discrete space of the agent at time t, and $u(t, x, y)$ be the concentration of u at time t and at position (x, y).

We denote with $M(x, y)$ the *Moore neighbourhood* of (x, y), i.e. the eight discrete points surrounding (x, y) (here included)[2], as shown in Figure 12.

2 Technically, the Moore neighbourhood of a central point does not include the point itself.

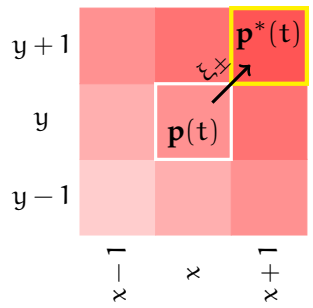

Figure 12: Molecular bias and random walk. The movement is directed to the neighbour with the highest concentration.

Let $u^*(t,x,y) = \max_{(x',y')\in M(x,y)} u(t,x',y')$ be the maximum concentration of u in the neighbourhood of (x,y) and $\mathbf{p}^*(t) = (x^*,y^*)$ be the position at which u is maximum, i.e. $u(t,x^*,y^*) = u^*(t,x,y)$. The bias $\xi_{\pm}$ is calculated as:

$$\xi_{\pm} = U[0,1]\,(\mathbf{p}^*(t) - \mathbf{p}(t))\,\frac{1+u^*(t,x,y)}{1+u(t,x,y)}$$

where $U[0,1]$ is a uniformly distributed random value between 0 and 1.

In other words, the bias $\xi_{\pm}$ is directed towards the neighbour with the highest RANKL molecular concentration, and its intensity is a random value weighted by the ratio between the target concentration and the current one.

OSTEOCYTES. We assume that osteocytes produce RANKL, since osteocytes' signalling has the effect of attracting osteoclasts to the source of the signal, similarly to RANKL signalling by pre-osteoblasts. Osteocytes' initial positioning in the bone matrix is not pre-determined, and the outcome of different shapes for osteocytes' positioning is discussed in Section 3.5.2.

OSTEOCLASTS. In normal conditions, the number of osteoclasts in the BMU is subject to little variations from the average $n_{Oc} = 20$. Higher perceived densities of RANKL in the environment, which are caused by an inflammation or a signalling defect, lead to a higher production of osteoclasts. Their motion law is a biased random walk affected by the RANKL concentration gradient, with a diffusion coefficient $D_{Oc} = 10^{-2}mm^2d^{-1}$. The expected lifetime t_{Oc} is 10 days, but they can undergo apoptosis before t_{Oc} if a high concentration of osteoblasts is detected in the neighbourhood. Once reached the portion of bone to consume, an osteoclast reduces the percentage density in that part of bone by $k_{Oc} = 2.5$ per day.

OSTEOBLASTS. The number of osteoblasts in the system varies randomly around the average $n_{Ob} = 2000$. They move according to a biased random

walk affected by the osteoclasts' death factors, with a diffusion coefficient $D_{Ob} = 2.15 \times 10^{-2} mm^2 d^{-1}$. Moreover, osteoblast precursors emit RANKL which contributes to osteoclasts' production and stimulation. Mature osteoblasts inhibits RANKL signalling by binding with the OPG channel. The lifetime of an osteoblast is about 20 days: 5 days as a precursor, 15 days as a mature cell active in the formation process. When active, it increases the bone density of a factor $k_{Ob} = 0.25$ per day. It can die before its lifetime has passed, if the number of active osteoclasts in the system is higher than expected.

3.5 ANALYSIS AND SIMULATION

We analyse how even small variations in RANKL signalling lead to defective remodelling dynamics and in turn to disease conditions, especially when ageing factors are involved.

In order to describe these aspects, we introduce two parameters, k_{RANKL} and k_{ageing}, modelling respectively the RANKL production rate; and the ageing factor defined in terms of a reduced cellular activity. By varying such parameters, we obtain two parameter configurations:

CONTROL CONFIGURATION: where RANKL production and cellular activity is normal ($k_{RANKL} = 1$, $k_{ageing} = 1$);

OSTEOPOROTIC CONFIGURATION , with an overproduction of RANKL and a reduced cellular activity ($k_{RANKL} = 2$, $k_{ageing} = 2$).

When running the osteoporotic configuration, the higher production of RANKL leads to a higher number of recruited osteoclasts, hence to a higher resorption activity. On the other hand, osteoblasts are not effective enough to completely repair the consumed bone, due to the ageing factor responsible for a lower and less effective cellular activity. This causes a decreased total bone density, weaker trabeculae and consequently more frequent and more consistent micro-fractures in osteoporotic patients.

It is worth noting that in absence of ageing factors, like in a young patient, an overproduction of RANKL does not lead normally to negative remodelling and bone diseases. Indeed, an unexpected high absorbing activity can be successfully balanced by recruiting a higher number of osteoblasts, which would not be possible in an old patient characterized by a lower cellular activity. Conversely, if we consider an old patient with a regular RANKL signalling, less effective osteoclasts are balanced by less effective osteoblasts and we do not observe relevant negative remodelling phenomena.

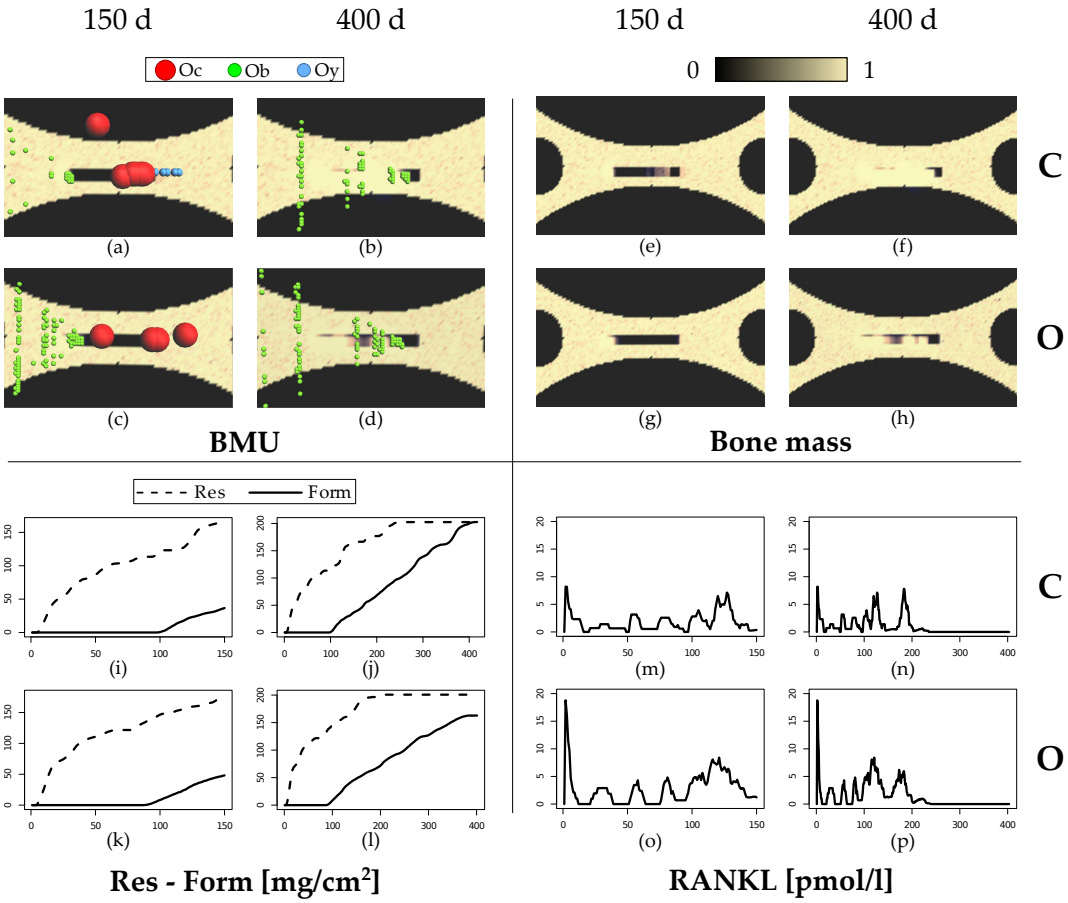

Figure 13: Simulation of control (C) and osteoporotic (O) configurations. (a)-(d) and (e)-(h) show the position of bone cells in the BMU and the density of the trabecula, resp. Graphs in (i)-(l) display the cumulative values of bone resorption and formation. RANKL concentration is plotted in (m)-(p).

Figure 13 groups the key snapshots taken during a simulation of one trabecular remodelling cycle, comparing the control and the osteoporotic configurations. We evaluate the location of bone cells in the BMU, the bone micro-structure, resorption and formation activities, and the RANKL concentration at the following time points:

$t = 150$: the first osteoblasts (green spheres) are being recruited and osteoclasts (red spheres) have almost concluded the resorption phase. Osteoblasts starts to fill the cavities excavated by osteoclasts, following them in a highly coordinated manner. At this stage, osteocytes (blue spheres) have been absorbed almost entirely. While there are no significant differences in the bone mass, we observe that RANKL con-

centration is higher in the osteoporotic case, as expected. This causes a faster resorption, leading in turn to a faster overall remodelling activity, evidenced by the fact that osteoblasts are recruited earlier than in the control scenario.

$t = 400$: the remodelling cycle is almost ended. Differences in the bone density are quite prominent between the two configurations: in the control patient, the cavities have almost been repaired (Fig. 13 (f)); while in the osteoporotic case, there are several holes left in the trabecular structure (Figure 13 (h)), due to the reduced osteoblastic activity. This can be observed also in the cumulative plots of bone resorption and formation in Fig. 13 (j),(l). In healthy conditions, formation (solid line) compensate resorption (dashed line), while in the osteoporotic case formation does not counterbalance resorption, even if the resorption activity is not greater than in the control case. This corresponds to a negative remodelling of about 50 mg/cm^2 which might appear a minor disruption, but we remark that the effects are amplified after a number of negative remodelling cycles. In addition, we notice a lower RANKL concentration in the second half of the remodelling cycle, due to the fact that signalling osteocytes have been completely absorbed and RANKL-producing pre-osteoblasts have matured into bone-forming osteoblasts.

Figure 14 compares the bone mineral density in the control and in the osteoporotic case, averaged over forty simulations of a single remodelling cycle for each configuration. Initial density values are taken from population-wide statistical data [101] and are given by the hip density of a Caucasian woman aged 25 (a more detailed explanation of how statistical data is incorporated into the model is given in Section 3.5.1).

In normal conditions we observe that at the end of remodelling the initial bone density is re-established (bone homeostasis), and that variations from the mean density are limited. By running the osteoporotic parameters, the minimal values of mean BMD are reached during resorption, and the final density is lower than the initial one (negative remodelling), since the osteoblastic activity is not effective enough to counterbalance resorption. In addition, the pathological case is characterized by a higher standard deviation. However the sum of the mean density and its standard deviation at the end of remodelling is still below the optimal density. Assuming normally distributed simulation outcomes, this implies that in more than the 68.2% of cases the outcome of bone remodelling will be negative in the osteoporotic configuration.

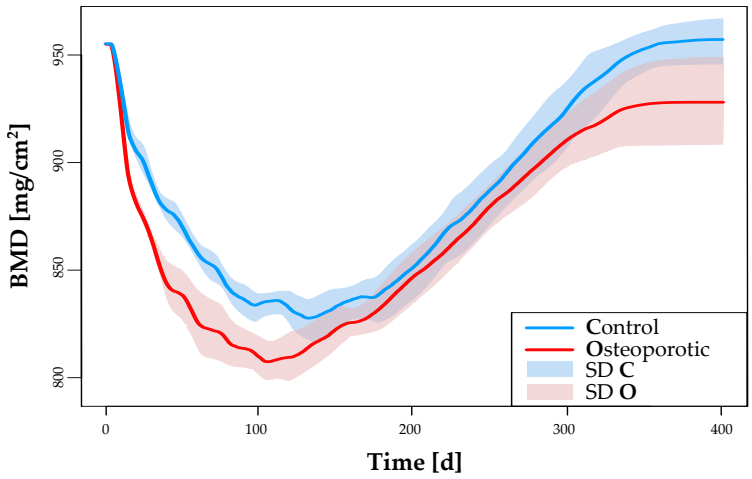

Figure 14: Simulated BMD dynamics along one remodelling cycle. Plots are obtained after 40 simulations. Continuous curves represent the mean density. Filled areas span the interval *mean* ± *standard deviation*.

3.5.1 Validation with Statistical Data

Sources of biomedical data on bone remodelling and bone-related diseases include aggregated statistics of clinical values (typically, bone density measurements) or, as reported in Appendix D for the case study of osteomyelitis, gene expression data of control patients and of patients affected by a specific bone disease.

Here we validate the outputs of the agent-based model against population wide survey data. In particular we refer to the *National Health and Nutrition Examination Survey* (*NHANES III*, 1988-94) [101], a survey conducted to assess the health and nutritional status of adults and children in the United States. Hip density values are taken from [116].

Bone Mineral Density (BMD) is an indicator of the quality of the bone and it is measured with clinical techniques, the most used of which is DEXA (Dual Energy Xray Absorptiometry). Based on BMD measurement and according to the patient's gender and ethnicity, it is possible to determine the presence of bone pathologies by comparing BMD measurements with statistical data and according to the following definitions [154]:

- *Osteopenia*, when the BMD is between 1 standard deviation (SD) and 2.5 SD below the mean of the young reference group (25 years old).
- *Osteoporosis*, when the BMD is 2.5 SD or more below the mean of the young reference group.

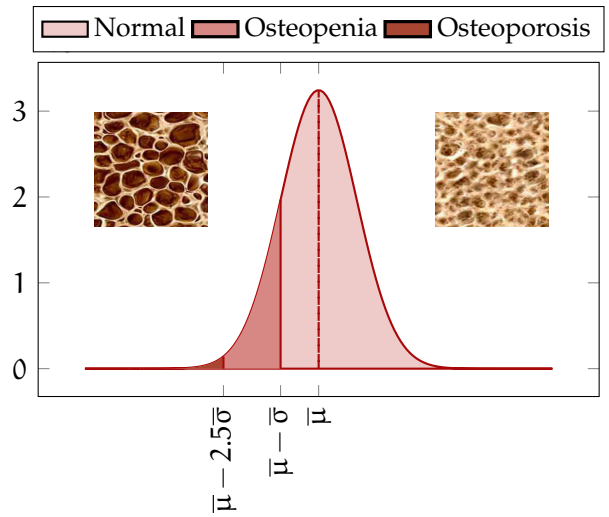

(a) Caucasian women, 25 yo. $\bar{\mu} = 955\ mg/cm^2; \bar{\sigma} = 123$.

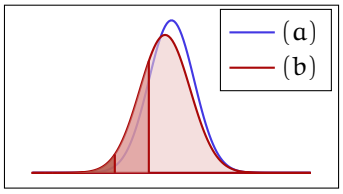

(b) Caucasian women, 45 yo. $\mu = 920\ mg/cm^2; \sigma = 136$.

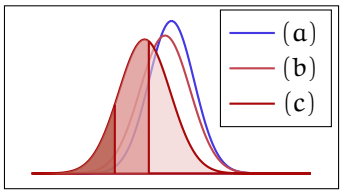

(c) Caucasian women, 65 yo. $\mu = 809\ mg/cm^2; \sigma = 140$.

Figure 15: Hip BMD distribution in Caucasian women from statistical data. a) refers to the young reference group (25 years) with mean BMD $\bar{\mu}$ and standard deviation $\bar{\sigma}$. b) and c) show the BMD distributions at 45 and 65 years, respectively.

Figure 15 shows the reference values of hip bone density for Caucasian women at 25 years a) (the young reference group); 45 years b); and 65 years c). The filled areas below the curve and the different shades of red identify patients with normal bone, osteopenia and osteoporosis. In b) and c), an increasing incidence of osteopenia and osteoporosis can be clearly observed.

By running the simulator with an initial density equal to the young reference one, we report that after a single remodelling cycle, both the control and the osteoporotic configurations give final density values within the normal density range $\bar{\mu} \pm \bar{\sigma} = 955 \pm 123$, determined by the BMD distribution of the young reference group (see Fig. 15). In particular, after 40 simulation runs the mean $\pm$ standard deviation values have been obtained at the end of a single remodelling cycle:

- **Control configuration:** $955.01 \pm 14.41 \subset \bar{\mu} \pm \bar{\sigma}$
- **Osteoporotic configuration:** $921.86 \pm 19.36 \subset \bar{\mu} \pm \bar{\sigma}$

Although in the pathological configuration we observe a lower mean density, in both cases no particular bone pathologies are diagnosed, since the values are within the normal density range. As one can expect, it is very unlikely that pathological conditions can occur after just one remodelling

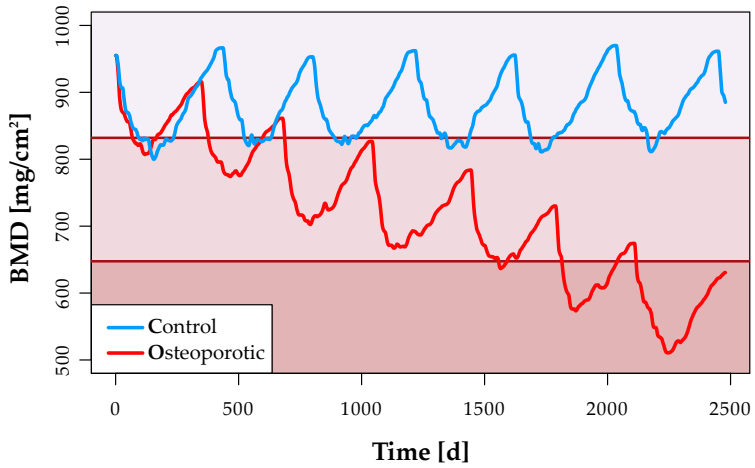

Figure 16: Changes in BMD during the simulation of seven remodelling cycles. Different shades of red determine the density ranges for normal bone, osteopenia and osteoporosis. In the control configuration (blue curve), the initial density is maintained after each remodelling cycle. In the osteoporotic configuration (red curve), bone density keeps decreasing, going below the threshold under which osteoporosis is diagnosed.

cycle (corresponding to about 400 days) and starting from an optimal bone density.

Instead, osteopenia and osteoporosis are diseases resulting after several years of negative remodelling. We experiment this scenario by running a single simulation lasting seven consecutive remodelling cycles (Figure 16), which roughly corresponds to seven years. In this case we report that when running the osteoporotic configuration, bone mineral density keeps decreasing throughout the years. At about $t = 700$ d, density reaches the range $[\bar{\mu} - 2.5\bar{\sigma}, \bar{\mu} - \bar{\sigma}]$, meaning that osteopenia would be diagnosed after less than two years. Moreover at about $t = 2100$, bone density goes below the level $\bar{\mu} - 2.5\bar{\sigma}$. Therefore running the osteoporotic configuration, osteoporosis would be diagnosed after less than six years of simulation, which is in agreement with clinical studies on the bone density of menopausal women (see e.g. [77]).

3.5.2 Osteocytes' positioning affects bone micro-structure

Here we exploit the spatial capabilities of the model to evaluate how the positioning of active (signalling) osteocytes affects in the long run the bone density and micro-structure. Keeping in mind that we model only signalling osteocytes, their initial positions are mainly determined by factors at tissue

level. Osteocytes act as mechanosensors by providing a molecular response at the cellular level to the mechanical stresses at tissue level, and they also activate along micro-fractures in the bone matrix. Considering that osteocytes are responsible for the activation of bone remodelling, this kind of analysis could explain the multiscale loop involving the following phases:

- the origination of mechanical stimuli at the tissue level, driven by the optimization of the bone micro-structure;
- the activation of a specific number of osteocytes at specific positions in the bone matrix, determined by the entity of the mechanical stimuli;
- depending on osteocytes' positioning, the outcome of bone remodelling in terms of bone density and micro-structure, which in turn triggers a new mechanical adaptation process.

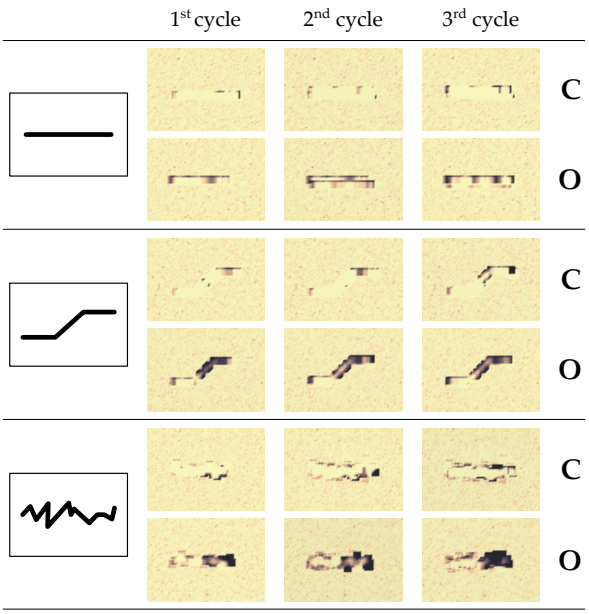

Figure 17: Simulation of the effects of different osteocytes' positioning (straight, zig-zag, and random) on bone density and structure, comparing the control (**C**) and the osteoporotic (**O**) parameters. Colour code is as in Figure 14 (a-h).

Figure 17 summarizes the results obtained after three remodelling cycles, comparing control and osteoporotic parameters and three different positioning patterns: straight, zig-zag, and random.

Firstly we observe that mineral homeostasis and bone micro- structure is successfully maintained in the healthy configuration, regardless of the initial positioning of osteocytes. There are just few parts characterized by a lower density, which can be ascribed to the stochastic fluctuations in the agent-based model. Indeed, we notice that osteoblasts are able to fill any hole left in the previous remodelling cycles, but their stochastic behaviour may allow some parts not to be completely repaired. On the other hand, a progressive micro-structural weakening is observed in the osteoporotic configuration, thus reproducing the expected defective dynamics.

3.6 SUMMARY

We have investigated the complex multiscale dynamics that connects disorders in the RANKL signalling at the molecular level, to bone diseases like osteoporosis that are characterized by a lower bone mass and disruptions at tissue level. In particular our computational study suggests that defective bone diseases arise when a RANKL over-signalling occurs in older patients characterized by a reduced activity of osteoblasts and osteoclasts. Simulation results have been validated over statistical data available from population-wide surveys. We focus on the spatial and temporal scale of the BMU, which is expressive enough to analyse the cellular activity in a remodelling cycle. In the control configuration, the simulator is able to reproduce the homeostatic process of remodelling, where resorption is counterbalanced by formation. On the other hand, when we execute in the osteoporotic configuration, osteoporosis can be potentially diagnosed after six years of simulation, even if starting from an optimal bone density. Finally, we have analysed the connection between the spatial location of signalling osteocytes and the bone micro-structure in the long run, in order to relate structural patterns at the tissue level and the origin of the disruptions that activate the process of remodelling.

From the methodological point of view, we have defined a multi-level computational framework that could be successfully employed also in other areas of biology and biomedicine. At the specification level, we describe the process of bone remodelling through a process-algebraic language, the Shape Calculus, which proved to be particularly suitable for expressing the spatial and multiscale nature of bone remodelling. The executable side consists of a stochastic agent-based simulator supporting the Shape Calculus-based specifications, and featuring a variety of analysis and runtime monitors. We report that the stochastic agent-based simulation results agree with those obtained from well-established mathematical models like [86, 135].

Besides being a biomedical problem of growing importance, osteoporosis and bone remodelling are characterized by complex multiscale mechanisms not entirely explained yet, thus they represent a testbed for novel modelling paradigms and techniques. The combination of formal languages with state-of-the-art modelling and simulation tools has provided us with a deeper understanding of this challenging field of research; and with a general modelling framework that could be applied to a wider class of problems in Computational Systems Biology.

4 MATHEMATICAL AND FORMAL ANALYSIS OF BONE PATHOLOGIES: MULTIPLE MODELS FOR MULTIPLE BIOLOGICAL PROPERTIES

Chapter Outline

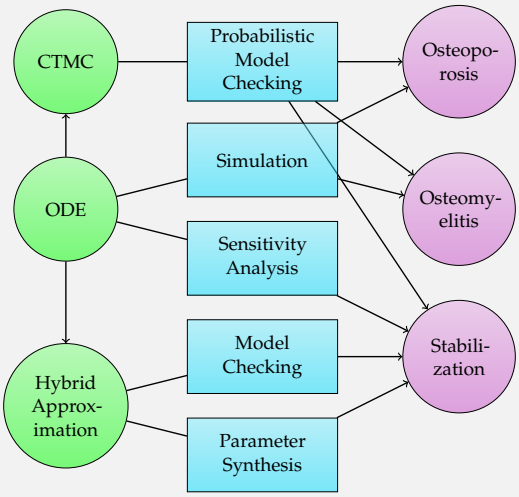

In this chapter, we present a set of formal techniques and a methodology for a composite formal analysis at the tissue and organ level, focusing on the verification of quantitative properties and disease dynamics in the process of bone remodelling. Starting from a differential equation model, we derive a stochastic model and a piecewise multi-affine approximation in order to perform model checking of stabilisation properties for the biological tissue, and to assess the differences between a regular remodelling activity and defective activity occurring in osteoporosis and in osteomyelitis, a bacterial infection caused by *Staphylococcus aureus*.
The complex nonlinear dynamics of bone remodelling is analysed with a variety of techniques: sensitivity analysis for the differential equation model; quantitative probabilistic model checking for the stochastic model; and classical model checking and parameter synthesis on the piecewise multi-affine model. Such analyses allow us to extract a wealth of information that is not only useful for a deeper understanding of the biological process but also towards medical diagnoses, where quantitative verification-based clinical estimators proved to be effective in the detection of osteoporosis and osteomyelitis.

TRADITIONALLY, Systems Biology has been described by using continuous deterministic mathematical models like ODEs and PDEs. A growing amount of experimental results is nowadays showing that biochemical kinetics at the single-cell level are intrinsically stochastic, suggesting that stochastic models are more effective in capturing the multiple sources of heterogeneity needed for modelling a biological system in a realistic way. In particular biological systems have also developed strategies for both exploiting and suppressing biological noise and heterogeneity.

The emergence of new computational frameworks that enable the formal analysis of complex biological systems with stochastic [49, 90, 25, 93], ordinary differential equations [57, 87, 24, 80] and hybrid semantics [26, 29, 14, 54, 62] has changed cell biology from a pure wet lab-based science to also an engineering and information science.

In this chapter, we present a set of formal techniques and a methodology suitable to specify and analyse bone remodelling, which is representative of a variety of physiological processes characterized by a multiscale interplay between different populations of cells that regulate together tissue homeostasis.

We give a mesoscopic description of the bone remodelling process, able to capture the essential features leading to tissue phenotype changes and to the emerging of a disease condition. Starting from a mathematical continuous model, we implement different encodings for deriving a stochastic model and a piecewise multi-affine discrete abstraction, in order to tackle the complexity of the bone remodelling system with formal analysis methods like sensitivity analysis, quantitative verification and parameter synthesis. Further, we extend the model for describing pathological remodelling dynamics, particularly focusing on osteoporosis and osteomyelitis (introduced in Section 2.1).

Formal Analysis of Bone Remodelling Dynamics

From a methodological viewpoint, we address the following problem: *Given a system* S *and a property to verify* P*, which is the most suitable model for* S *to prove* P *over* S*?*. We instantiate this problem in the context of biological systems, consider a set of stabilization properties and disease dynamics over three different models of BR:

- **ODE model.** It describes the continuous changes of, and the interactions between osteoclasts and osteoblast. Bone density is given by the difference between the formation activity (proportional to osteoblasts concentration) and the resorption activity (proportional to osteoclasts

concentration). Besides numerical simulations of the system and the analytical solution of steady states, *sensitivity analysis* is used for evaluating the effects on the system when parameters vary over large ranges.

- **Stochastic model.** We define a stochastic model from the ODE specification, for reasoning on the random fluctuations and the discrete changes of bone density and bone cells. After showing a good fitting between the continuous model and the expected values of the stochastic one, we employ *probabilistic model checking* for giving precise quantitative insights into the system.

- **Piecewise multi-affine (PMA) model.** We derive an optimal PMA approximation of the ODE model, following the approach presented in [67]. This class of hybrid systems provides a suitable discrete abstraction of the reachable sets and their possible trajectories over which classical *model checking* and *parameter synthesis* techniques can be applied.

This pipeline of models and analysis methods has been developed with the aim to assess the following properties:

- **Stabilisation.** It is a crucial property in our system as well as in a broad class of biological examples. Indeed the stabilisation of bone density to its initial level is a desirable feature, since it underlies tissue homeostasis and therefore the correct functioning of the whole skeleton. In turn bone stabilisation strongly depends on the balanced alternation, and consequently on the stabilisation of osteoclasts and osteoblasts at the end of their resorption and formation activity, respectively. In many cases stabilisation is defined as the existence of a unique fixpoint state that is always eventually reached [51]. In this work we prove stabilisation-related properties that are:

  1. Robustness of stabilisation with respect to initial conditions (ODE and stochastic model)

  2. Down-regulation of osteoclasts by osteoblasts (stochastic and PMA model)

  3. Boundedness of osteoclasts and osteoblasts (PMA model)

- **Defective bone dynamics.** We extend the ODE and stochastic models in order to describe the dynamics of osteoporosis and osteomyelitis. In particular, we introduce factors for modifying the death rates of bone cells and the regulatory interactions between osteoclasts and

osteoblasts, in order to reproduce the alteration in the RANK/RANKL/OPG signalling pathway. The growth function for the bacterial population has been modified to simulate the dosage of bacteriostatic and antibiotic drugs.

Structure of the chapter

SECTION 4.1 We present the ODE model for bone remodelling, and we give an overview of the method followed for calibrating model parameters.

SECTION 4.2 We encode a stochastic version of the ODE model and by using the PRISM model checker we compute the expectations of stochastic variables and the transient probability distribution.

SECTION 4.3 We derive a piecewise multi-affine over-approximation out of the non-linear equations, resulting in a transition system model.

SECTION 4.4 We compare the three methods in the formal analysis of stabilization properties and of bone pathologies (osteoporosis and osteomyelitis).

4.1 ODE MODEL

In this part we define a continuous mathematical model for cellular bone remodelling based on the work by Komarova et al. [86], where the authors developed an important model for BR based on experimental results described in Parfitt's work [121] which has inspired many other similar models.

It describes the temporal changes in osteoclast (x_1) and osteoblast (x_2) populations in a Basic Multicellular Unit (BMU) and the resulting bone density (z) as a function of the concentrations of x_1 and x_2.

$$\dot{x}_1 = \alpha_1 x_1^{g_{11}} x_2^{g_{21}} - \beta_1 x_1 \tag{1}$$
$$\dot{x}_2 = \alpha_2 x_1^{g_{12}} x_2^{g_{22}} - \beta_2 x_2 \tag{2}$$
$$\dot{z} = -k_1 x_1 + k_2 x_2 \tag{3}$$

Model parameters (listed in Table 9) have been calibrated so that variables x_1 and x_2 represent the actual number of osteoclasts and osteoblasts in a BMU. Recent experimental evidences based on the measurement of bone cells surfaces [122] suggest that in control subjects the ratio between os-

teoblasts and osteoclasts in a BMU varies around a mean value of 10. Given that the number of osteoclasts during resorption is estimated to 10 [121, 86], we make x_1 and x_2 range in the interval $[0, 10]$ and $[0, 100]$ respectively, as shown in the simulation plots (Fig. 18). Further details on the parameter estimation procedure are given in Section 4.1.1.

The parameters g_{ij} describe the effectiveness of autocrine and paracrine regulation. In the autocrine process the cell signals itself by secreting a chemical that binds with receptors on the surface of the same cell. In the paracrine process a chemical signals that diffuse into the area interacts with receptors on nearby cells. Here g_{11} describes the osteoclast autocrine regulation, g_{22} the osteoblast autocrine regulation, g_{21} is the osteoblast-derived paracrine regulation, and g_{12} is the osteoclast paracrine regulation.

The nonlinearities of these equations are approximations for the interactions of the osteoclast and osteoblast populations in the proliferation terms of the equations. As reported in Table 9, the autocrine signalling has a positive feedback on osteoclast production ($g_{11} > 0$), and paracrine signalling has a negative feedback on osteoclast production ($g_{21} < 0$). The autocrine signalling has a positive feedback on osteoblast production ($g_{22} > 0$), while the paracrine signalling does not affect osteoblast production ($g_{12} = 0$).

The resulting relative bone density (z) is calculated as the difference between the formation ($k_2 x_2$) and the resorption ($k_1 x_1$) activity, where k_1 and k_2 are the resorption and formation rates, respectively. The variable z measures the percentage changes in bone density with respect to an initial optimal value, which is set to zero.

The non-trivial steady state solution $(\bar{x}_1, \bar{x}_2)$ (obtained analytically by setting $\dot{x}_1 = 0$ and $\dot{x}_2 = 0$) is given by the equations

$$\bar{x}_1 = \left(\frac{\beta_1}{\alpha_1}\right)^{(1-g_{22})/\Gamma} \left(\frac{\beta_2}{\alpha_2}\right)^{g_{21}/\Gamma} \tag{4}$$

$$\bar{x}_2 = \left(\frac{\beta_2}{\alpha_2}\right)^{(1-g_{11})/\Gamma} \left(\frac{\beta_1}{\alpha_1}\right)^{g_{12}/\Gamma}, \tag{5}$$

where $\Gamma = g_{12}g_{21} - (1 - g_{11})(1 - g_{22})$. With the considered parameters we obtain $\bar{x}_1 = 1.265 \times 10^{-3}$ and $\bar{x}_2 = 2.531 \times 10^{-1}$.

S-SYSTEMS The set of ODEs considered in (1-3) belong to the class of S-Systems, a class of systems conceived for the modelling of biochemical systems and described in details in [114, 23]. The general format of a S-System describes the evolution of a set of dependent variables $(x_1, \ldots, x_n)$ consid-

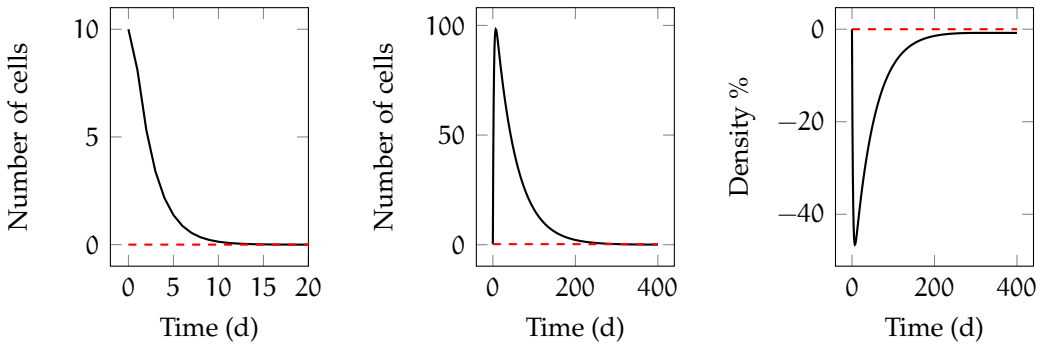

(a) Osteoclasts **(b)** Osteoblasts **(c)** Relative bone density

Figure 18: Simulation results of a single remodelling cycle in the ODE model. Dashed lines mark the steady state concentrations for osteoclasts and osteoblasts, and the initial bone density. The remodelling cycle is triggered by an increase in the number of osteoclasts from their steady level, such that the initial conditions are $(x_1^0, x_2^0) = (10 + \bar{x}_1, \bar{x}_2)$. The stabilisation of osteoclasts is achieved at about $t = 20$ days, and at the end of the cycle, we observe the stabilisation of osteoclasts and osteoblasts, and the initial bone density being re-established. In this model, $\bar{x}_1 = 1.265 \times 10^{-3}$ and $\bar{x}_2 = 2.531 \times 10^{-1}$.

ering an additional set of independent variables $(x_{n+1}, \ldots, x_{n+m})$ by the following differential equations:

$$\dot{x}_i = \alpha_i \prod_{j=1}^{n+m} x_j^{g_{ij}} - \beta_i \prod_{j=1}^{n+m} x_j^{h_{ij}}$$

where α_i and β_i are the production and degradation rates, respectively, of the i-th variable; g_{ij} and h_{ij} are called *kinetic orders* and they represent the strength of the interaction of X_j in the production or degradation of X_i. In our bone remodelling model, kinetic orders correspond to the autocrine and paracrine regulation factors g_{ij}.

SIMULATION RESULTS Figure 18 depicts the simulation plots for x_1, x_2 and z during a single remodelling cycle (about 400 days). The initiation of a remodelling cycle is modelled with a momentary increase of x_1 from $\bar{x}_1$ at time 0. Osteoclasts' lifespan is much shorter than osteoblasts, and consistently with the experimental data reported in [121], maximal erosion is reached at $t = 10$ days. Henceforth, osteoblasts mineralize the consumed bone and at about $t = 400$ days, the initial steady level of bone density is achieved (bone homeostasis), and both osteoclasts and osteoblasts reach their stable states.

Param	Value	Description
α_1	0.5 day^{-1}	Oc growth rate
α_2	4 day^{-1}	Ob growth rate
β_1	0.51 day^{-1}	Oc death rate
β_2	0.02 day^{-1}	Ob death rate
g_{11}	1.1	Oc autocrine regulation
g_{22}	0	Ob autocrine regulation
g_{12}	1	Oc paracrine regulation
g_{21}	-0.5	Ob paracrine regulation
k_1	1.9 $cell^{-1}$ day^{-1}	Resorption rate
k_2	9.48×10^{-3} $cell^{-1}$ day^{-1}	Formation rate

Table 9: Parameters of the ODE model for bone remodelling. Details on parameter estimation can be found in Sect. 4.1.1.

4.1.1 Calibration

Model parameters have been calibrated in order to meet recent experimental evidences [122] stating that the number of osteoclasts in a BMU (variable x_1) during resorption consists of about 10 units, and that the number of osteoblasts (variable x_2) during the formation phase consists of about 100 units, which contradicts the results obtained with the original parametrization of the model [86], where a 4 times higher abundance of osteoblasts is reported.

Parameter estimation has been performed using the R statistical software and the package FME [136] that provides algorithms for inverse modelling, sensitivity and Monte Carlo analysis. In the following, we sketch the procedure followed for the estimation of the model parameters.

SENSITIVITY ANALYSIS OF BONE CELL POPULATIONS *Sensitivity Analysis (SA)* is a technique to determine how sensitive a system is with respect to the change of parameters, and to identify key parameters that have more impact on the system's outcomes. Generally, it computes the variation of the model outputs w.r.t. variations to model inputs, and thus gives a measure of the *robustness* of a system, i.e. the ability of a system to maintain its functions against perturbations.

In this analysis, we consider two classes of sensitivity measures: the so-called local and global sensitivity. *Local sensitivity* is a dimensionless quantity which evaluates the effects of a small (infinitesimal) variation of an in-

put parameter θ_j over an output variable θ_j, at a particular time t. It is calculated as the derivative of y_i w.r.t. θ_j:

$$\frac{\partial y_i}{\partial \theta_j} \cdot \frac{w_{\theta_j}}{w_{y_i}},$$

where w_{θ_j} and w_{y_i} are a scaling factors applied to θ_j and y_i, usually equal to their respective original values.

We evaluate the local sensitivity of variables x_1 (osteoclasts) and x_2 (osteoclasts) with respect to their growth and death rates (α_i and β_i, $i = 1, 2$), in order to identify the candidate parameters (those leading to higher variations) to be tuned in the calibration process. We exclude the parameters describing autocrine and paracrine factors g_{ij}, since their modification results in a major change in the qualitative dynamics of BR (inducing for instance periodicity). From the sensitivities plotted in Figure 19, we observe that α_1 and β_1 mainly affect the output of variable x_1, and that β_1 has the most (negative) effect also on x_2, because of the positive paracrine regulation of Ocs on Obs. This also evidenced by the mean sensitivity values reported in the same figure. Therefore we have chosen parameters α_1 and β_1 as candidates for model calibration.

Additionally, we performed a Monte Carlo analysis for evaluating the *global sensitivity* of α_1 and β_1 on the maximum number of osteoclasts (max_{x_1}) and osteoblasts (max_{x_2}). Global sensitivity analysis is performed by making parameters vary in a specified range according to some predefined distribution (here uniformly distributed), and by running the model with each of these parameter combinations, for a given number of runs (here, 200 runs). With this analysis, we aim at identifying values for α_1 and β_1 so that max_{x_1} is close to 10 and max_{x_2} is close to 100.

Figure 21 display the results of the global sensitivity analysis on max_{x_2} with $\alpha_1 \in [0, 1]$ and $\beta_1 \in [0.5, 1]$. max_{x_1} has not been reported since constantly takes the desired value (10) for each α_1 and β_1, while max_{x_2} increases with higher values of α_1 and decreases with higher values of β_1. The desired maximum number of osteoblasts (100) is reached approximately with either $\alpha_1 = 1$ or $\beta_1 = 0.5$.

FITTING *Non-linear data fitting* techniques have been applied for calibrating α_1, β_1, k_1, and k_2 in order that the new model fulfils the condition of remodelling equilibrium and reflects the desired ratio of 10:100 between osteoclasts and osteoblasts. Nonlinear fitting is a class of optimization algorithms that takes in input a function to minimize, i.e. the residuals of the model output versus the observed data, and the initial values (and possibly

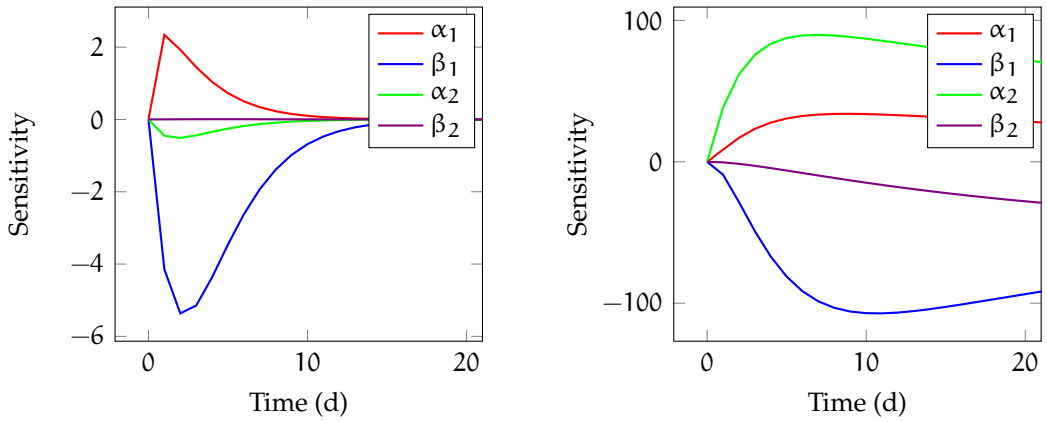

(a) Local sensitivity of osteoclasts

(b) Local sensitivity of osteoblasts

Parameter	Mean x_1 sensitivity	Mean x_2 sensitivity
α_1	0.02240	5
α_2	-0.00642	13
β_1	-0.07861	-16
β_2	0.00013	-14

Figure 19: Local sensitivity functions of variables x_1 (number of osteoclasts) and x_2 (number of osteoblasts) with respect to growth and death rates of bone cells (α_i and β_i, $i = 1, 2$).

upper and lower bounds) of the parameters to be optimized. It returns the calibrated parameters and the optimally minimized residuals.

In this case, observations are generated from the model with the original parameters (as in [86]), after scaling simulation outputs in order to reflect the numbers of cells experimentally measured, and after adding uniformly distributed random noise. The initial parameter values passed to the optimization algorithm are: $\alpha_1 = 0.5$, $\beta_1 = 0.75$, $k_1 = 0.24$ and $k_2 = 1.7 \times 10^{-3}$ (the last two are as in [86]). After evaluating the fitting algorithm with different initial values, we set α_1 and β_1 to the central value of their respective domains, as considered in the global sensitivity analysis. Table 10 reports the optimized parameters, compared with those in Komarova's work [86]. Figure 20 displays the output of the bone remodelling model simulated with the fitted parameters, whose outcome well agrees with the (scaled) output of the original model.

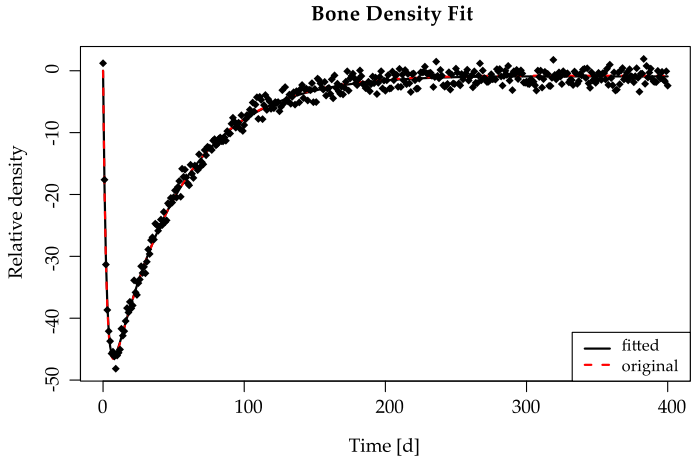

Figure 20: Relative bone density simulated with calibrated parameters. Black dots represent observations; the dashed red curve indicates the output of the original model; the black curve indicates the fitted output.

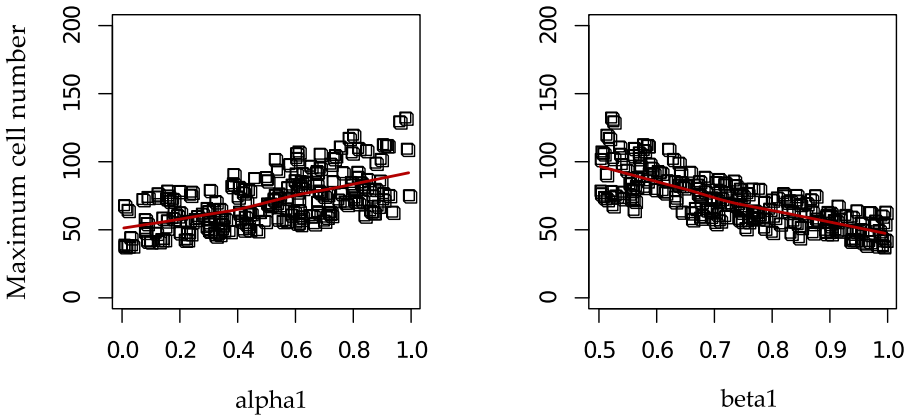

Figure 21: Global sensitivity on the maximum amount of osteoblasts, plotted as a function of osteoclasts' growth and death rates (α_1 and β_1). Both plots are obtained by the uniform sampling of $\alpha_1 \in [0, 1]$ and $\beta_1 \in [0.5, 1]$. The solid line indicate the LOWESS smoother.

Param	Original value	Calibrated value	Units	Description
α_1	3	0.5	day^{-1}	Oc growth rate
β_1	0.2	0.51	day^{-1}	Oc death rate
k_1	0.24	1.9	$cell^{-1}\ day^{-1}$	Resorption rate
k_2	1.7×10^{-3}	9.48×10^{-3}	$cell^{-1}\ day^{-1}$	Formation rate

Table 10: Comparison of original (as in [86]) and calibrated parameters. Osteoclasts' growth and death rates have been modified to reflect the actual ratio between osteoclasts and osteoblasts in a BMU. Resorption and formation rates have been estimated for ensuring the remodelling equilibrium, by means of data fitting algorithms.

4.2 STOCHASTIC MODEL FOR QUANTITATIVE VERIFICATION

Randomness and stochasticity are inherent features of biological systems. Living cells are complex mixtures of a variety of complex molecules that are constantly undergoing reactions with one another, and such reactions typically have an exponential distribution associated [65]. Stochasticity plays a key role in bone remodelling, e.g. the fluctuations in molecular concentrations (RANKL and OPG) produce changes in the chemotaxis, that is the process by which cells move toward attractant molecules, of osteoclasts and osteoblasts. This may affect for example the cell differentiation, number and arrival time, and consequently the whole remodelling process. Moreover, autocrine and paracrine regulation among osteoblasts and osteoclasts results from stochastic interactions whose propensity is determined by the availability of a particular class of cells, that are naturally discrete.

Being continuous and deterministic, the ODE model presented in Sect. 4.1 is not capable to express such crucial aspects. We thus define a stochastic model for bone remodelling and perform formal analysis by means of probabilistic verification techniques, for assessing the probability of a particular configuration of the biological system (usually expressed as a temporal logic property) being reached. In particular, we employ the probabilistic model checker PRISM [90], which has been largely adopted in several biological case studies, especially for modelling biochemical pathways [89, 37, 8, 130]. In this section, we extend this approach to cellular networks, in order to

[ ]	$0 < x_1 < x_1^{max} \wedge x_2 > 0 \rightarrow$	$\alpha_1 x_1^{g_{11}} x_2^{g_{21}}$	$: x_1 = x_1 + 1$
[ ]	$x_1 > 0 \rightarrow$	$\beta_1 x_1$	$: x_1 = x_1 - 1$
[resorb]	$x_1 > 0 \rightarrow$	$k_1 x_1$	: true

(a) Osteoclasts

[ ]	$0 < x_2 < x_2^{max} \wedge x_1 > 0 \rightarrow$	$\alpha_2 x_1^{g_{12}} x_2^{g_{22}}$	$: x_2 = x_2 + 1$
[ ]	$x_2 > 0 \rightarrow$	$\beta_2 x_2$	$: x_2 = x_2 - 1$
[form]	$x_2 > 0 \rightarrow$	$k_2 x_2$	: true

(b) Osteoblasts

[resorb] true : 1

(c) Bone resorbed reward

[form] true : 1

(d) Bone formed reward

Table 11: Stochastic model for bone remodelling. Maximum values have been set to $x_1^{max} = 15$ and $x_2^{max} = 150$. Initial values are $x_1^0 = 10$ and $x_2^0 = 1$. The other parameters are listed in Table 9

give theoretically justified and quantitative insights in the remodelling process and in the development of defective bone pathologies.

In our settings we use *Continuous Time Markov Chains (CTMC)* (introduced in Sect. 2.3), following a *population-based* approach where osteoclasts and osteoblasts are defined as PRISM modules. Each module is equipped with a random state variable modelling the discrete number of cells; and with a list of guarded and stochastic transitions of the form

$$[\mathtt{label}]\ \mathtt{guard} \rightarrow \mathtt{rate} : \mathtt{update}$$

where $\mathtt{label}$ is an optional transition label; $\mathtt{guard}$ is a predicate over the state variables determining whether the transition is enabled or not; in the CTMC settings, $\mathtt{rate}$ is the speed/propensity of the action, giving rise to an exponentially distributed duration of the transition with mean $1/\mathtt{rate}$ (faster action have a higher probability of being taken than slower one); and $\mathtt{update}$ optionally sets new values to state variables.

The PRISM model has been derived from the ODE in Section 4.1 in the standard way which exploits the inherent population structure of the BR

model as follows. Let $\dot{x} = \alpha - \beta$, with $\alpha, \beta > 0$, be a generic population model. The corresponding stochastic transitions would be:

$$\begin{aligned} x < x_{max} &\rightarrow \alpha : x = x + 1 \\ x > x_{min} &\rightarrow \beta : x = x - 1 \end{aligned}$$

where x_{min} and x_{max} define the range within which the random variable x can vary. Typically, x is the number of individuals in the population, while α and β are possibly non-linear functions of the population counts. Table 11 summarizes the transitions of osteoclasts and osteoblasts. We do not assume any scaling factor between variables in the continuous model and variables in the stochastic model, so that the random variables x_1 and x_2 represent the discrete number of osteoclasts and osteoblasts, respectively, in a BMU. We use the calibrated ODE model to parametrize the CTMC. Command guards are set in order to avoid out-of-range updates and 0- or infinite-valued transition rates occurring because of nonlinearities in growth and death rates. Further, in order to reduce the state-space of the stochastic model, the relative bone density has not been implemented as a state variable, but as transition rewards, i.e. costs associated to osteoclasts'/osteoblasts' transitions.

Further details on the PRISM implementation and on the choice of upper bound for the random bone variables can be found in Appendix C.

4.2.1 Analysis of Bone Density and Bone Cells Properties

Bone cells concentrations and bone density are assessed through the verification of quantitative properties over the defined stochastic model. Properties to verify have been formulated in *CSL (Continuous Stochastic Logic)* [5] extended with rewards (presented in Sect. 2.3), and are:

- **Expected bone cells.** In order to compute the expected values of osteoblasts and osteoclasts during the remodelling cycle, we have defined the following instantaneous reward properties, where *expOc* and *expOb* are the state rewards associated to x_1 and x_2, respectively:

$$\begin{aligned} E(x_1)(t) &= \mathcal{R}^{expOc}_{=?}[\mathcal{I}^{=t}], \quad t = 0, 10, \ldots, 400 \\ E(x_2)(t) &= \mathcal{R}^{expOb}_{=?}[\mathcal{I}^{=t}], \quad t = 0, 10, \ldots, 400 \end{aligned}$$

- **Variance of bone cells.** Being the variance of a random variable X equals to $E(X^2) - (E(X))^2$, we have introduced two additional reward structures defined as the expected value of the squared number of os-

teoclasts ($squaredOc$) and osteoblasts ($squaredOb$). Therefore, the variance is computed with the following properties:

$$\sigma^2(x_1)(t) = (\mathcal{R}^{squaredOc}_{=?}[\mathcal{I}^{=t}]) - (E(x_1)(t))^2, \quad t = 0, 10, \ldots, 400$$
$$\sigma^2(x_2)(t) = (\mathcal{R}^{squaredOb}_{=?}[\mathcal{I}^{=t}]) - (E(x_2)(t))^2, \quad t = 0, 10, \ldots, 400$$

- **Ranges of the number of cells in a BMU.** Expected minimum and maximum concentrations of osteoclasts and osteoblasts have been verified by using PRISM filters, a particular kind of formulas capable to compute values simultaneously for several states. Filters are of the form $filter(op, prop, states)$, where op is the operator characterizing the type of filter, in our case $range$; $prop$ is the property to verify; and $states$ is the predicate identifying the set of states over which to apply the filter (if $true$ it can be omitted). The resulting properties are:

$$filter(range, E(x_1)(t)) \text{ and } filter(range, E(x_2)(t)),\ t = 0, 10, \ldots, 400$$

- **Expected relative bone density.** It is calculated as the difference between the cumulative reward for bone formed, and the cumulative reward for bone resorbed:

$$\mathcal{R}^{boneFormed}_{=?}[\mathcal{C}^{\leqslant t}] - \mathcal{R}^{boneResorbed}_{=?}[\mathcal{C}^{\leqslant t}], \quad t = 0, 10, \ldots, 400$$

Figure 23 displays the temporal changes in the expected values, standard deviations and ranges of osteoclasts, osteoblasts and bone density. Additionally, we have compared the expected quantities of the stochastic model with the results of the differential equation model of Sect. 4.1 (see Fig. 22). It is possible to observe a satisfying agreement between the two outputs, also confirmed by the low values obtained for the scaled *Sum of Squared Residual (SSR)* between the ODE curves and the stochastic ones. By calculating the scaled variant of the common (unscaled) SSR, we obtain a measure of fitting independent from the number of data points, that can considerably affect the result of the analysis.

Therefore the presented model provides a biologically sound and a numerically faithful stochastic extension of the ODE model, and enables at the same time a variety of rigorous quantitative analysis over the bone remodelling system.

On the other hand, transient analysis [139] evaluates the probability of all the states at a specific time instant, and it could detect behaviours like bistability (i.e. the coexistence of two distinct states with high probability), that

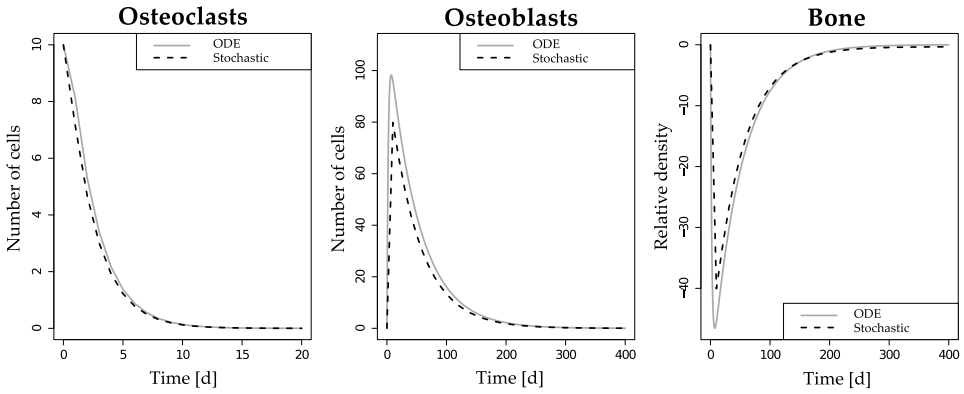

Figure 22: Comparison between the stochastic model (black dashed curves) and the ODE model (grey solid curves) of bone remodelling. For each variable, the squared distances between the curves of the ODE model and the stochastic one are $SSR_{x_1} = 0.00364$, $SSR_{x_2} = 0.489$ and $SSR_z = 0.0505$.

cannot be estimated by just computing the expected values of the random variables. For details on the transient probabilities of a CTMC, see Section 2.3 or the tutorial paper [88].

Figure 24 illustrates the transient probabilities computed at 5 and 20 days. Here and along the whole remodelling timespan, we do not observe any bistable behaviour and therefore the expected values are representative of the single mode and of its probability density.

4.3 PIECEWISE MULTIAFFINE APPROXIMATION

The formal analysis of the ODE model presented in Section 4.1 is intractable due to the presence of the nonlinear terms where the degree of some state variables is greater than one or not even an integer. The stochastic version presented in the previous section is amenable to quantitative analysis only with small numbers of osteoclasts and osteoblasts, but it suffers the state explosion problem with larger populations, e.g. with multiple BMUs.

In this section, we present an alternative method to tackle the problem. Following [67], we have identified a piecewise multi-affine (PMA) system [16] that best approximates the original one, opening to formal analysis techniques like model checking [12], reachability analysis [19] and parameter synthesis [14]. This class of hybrid systems, relying on the convexity property [16] of multi-affine functions, provides a conservative overapproximation of the reachable sets represented by hyper-rectangles in the state space.

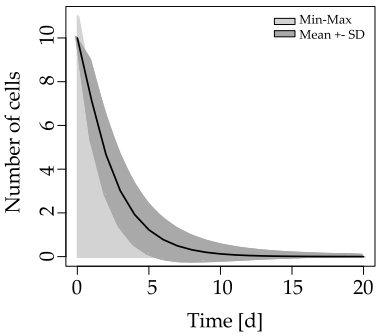

(a) Osteoclasts

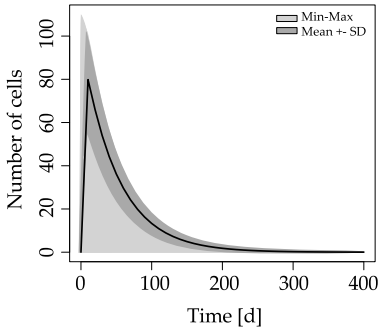

(b) Osteoblasts

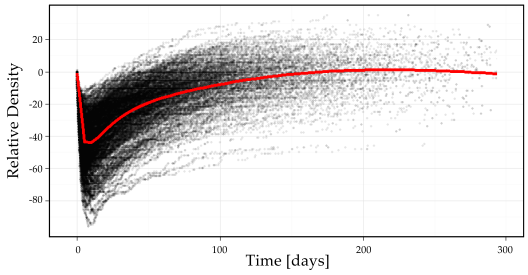

(c) Bone density

Figure 23: Stochastic fluctuations in the model variables of bone remodelling. Expected values, standard deviation and ranges of bone cells have been computed through the properties in Sect. 4.2.1. Bone density values have been obtained with 10.000 runs of the PRISM discrete-event simulator.

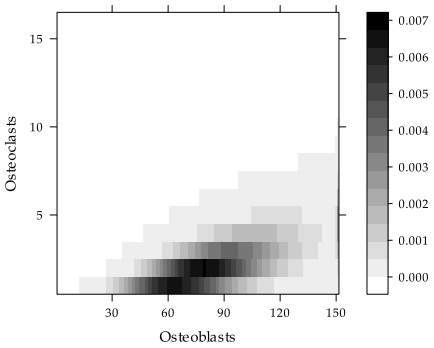

(a) 5 days

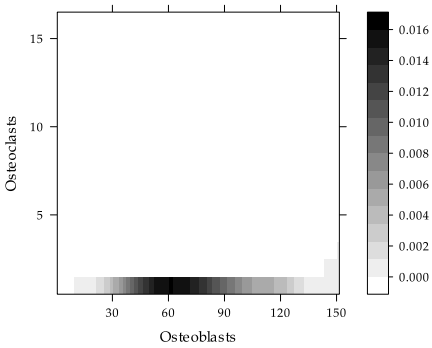

(b) 20 days

Figure 24: Transient probability distributions of the stochastic model. The x-axis gives the number of osteoblasts and the y-axis gives the number of osteoclasts. Darker points indicate states with higher probability density.

This powerful abstraction results in a discrete transition system, where the states are the reachable sets and the transitions represent the possible trajectories between two reachable sets. A multi-affine function [16] is a polynomial, where the product of different state variables is allowed, but the degree of each state variable is one or zero. We recall the definition of multi-affine function as presented in [19].

Definition 4.3.1 (Multi-affine function [19]). *A multi-affine function* $f : \mathbb{R}^n \to \mathbb{R}^n$ *has the following form:*

$$f(x) = \sum_{j=0}^{2^n-1} c_j x_1^{i_1(j)} x_2^{i_2(j)} \cdots x_n^{i_n(j)};\ c_j \in \mathbb{R}^n,$$

where $x = (x_1, \cdots, x_n)$ *and the concatenation* $i_1(j)i_2(j)\cdots i_n(j)$*, with* $\{i_1(j), \ldots, i_n(j)\} \in \{0,1\}^n$*, is a binary representation of the integer* j*.*

In [96] it is shown that any nonlinear function can be approximated with a piecewise affine function with an arbitrary accuracy and this allows us to recast our original model as a PMA. The accuracy of the approximation is not a marginal problem, for example a common question can be: how can we optimally fit the nonlinear terms with a fixed number of segments such that the least square error between the original curve and its approximation is minimum? This issue is solved by a dynamic programming algorithm proposed in [67]: given the sampled points of a set of nonlinear curves representing the dynamics of the system in a particular interval, it finds the optimal global linearisation for a fixed number of segments (or *ramps*) given in input. The resulting PMA identified in a region $[x_1^{min}, x_1^{max}] \times [x_2^{min}, x_2^{max}]$ partitions the concentrations of the osteoclasts and the osteoblasts respectively in ns_1 and ns_2 intervals as it follows:

$$\dot{x_1} = \alpha_1 \sum_{i=1}^{ns_1+1} r(x_1, \theta_i^{(1)}, \theta_{i+1}^{(1)}, y_i^{(1)}, y_{i+1}^{(1)})) \sum_{i=1}^{ns_2+1} r(x_2, \theta_i^{(2)}, \theta_{i+1}^{(2)}, y_i^{(2)}, y_{i+1}^{(2)})) - \beta_1 x_1 \tag{6}$$

$$\dot{x_2} = \alpha_2 x_2 - \beta_2 x_2 \tag{7}$$

$$\dot{z} = -k_1 x_1 + k_2 x_2. \tag{8}$$

with the following thresholds for the state variables x_1 and x_2:

$$\theta_1^{(1)} = x_1^{min} < \theta_2^{(1)} < \cdots < \theta_{ns_1+1}^{(1)} = x_1^{max} \tag{9}$$

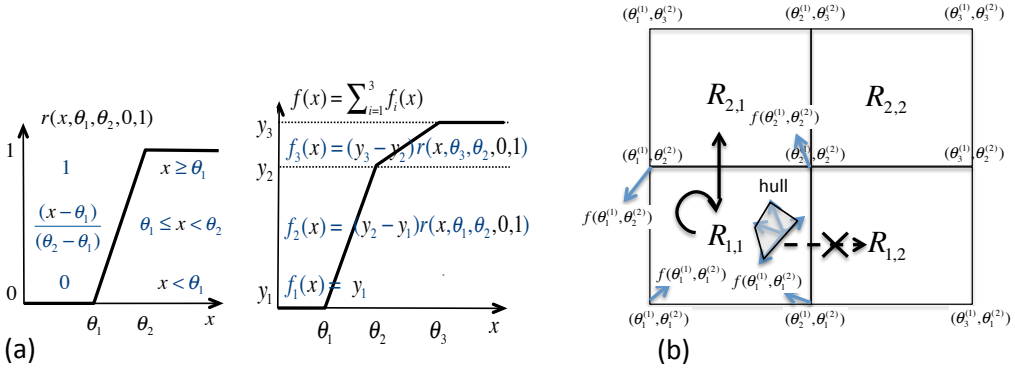

Figure 25: Piecewise multi-affine approximation. (a) On the left a single ramp and on the right the sum of two ramps. (b) The convexity property of hyper-rectangles with multi-affine dynamics can be used to determine if there are possible trajectories between two adjacent reachable sets.

$$\theta_1^{(2)} = x_2^{min} < \theta_2^{(2)} < \cdots < \theta_{ns_2+1}^{(2)} = x_2^{max} \tag{10}$$

The higher is the number of chosen intervals, the finer is the resulting abstraction, but the price of precision is the computational time spent in the identification and in the analysis of the system. Figure 25 (a) shows the ramp expression that is formally defined as it follows:

$$r(x,\theta_1,\theta_2,y_1,y_2) = \begin{cases} y_2 & \text{if} \quad x \geqslant \theta_2 \\ y_1 + (y_2 - y_1)\frac{(x-\theta_1)}{(\theta_2-\theta_1)} & \text{if} \quad \theta_1 \leqslant x < \theta_2 \\ y_1 & \text{if} \quad x < \theta_1 \end{cases} \tag{11}$$

The sum of ramps is a piecewise affine function, and the resulting model is piecewise multi-affine, because the right term of Eq. 6 contains the product of two piecewise affine functions. In the right term of Eq. 7, we omit x_1 from the production of the osteoblasts since in the reference model $g_{22} = 0$. The thresholds found after the piecewise multi-affine model identification partition the state space in hyper-rectangles adjacent and disjointed in which the dynamics is locally multi-affine.

Definition 4.3.2 (Hyper-rectangle [16]). *For $n \in \mathbb{N}$, a hyper-rectangle R is an n-dimensional rectangle described by:*

$$R = \{x = (x_1, \cdots, x_n) \in \mathbb{R}^n | a_i \leqslant x_i \leqslant b_i\}$$

where $a_i, b_i \in \mathbb{R}$, $a_i < b_i$, $i = 1, \cdots, n$.

Proposition 4.3.3 (Flow overapproximation [16]). *Let* $R \subset \mathbb{R}^n$ *a hyper- rectangle,* $f_R : R \to \mathbb{R}^n$ *be a multi-affine function and* $x \in R$*. Then* $f_R(x)$ *is a convex combination of the values of* f_R *at the* 2^n *vertices of* R*.*

This last property is very important to define an abstraction of the PMA system as a discrete transition system. Figure 25 (b) shows an example where a transition between the hyper-rectangles $R_{1,1}$ and $R_{2,1}$ can occur, because the vertical component of $f_{R_{1,1}}$ in one of the two vertices of their facet is greater than zero. A transition cannot instead occur between $R_{1,1}$ and $R_{1,2}$ because the horizontal component of $f_{R_{1,1}}$ in both vertices of their facet is less than zero.

4.3.1 PMA Identification

We have identified a PMA with 20 intervals for the concentration of the osteoblasts $[0, 2000]$ and 10 intervals for the concentration of the osteoclasts $[0, 15]$. Figure 26 shows a comparison between the original model and the approximated one.

The model obtained has been encoded as a specification for RoVerGeNe[1] [14], a tool designed for robustness analyses and parameters tuning of piecewise multi-affine differential equation models. The results of robustness analysis and parameters tuning are guided by the classical model checking, where a property is specified in Linear Temporal Logic (LTL) [127] and the discrete transition system is the abstraction of the PMA system discussed above. The LTL atomic predicates are of type $(x_i < \theta_j^{(i)})$ or $(x_i > \theta_j^{(i)})$, which can be combined with classical logical ($\neg$, $\wedge$, $\vee$) or temporal (X, $\mathcal{U}$, $\mathcal{F}$, $\mathcal{G}$) operators.

4.4 RESULTS

4.4.1 Analysis of Stabilisation Properties

Stabilisation is a property of high biological relevance in the bone remodelling system: stabilisation of bone density underlies tissue homeostasis and therefore the maintenance of its mechanical quality. Bone stabilisation depends in turn on the balanced alternation, and consequently on the stabilisation of osteoclasts and osteoblasts at the end of their resorption and formation activity, respectively.

1 http://iasi.bu.edu/~batt/rovergene/rovergene.htm

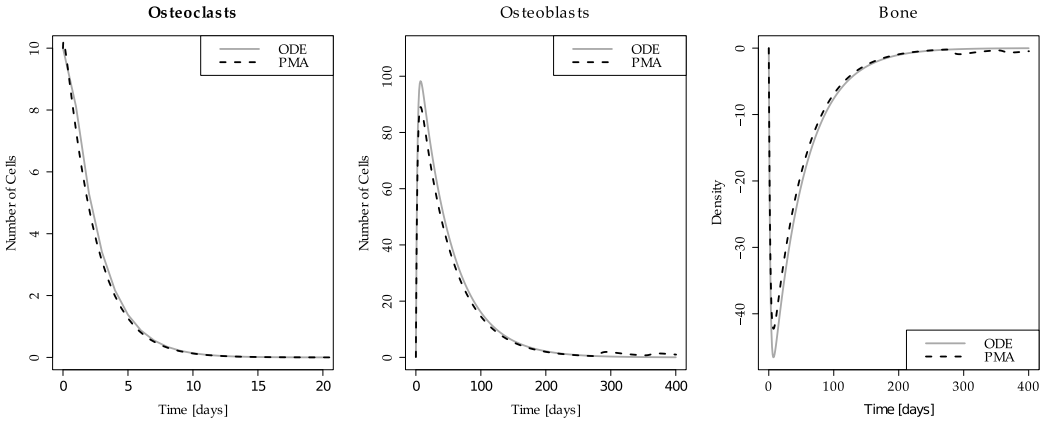

Figure 26: Comparison between the PMA model (black dashed curves) and the ODE model (grey continuous curves). In the PMA model, x_1 has been partitioned in 10 intervals: $\theta^{(1)} = \{0.000, 0.413, 1.178, 2.214, 3.482, 4.960, 6.626, 8.472, 10.490, 12.666, 15.000\}$. x_2 has been partitioned in 20 intervals: $\theta^{(2)} = \{0.000, 1.100, 2.101, 3.101, 4.102, 6.103, 9.104, 13.106, 19.109, 28.113, 41.118, 61.127, 90.141, 133.160, 196.188, 289.230, 426.292, 627.382, 923.516, 1358.711, 2000.000\}$. A good fitting can be observed between the ODE and the PMA curves, as evidenced by their SSR distances ($SSR_{x_1} = 0.000632$; $SSR_{x_2} = 0.0522$; and $SSR_z = 0.0114$).

In this part we show the analysis results for the following properties:

1. **Robustness of stabilisation with respect to initial conditions.** Since the starting of a remodelling cycle is simulated by an initial temporary increase of osteoclasts in the BMU, we are interested in assessing how changes in initial concentration of osteoclasts affect remodelling. In particular, we evaluate the effects on the stabilisation of bone cells and bone density, that is normally achieved with the original parameters. This analysis has been performed over the ODE and the stochastic model.

2. **Down-regulation of osteoclasts by osteoblasts.** We verify the effectiveness of the negative regulation that osteoblasts apply on osteoclasts. It is a key feature in the bone remodelling system since it ensures that the resorption phase comes to an end, and consequently that bone is protected from excessive resorption. In other words, we verify that osteoclasts cannot increase when osteoblast concentration is above a given threshold. Additionally we verify the converse property, stating that osteoclasts cannot decrease when the number of osteoblasts is below that threshold. This guarantees that osteoclasts can

proliferate in presence of small perturbations of osteoblasts. This analysis has been performed over the PMA and the stochastic model.

3. **Boundedness of osteoclasts and osteoblasts.** We perform parameter synthesis on the piecewise multi-affine model in order to find regions in the parameter space for which the concentrations of osteoblasts and osteoclasts are below fixed thresholds. The existence of an upper-bound ensures the bounded growth of bone cells and therefore, the absence of anomalous dynamics like the osteoclasts proliferation in bone metastases.

ROBUST STABILIZATION. Results show that both in the ODE and the stochastic model the stabilisation of x_1, x_2 and z is robust with respect to perturbations in the initial value of x_1 (x_1^0). In other words, homeostasis of bone density and bone cells is maintained regardless the initial concentration of osteoclasts.

In order to assess more formally how x_1^0 affects the remodelling dynamics in the ODE model, global sensitivity analysis (introduced in Sect. 4.1.1) has been performed over the three variables of the system. In this case we make x_1^0 range in the interval $[\bar{x_1}, 20 + \bar{x_1}]$, where $\bar{x_1}$ is the steady level of osteoclasts analytically solved in Sect. 4.1 (in the original model, $x_1^0 = 10 + \bar{x_1}$). As regards the stochastic model, we have computed the expected values of x_1, x_2 and z as explained in Sect. 4.1, with $x_1^0 = 0, 5, 10, 15, 20$. Figure 27 displays the results and the statistical summary of the three variables at the end of the remodelling cycle.

DOWN-REGULATION OF OSTEOCLASTS BY OSTEOBLASTS. From a formal verification viewpoint, stabilisation is often defined as the existence of a unique fixpoint state that is always eventually reached [51]. Translated into LTL, $\mathcal{FG}(s)$ must be verified, where s is the global fixpoint/ stable state. In our case, since we are more interested in locally stable behaviours, we restrict our analysis only to particular regions (i.e. low/high population of osteoblasts), and we use the following pattern: $p \rightarrow \mathcal{G}(s)$, where p identifies the region of interest in the state space, and s the property that is always verified in that region.

As explained before, we verify that if the population of osteoblasts is greater than the threshold $\theta_3^{(2)} = 2.101$, it will be always true that the population of osteoclasts will not grow, while the osteoblasts remain greater than

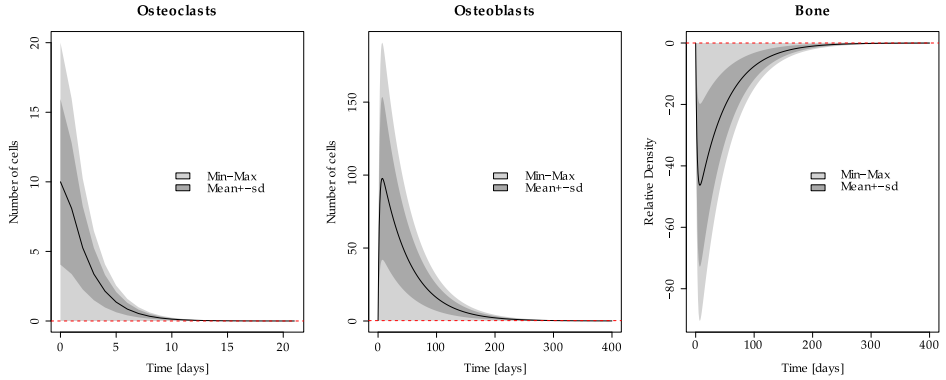

(a) ODE model

$(t = 400)$	μ	σ	min	max	$stable$
x_1	7.37×10^{-4}	2.76×10^{-4}	2.75×10^{-4}	1.26×10^{-3}	1.26×10^{-3}
x_2	4.46×10^{-2}	3.71×10^{-2}	2.63×10^{-3}	2.53×10^{-1}	2.53×10^{-1}
z	-1.37×10^{-2}	7.23×10^{-2}	-1.35×10^{-1}	-1.11×10^{-1}	0

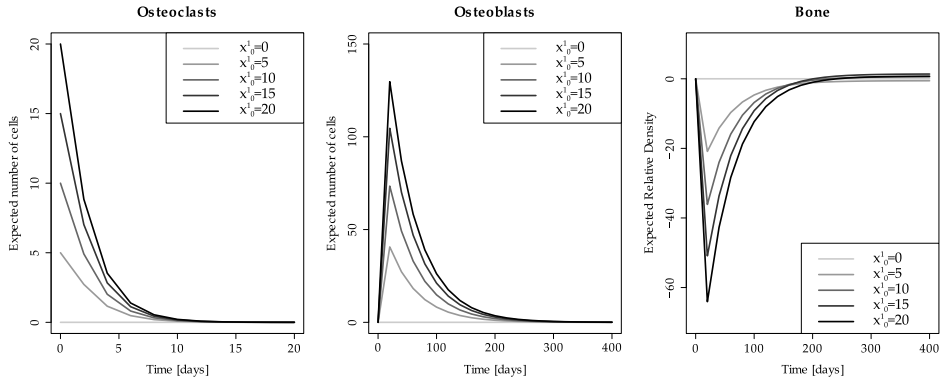

(b) CTMC model

$(t = 400)$	μ	σ	min	max	$stable$
x_1	1.096×10^{-3}	7.293×10^{-4}	0	1.871×10^{-3}	0
x_2	3.486×10^{-2}	2.568×10^{-2}	0	6.49×10^{-2}	0
z	0.4234	0.736	-0.566	1.366	0

Figure 27: Stabilisation of the system under perturbations in the initial value of osteoclasts. a) global sensitivity analysis on the ODE model, with $x_1^0 \in [\bar{x_1}, 20 + \bar{x_1}]$ and distributed uniformly. Black curves indicate the mean values μ; dark gray areas indicate the interval $[\mu - \sigma, \mu + \sigma]$; and light gray areas represent the interval between the maximum and the minimum values. b) increasing grey tones show the expected values of the random variables in the stochastic model with $x_1^0 = 0, 5, 10, 15, 20$. The statistical summaries (columns μ, σ, min and max) refer to the variables at the end of the remodelling cycle ($t = 400$ days), and demonstrate that variable values tend or are close to their steady levels (column $stable$).

$\theta_3^{(2)}$. We have verified the robustness of the following LTL property on the PMA system with RoVerGeNe:

$$(x_2 > \theta_3^{(2)}) \rightarrow \mathcal{G}(\wedge_{i=2}^{11}(x_1 < \theta_i^{(1)} \wedge x_2 > \theta_3^{(2)}) \rightarrow \mathsf{X}(x_1 < \theta_i^{(1)})).$$

In addition, we demonstrate that the corresponding PRISM property holds also in the stochastic model. Indeed for each $\theta^{(1)} = 1, \ldots, x_1^{max} = 15$, the following formula holds:

$$\mathcal{P}_{=1}\,[\mathcal{G}((x_1 < \theta^{(1)} \wedge x_2 > \lfloor\theta_3^{(2)}\rfloor) \rightarrow \mathsf{X}(x_1 < \theta^{(1)}))]$$

The attentive reader will notice that the above formula is not CSL, in which temporal operators cannot be combined. The property specification language of PRISM supports also LTL-style path properties, thus making possible to combine temporal operators.

We are also interested in the converse property of down-regulation that is, the proliferation of osteoclasts with small perturbations of osteoblasts. Stated differently we verify that if the population of the osteoblasts is less than $\theta_2^{(2)} = 1.1$, it will be always true that the population of osteoclast will not decrease while the osteoblasts remains lower than $\theta_2^{(2)}$. The LTL formula verified on the PMA system is

$$(x_2 < \theta_2^{(2)}) \rightarrow \mathcal{G}(\wedge_{i=4}^{11}(x_1 > \theta_i^{(1)} \wedge x_2 < \theta_2^{(2)}) \rightarrow \mathsf{X}(x_1 > \theta_i^{(1)})).$$

Similarly to the previous case, the proliferation property holds also in the stochastic model. Indeed, the PRISM formula

$$\mathcal{P}_{=1}\,[\mathcal{G}((x_1 > \theta^{(1)} \wedge x_2 < \lfloor\theta_1^{(2)}\rfloor) \rightarrow \mathsf{X}(x_1 > \theta^{(1)}))],$$

holds for each $\theta^{(1)} = 1, \ldots, x_1^{max} = 15$.

4.4.2 Parameter Synthesis of PMA Model

BOUNDEDNESS OF OSTEOCLASTS AND OSTEOBLASTS. We exploit the parameter synthesis feature of RoVerGeNe [14] in order to find the ranges of parameter for which the concentrations of osteoclasts and osteoblasts admit a fixed upper bound in the piecewise multi-affine model. In particular we are interested in finding the regions in the parameter space of β_1 and β_2 (the death rates of x_1 and x_2 resp.), such that the population of the osteoclasts is

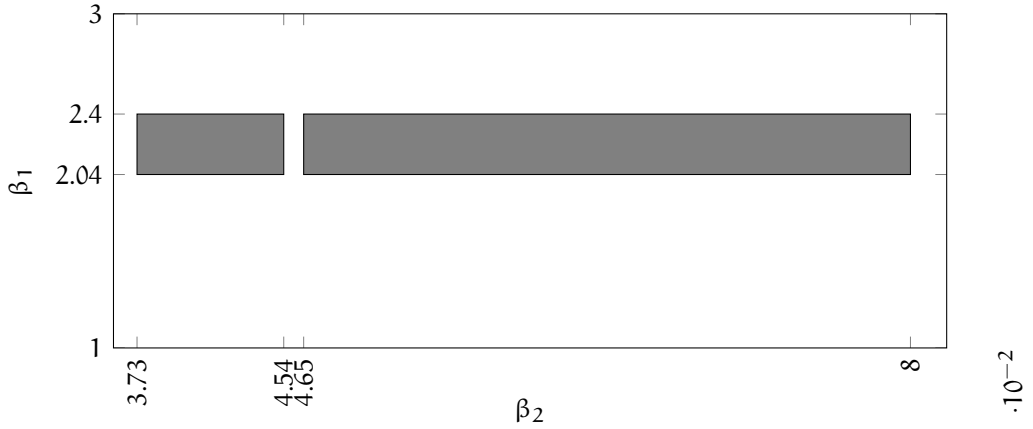

Figure 28: Parameter synthesis for boundedness of bone cells $(((x_1 < \theta_{10}^{(1)})) \wedge (x_2 < \theta_{20}^{(2)})) \rightarrow \mathcal{G}((x_1 < \theta_{10}^{(1)})) \wedge (x_2 < \theta_{20}^{(2)})))$, with $\beta_1 \in [0.6, 2.4]$ and $\beta_2 \in [0.02, 0.08]$. Synthesized regions are $2.0381 \leqslant \beta_1 \leqslant 2.4 \wedge 0.0373 \leqslant \beta_2 \leqslant 0.0454$ and $2.0381 \leqslant \beta_1 \leqslant 2.4 \wedge 0.0465 \leqslant \beta_2 \leqslant 0.08$.

always less than $\theta_{10}^{(1)} = 15$ and the population of the osteoblasts is always less than $\theta_{20}^{(2)} = 2000$. The corresponding LTL property is

$$((x_1 < \theta_{10}^{(1)})) \wedge (x_2 < \theta_{20}^{(2)})) \rightarrow \mathcal{G}((x_1 < \theta_{10}^{(1)})) \wedge (x_2 < \theta_{20}^{(2)})).$$

By setting the initial range for β_1 to $[0.6, 2.4]$ and for β_2 to $[0.02, 0.08]$, the synthesis algorithm returns two regions in the parameter space satisfying the boundedness property (see Fig. 28): $2.0381 \leqslant \beta_1 \leqslant 2.4 \wedge 0.0373 \leqslant \beta_2 \leqslant 0.0454$ and $2.0381 \leqslant \beta_1 \leqslant 2.4 \wedge 0.0465 \leqslant \beta_2 \leqslant 0.08$.

4.4.3 Osteoporosis and Osteomyelitis

We extended the bone remodelling model in order to analyse defective dynamics arising from bone pathologies, namely osteoporosis and osteomyelitis. In osteoporosis, an increased death rate for osteoclasts and osteoblasts is assumed, motivated by the fact that the occurrence of defective bone pathologies in elderly patients is partly attributable to the reduced cellular activity typical of those patients. Therefore we introduced a parameter k_{ageing} as a factor multiplying the death rates β_i. On the other hand, we modified the regulation factors in order to model an increased RANKL expression by osteoblasts, which results both from the analysis performed on gene expression data (reported in Appendix D) and from experimental evi-

dences [111]. In our model g_{21} is the result of all the factors produced by osteoblasts that activates osteoclasts and as explained in [86], $g_{21} = \mathrm{RANKL} - \mathrm{OPG}$ where RANKL is the effectiveness of RANKL signalling while OPG is the effectiveness of OPG signalling. Therefore a further parameter g_{por} has been included as a factor incrementing g_{21}, in order to incorporate the changes in the system RANKL, OPG associated to osteoporosis.

The resulting equations are:

$$\begin{aligned}
\dot{x}_1 &= \alpha_1 x_1^{g_{11}(1+f_{11}\frac{B}{s})} x_2^{g_{21}(1-f_{21}\frac{B}{s})+g_{por}} - k_{ageing}\beta_1 x_1 \\
\dot{x}_2 &= \alpha_2 x_1^{g_{12}/(1+f_{12}\frac{B}{s})} x_2^{g_{22}-f_{22}\frac{B}{s}} - k_{ageing}\beta_2 x_2 \\
\dot{B} &= (\gamma_B - V)B \cdot \log(\frac{s}{B}).
\end{aligned}$$

where the density of *S. aureus* follows a Gompertz curve with growth rate γ_B and carrying capacity (i.e. the maximum population size) s. Additionally, we introduced four parameters f_{ij} used to model the effects of the infection on the autocrine and paracrine regulation factors g_{ij}.

This model has been inspired from Ayati's work on multiple myeloma bone disease [3] and the key difference with respect to Komarova's model [86] is the addition of the terms $f_{ij}B/s$ that couple the bacterial density and its maximum size to the power laws for the osteoclast/osteoblast interactions. The bacterial parameters f_{11}, f_{12}, f_{21}, f_{22} are all nonnegative. The *S. aureus*-induced infection affects the normal remodelling activity by:

- reducing osteoblasts' growth rate: in fact, the paracrine promotion of osteoblasts is reduced ($g_{12}/(1 + f_{12}\frac{B}{s}) < g_{12}$, since $g_{12} > 0$), and the autocrine promotion of osteoblasts is reduced as well ($g_{22} - f_{22}\frac{B}{s} < g_{22}$);
- increasing RANKL and decreasing OPG expression: the paracrine inhibition of osteoclasts is a negative exponent resulting from the difference between the effectiveness of OPG signalling and that of RANKL signalling. Since $g_{21}(1 - f_{21}\frac{B}{s}) > g_{21}$, the infection causes an increase in RANKL expression and therefore a decrease in OPG expression.

In addition the infection increases the autocrine promotion of osteoclasts (since $g_{11} > 0$). We have taken γ_B to be independent of bone loss. The parameter V describes the effectiveness of the antibiotic treatment as a factor decreasing the growth rate γ_B of bacteria. Two different kinds of treatment can be distinguished: bacteriostatic treatments that stop bacteria proliferation ($V = \gamma_B$); and bacteriocide treatments which kill bacteria ($V > \gamma_B$).

Param	Value	Description
α_1	3 day^{-1}	Oc growth rate
α_2	4 day^{-1}	Ob growth rate
β_1	0.2 day^{-1}	Oc death rate
β_2	0.02 day^{-1}	Ob death rate
g_{11}	1.1	Oc autocrine regulation
g_{22}	0	Ob autocrine regulation
g_{12}	1	Oc paracrine regulation
g_{21}	-0.5	Ob paracrine regulation
k_1	0.0748 $cell^{-1}$ day^{-1}	Resorption rate
k_2	0.0006395 $cell^{-1}$ day^{-1}	Formation rate
k_{ageing}	[1, 2]	Ageing factor
g_{por}	0.1	RANKL factor
γ_B	0.005 day^{-1}	*S. aureus* growth rate
s	100	*S. aureus* carrying capacity
V	(0.005, 0.007) day^{-1}	Effectiveness of antibiotic treatment
t_{treat}	(200, 400, 600) days	Dosage time
$(f_{11}, f_{12}, f_{22}, f_{21})$	(0.005, 0, 0.2, 0.005) day^{-1}	Effect of infection on regulation factors

Table 12: Parameters for osteoporosis and osteomyelitis. Values have been mainly adapted from [86, 3]. The ageing factor (k_{ageing}) varies between 1 (control patient) and 2 (osteoporotic patient).

Here we report only the differential equation-based model, from which the derivation of the stochastic one is quite standard (see Table 17, App. C for the full CTMC model).

In this study, we are particularly interested in assessing the long-term effects of bone defective dynamics, and to this purpose we consider the same parameters values reported in [86, 3] that, even if over-estimating the number of bone cells, are able to reproduce the oscillatory behaviour typical of subsequent remodelling cycles. Parameters for the three different models (control, osteoporosis and osteomyelitis) are given in Table 12.

Simulation results under the three different scenarios are compared in Figure 29. The plots show that both osteoporosis and osteomyelitis are characterized by a negative remodelling balance, but in the latter case the bone loss becomes much more critical after 600 days. In the osteoporotic case, the remodelling period is shorter than in the control case, mimicking the fact that in older patients microfractures and consequently remodelling occur

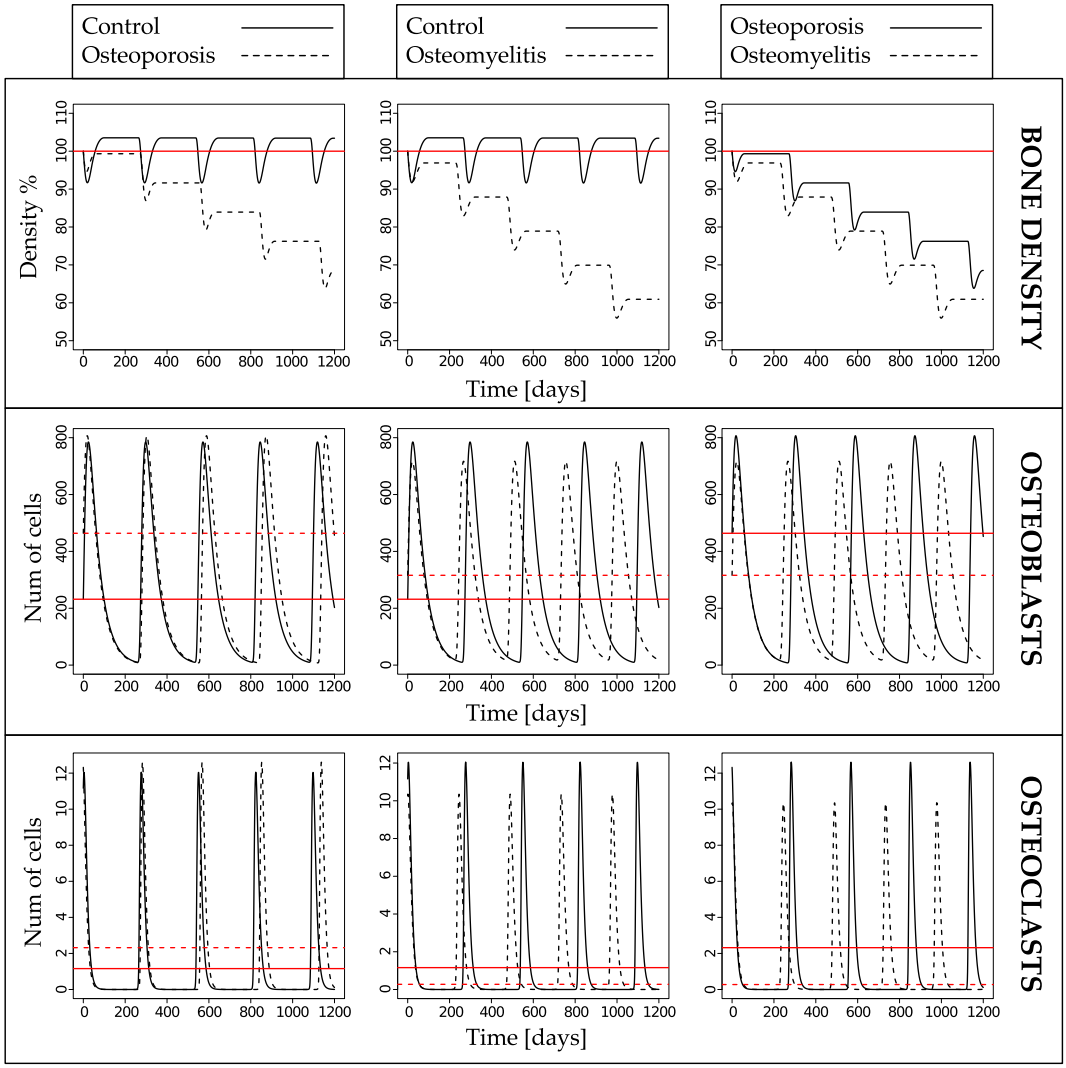

Figure 29: Comparison of the ODE results in control, osteoporosis and osteomyelitis configurations. Bone density (first row), number of osteoblasts (second row), and number of osteoclasts (third row) are compared between control and osteoporotic (first column); control and osteomyelitis (second column); osteoporotic and osteomyelitis (third column). Red lines mark the steady state values.

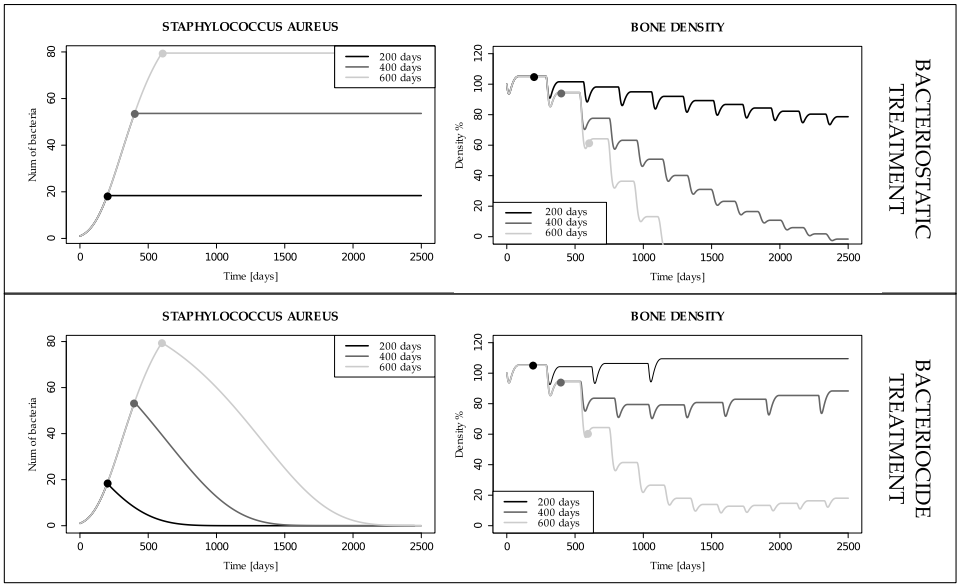

Figure 30: Simulation of a bacteriostatic ($V = 0.005 = \gamma_B$) and a bacteriocide ($V = 0.007 > \gamma_B$) treatments for *S. Aureus* at different dosage times (200, 400 and 600 days). Dots on the plots mark the points when treatment is given.

more frequently, in a vicious cycle that progressively weakens the structure and density of the bone [153]. On the other hand, the regular cycles of the normal bone model above are perturbed by the presence of the infection (chronic), and we observe longer and unstable remodelling periods.

SIMULATION OF DRUG DOSAGE We simulate the dosage of a bacteriostatic treatment ($V = 0.005 = \gamma_B$) and of a bacteriocide treatment ($V = 0.007 > \gamma_B$) for *S. Aureus* at different dosage times $t_{treat} = 200$, 400 and 600 days. Figure 30 shows that when applying the bacteriostatic drug (e.g. fusidic acid), the severe bone loss characterizing osteomyelitis can be limited only if the treatment is administered at $t = 200$ days. With later dosages the normal remodelling activity cannot be re-established, even if the situation is considerably better w.r.t. an untreated infection. Conversely, the bacteriocide treatment looks more effective than the bacteriostatic one, and the bone activity is able to recover regardless the dosage time. However the recovery time increases with the dosage time t_{treat}. It is evident that in both antibiotic treatments timeliness is a crucial factor in order to effectively operate against the infection. To this purpose, in Chapter 5 we will discuss methods to investigate more systematically the optimal dosage of drugs.

QUANTITATIVE VERIFICATION We evaluate the bone density, together with its change rate and variance in the stochastic model through probabilistic model checking. We show how the results of quantitative verification could serve as diagnostic and clinical estimators for assessing and predicting the onset of bone diseases. Indeed, the expected bone density corresponds to bone mineral density (BMD) measurements that are typically taken in clinical practice, and its variance is helpful in grasping abnormal remodelling dynamics that might not be immediately evident by looking at just the net bone density.

Finally, the *density change rate* allows to assess rapid negative and positive changes in bone density, which could be particularly helpful in detecting osteomyelitis, typically characterized by a higher negative change rate than osteoporosis. Let $f_{BD}(t)$ be expected bone density at time t, i.e. the output of the formula introduced in Sect. 4.2.1:

$$f_{BD}(t) = \mathcal{R}_{=?}^{\text{boneFormed}}[\mathcal{C}^{\leqslant t}] - \mathcal{R}_{=?}^{\text{boneResorbed}}[\mathcal{C}^{\leqslant t}]$$

Then, the density change rate is simply defined as the difference quotient of f_{BD} over a time interval Δt, that could represent the time between subsequent medical check-ups (e.g. 10 days):

$$\frac{f_{BD}(t+\Delta t) - f_{BD}(t)}{\Delta t}$$

Figure 31 and Figure 32 illustrate bone density, standard deviation and density change rate functions for the control (a), osteoporosis (b) and osteomyelitis (c) cases, respectively. Clearly the osteomyelitis case shows quicker decrease than control and osteoporosis cases.

4.5 SUMMARY

We have presented a set of formal techniques for reasoning about biological systems, focusing on bone remodelling as our case study. We showed how to derive, from the classical ODE model, a stochastic model and a piecewise multi-affine system that best approximates the original one. In the stochastic model the dynamics is locally regulated by the discrete entities (osteoblasts and osteclasts) involved. This model allows us to study the more realistic stochastic fluctuations of the system, but is amenable to quantitative analysis only with small populations of entities, suffering the state explosion problem. In the piecewise multi-affine model the dynamics of the system is

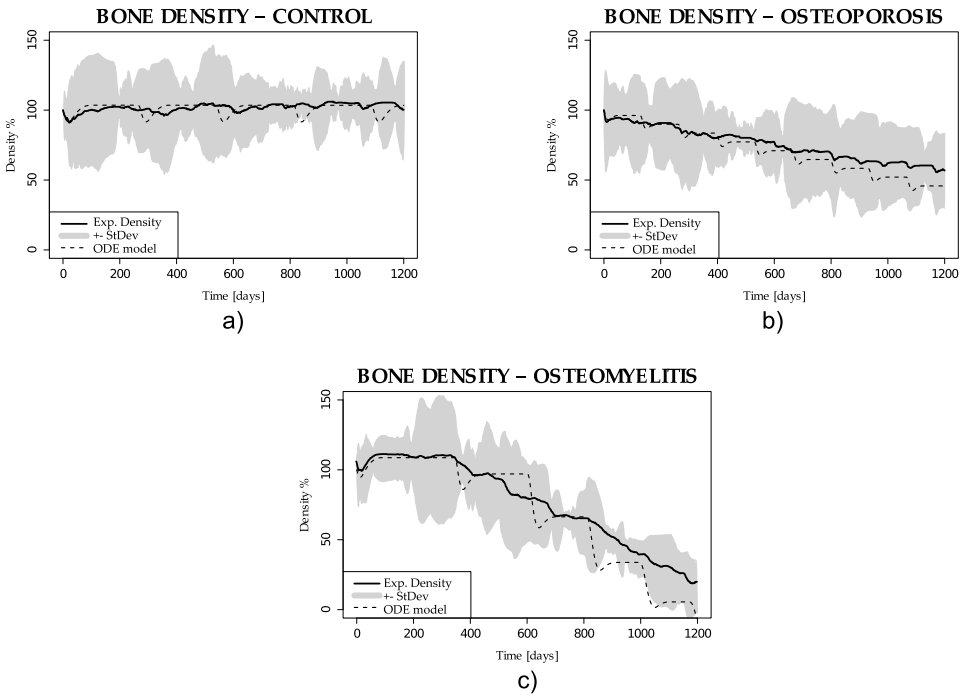

Figure 31: **Verification of expected density and variance in control (a), osteoporosis (b) and osteomyelitis (c).** Solid curves illustrate the expected densities of the stochastic model, compared with the ODE values (dashed ones). Gray areas indicate the standard deviation of bone density.

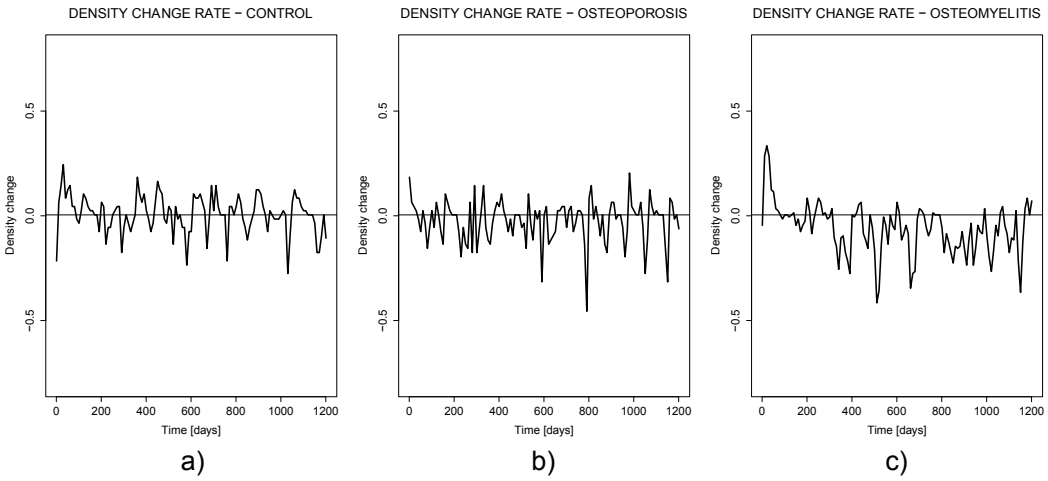

Figure 32: **Verification of bone density change rate for the control (a), osteoporosis (b) and osteomyelitis (c) configurations**.

governed by hyper-rectangles with locally multi-affine dynamics that partition the continuous state space. The convexity property of the multi-affine functions provides a powerful abstraction resulting in a discrete transition system, where the states are the reachable sets and the transitions represent possible trajectories between the reachable sets.

Stabilisation properties in a region of the state space can be checked on the models with both the stochastic and the PMA semantics. We showed how the parameter synthesis problem, guided by the satisfaction of stabilisation properties, can be approached in the PMA model by using the approach described in [67, 14]. The analysis of the PMA system represents an advantage over the ODEs in terms of behaviour interpretability and provides means to compare parameters with those used in the stochastic model. The combined use of both allows us to identify general trends and variability which could, in future, be associated to disease progression.

From a methodological viewpoint, we address the problem of choosing the most suitable model according to the biological property to analyse and to the formal techniques supported. This approach could be also helpful in the area of computational medicine, relatively to the prediction of bone-related diseases and more generally, of diseases where disruptions at the cellular scale affect the stability of the tissue and the organ scales. Finally, we showed how the quantitative verification of the stochastic model could provide effective diagnostic tools in the detection of defective remodelling dynamics occurring in osteoporosis and osteomyelitis.

5 HYBRID MODELLING OF DISEASE PROCESSES AND THERAPIES

Chapter Outline

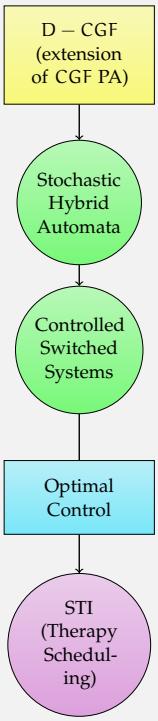

In this chapter, we investigate the use of formal languages and hybrid techniques in the modelling of disease processes and in the synthesis of treatment strategies. Hybrid models provide effective means for complex disease modelling where the action and dosage of a drug or a therapy could be meaningfully investigated: the infection dynamics can be classically described in a continuous fashion, while the scheduling of multiple drugs discretely.
From a methodological viewpoint, we define a process-algebraic language for specifying general disease processes and treatments, called D-CGF (an extension to the CGF process algebra), from which multiple semantics can be derived: stochastic hybrid automata and hybrid dynamical systems. Then, the application of control-theoretic tools is proposed in order to compute the optimal scheduling of multiple therapies.
The potentialities of our approach are shown in the case study of an epidemic model of the H1N1 influenza occurred in the US in 2009, where we seek to find the optimal combination of vaccination and antiviral treatments. By setting up multiple scenarios where we assign different costs/penalties to the two treatments, we found that a strategy of repeated pulse vaccinations is much more effective in controlling and counteracting the course of the infection at the population level than any strategy based on the antiviral treatment.

EPIDEMIC modelling is one of the most established tools for predicting the progress and the spread of a disease in large populations, thus providing useful suggestions to policy-makers to prevent and estimate the risk and control the outbreak of epidemics. The development of computational

methodologies and tools has provided major insights and explanation into the molecular and population processes that drive epidemics.

Infectious diseases can be broadly classified into three groups (Fig. 33): acute, latent persistent and chronic persistent. Acute diseases like the common cold, the Rhinovirus, the Yellow Fever, the Influenza or some strains of the Staphylococcus Aureus (Osteomyelitis) are characterized by a single disease episode after which they do not occur anymore. Latent persistent ones like the Herpes simplex, the Varicella-zoster or the Measles-SSPE arises also after the first disease episode and a non-infectious and latent period. Chronic persistent diseases (e.g. Hepatitis B, HIV, HTLV-1 leukemia, chronic Osteomyelitis) can protract their effects on the host organism for several years.

Epidemic models commonly divide the population into compartments representing different classes of individuals: Susceptible, Exposed, Infected and Recovered. According to the possible flows among such compartments, i.e. the stages of illness an individual can evolve into, different models arises, like the SIR (Susceptible $\rightarrow$ Infected $\rightarrow$ Recovered) model [84], SIS, SIRS, SEIR and SEIRS.

The SIR model represents the firstly proposed one, and via a set of coupled ODEs, computes the density of each compartment in a closed population, meaning that birth, death, immigration and emigration are not taken into account. Since then, several variants have been defined with more complex features: open population; stochasticity; spatial information; introduction of further compartments like the population of immune infants; or network models where the disease transmission occurs between connected nodes.

Similar compartments can be identified not only at the human population level, but also at the cellular population level, where the pathogen typically acts by infecting susceptible cells. As a matter of fact, infections are characterized by multiscale dynamics that affect the organism at multiple levels in the biological hierarchy, as shown on the left side of Fig. 34: at the *intracellular* level, in case of infection of a cell by a pathogen; at the *intercellular/cellular population* level, in case of infection of susceptible cells by infected cells; at the *tissue* level, when multi-cellular ensembles are involved; at the *organ/individual* level, when infection spreads to other parts of the body; and at the *human population* level, if the disease is transmitted among individuals. A further scale above the human population one could be the consciousness level for which several psychological and cognitive behaviour models exists. Just consider that psychological states like fear or stress can even affect (negatively) the immune system: a demonstration that all the scales in the biological hierarchy are intimately connected to each other. Their inherent

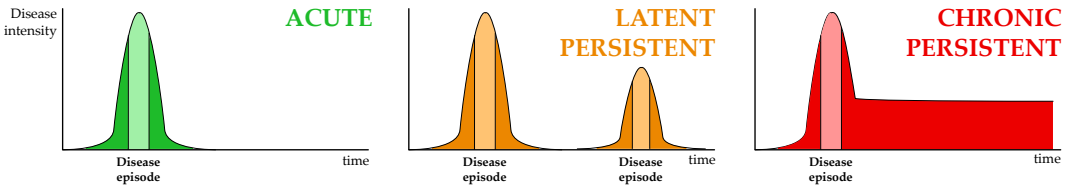

Figure 33: Simplified classification of infectious diseases. The disease intensity follows a Gaussian curve approximately partitioned in three stages. In the first one, the infection starts but any symptom is reported. In the second one called "disease episode" symptoms are reported and the disease can be transmitted to other individuals. In the last stage, the disease is over if it is acute or latent persistent. However some diseases can become chronic.

multiscale dynamics make the modelling of infective processes a challenging and intriguing field of research. Indeed, pathogens and infective agents generally act at the cellular scale, but they need to exploit mechanisms at the human population level to spread and survive in other host organisms.

Recent evidences [53] suggest a connection between cancer and infectious diseases according to which cancer cells behave like infectious agents and move from one host to another, in the case of canine transmissible venereal tumour. Generally cancer is not transmitted among individuals, although an important percentage of cancer deaths are due to infectious agents that, instead, enable the transmission at the human population level. In addition, even the non-infectious cancer is characterized by multiscale dynamics similar to infections, since metastases can occur and the disease spreads to different parts of the body.

Formal Languages, Hybrid Approaches and Control in Disease Modelling

We want to stress the role that hybrid modelling could play in unravelling the complexity of the multiscale dynamics occurring in infectious diseases. We refer to "hybrid modelling" not just with its classical meaning, i.e. the modelling of those systems characterized by the co-existence of continuous and discrete dynamics, but also with a methodological meaning. In multiscale systems different scales are typically approached with different methodologies, thus leading to the co-existence of heterogeneous modelling techniques, in other words to approaches that are methodologically hybrid. The cellular level is typically represented with agent-based or ordinary differential equation models, while the tissue and organ levels are often described using image-based finite element modelling (partial differ-

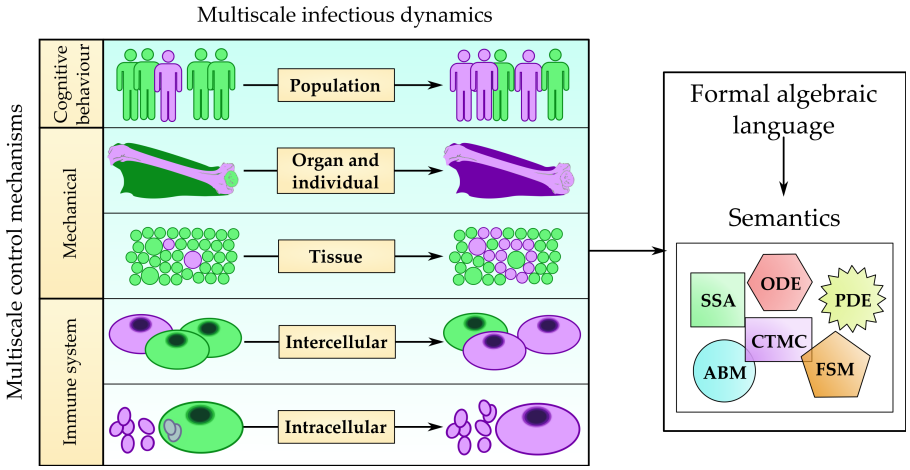

Figure 34: Modelling of multiscale infective dynamics. Infections involve the intracellular level (a cell infected by a pathogen); the intercellular level (infection among cells); the tissue level (infection among collections of cells); the organ level (infection among different parts of the body); and the human population level (transmission among individuals). Each biological scale can be implemented with different modelling techniques like Gillespie's SSA, Continuous Time Markov Chains, ordinary/partial differential equations, agent-based models, or finite state machines. Such heterogeneous semantics can be wrapped by a common formal language.

ential equations). In the context of disease modelling the determination of suitable intervention strategies, including drug and therapy administration, adds another level of description that affects multiple biological scales.

This kind of integrative models are composed of single-scale models, describing the biological process at different characteristic space-time scales, and scale bridging models, which define how the single-scale models are coupled to each other [150]. In this context, formal modelling languages can help in giving a general homogeneous formulation for the different scales in a multiscale biological system. In general, formal descriptions of biosystems cannot be directly executed or simulated, but can be encoded into multiple executable semantics (e.g. transition systems, differential equations and Markov chains).

In particular process-algebraic languages (introduced in Sect. 2.2) are a class of formal languages that, though initially developed for modelling software systems, has been extensively used and extended in order to describe biological systems. In a seminal paper [40], Cardelli showed that a subset of stochastic CCS, called *Chemical Ground Form (CGF)*, is powerful enough to encode both systems of reactions in the stoichiometric form and systems

of ordinary differential equations. Another example is given by the formal modelling framework discussed in Chapter 3, where a process-algebraic formulation of bone remodelling is encoded into a runnable stochastic agent-based model.

Consequently, formal languages could serve as a wrapping language able to homogeneously describe the different scales of a complex multiscale system, where each level can be instantiated into a runnable model according to the most suitable semantics, in the same spirit of the work presented in Chapter 4, where the dynamics of bone remodelling and bone pathologies are described with different semantics according to the biological property to analyse. Figure 34 sketches the idea of the heterogeneous semantics associated to a multiscale model of infection and described through a common formal language.

Furthermore, the importance of being hybrid in the classical sense is demonstrated by several biological evidences. For instance, genetic regulatory networks naturally exhibits hybrid dynamics, for which the continuous concentration of proteins is interrupted by the discrete switches dictated by changes in gene expression [13, 27, 67]. Moreover in population biology it happens that some species are present in high concentration, so they can be approximately modelled by continuous variables; conversely, small populations are opportunely modelled as discrete stochastic variables [94].

Another crucial aspect is related to the self-regulation and control of biological systems: in normal conditions, biological entities and functions are self-regulated and several multiscale control mechanisms naturally exists. One of the most striking example is the control operated by the immune system that protect the organism in case of disease. In fact, lymphocytes are able to detect the presence of a pathogen and produce an appropriate immune response by secreting immunoglobulins. However, in many severe diseases the immune system cannot apply an effective control anymore. Drugs and therapies represent a form of control which is external to the organism and is extremely significant when dealing with models of diseases that can be counteracted by appropriate medical interventions. The control operated by medical therapies can be much more effective than immune mechanisms, but has to take into account their (negative) impact on the organism due to possible side effects, by formulating appropriate control laws.

While drug administration strategies are determined at the human population level, the effect of a drug in the organism involves multiple lower scales (in most of the cases, the cellular and subcellular scale). Other examples of multiscale control are the mechanical control at the organ and tissue level that regulates the functioning of bone cells in the bone remod-

elling process; or in an infection scenario, the cognitive behaviour at the human level that avoids or limits the interactions with other individuals possibly affected by the disease. A work by Bagnoli et al. [7] embeds this aspect of human behaviour into a SIR epidemic model by allowing individuals to perceive the risk of being infected by ill neighbours. Therefore, the use of control-theoretic tools seems promising for describing the biological mechanisms of multiscale self-regulation and self-adaptiveness, as well as for implementing externally imposed control mechanisms.

STI PROBLEMS *Structured Therapy Interruption (STI)*, i.e. drug holiday, is the programmed interruption of a medication for a period of time. It has several advantages, e.g. regaining effectiveness after a period of continuous use and combinations of alternating therapies are typically administered (e.g. the HAART therapy for HIV).

We consider STI problems that, given a dynamic disease model, aims at finding an optimal scheduling of multiple drugs. The optimality of a therapy strategy is typically measured through an objective function that seeks to trade off the effectiveness of the treatment and its impact on the organism/patient, and current approaches solve the problem of finding such a drug cocktail by (non-linear, hybrid) optimal control techniques, where the controller represents the automated therapist and the disease or pathogen represents the controlled system.

In this chapter, we present a hybrid approach to the STI problem suitable for describing generic diseases and for scheduling optimal treatments. Hybrid models are able to effectively express this class of problems: disease dynamics are described in a continuous fashion, while the administration of multiple on-off therapies, discretely. We formulate disease processes by means of an extension to Cardelli's CGF process algebra, called *D-CGF (Disease CGF)*, where we consider two kind of processes: drugs (used to model treatments) and species (used to model the disease dynamics). From a D-CGF model, we formulate a method inspired by [26, 28, 31] to derive a hybrid semantics in terms of *Stochastic Hybrid Automata (SHA)*, where a location represents a possible combination of discretely-dosed drugs (a therapy) and where the disease dynamics under that particular therapy are given by a set of differential equations. From a SHA model, we show how to extract a semantics in terms of *hybrid dynamical systems*, obtained by assuming instantaneous transitions between different therapies, and where drug processes correspond to the discrete control inputs and species to the continuous state variables. Then, the control problem for finding the optimal treatment strategy is formulated for the non-linear hybrid dynamical system as a Model Predictive Control (MPC) problem and solved through an

approximate method based on the relaxation of the discreteness constraints, but able to synthesize (sub-)optimal discrete moves. Finally, we apply our methodology to a SIR model with vaccination and antiviral therapies for the case study of the pandemic influenza A(H1N1) occurred in the US in 2009, following [58] where a parametric study of disease control strategies is presented.

Related work

Examples of control-theoretic tools applied in the STI context include the synthesis of optimal HIV therapies [45, 46, 117, 147], and the optimization of hormone therapy for prostate cancer [140, 30]. A more formal perspective on this problem is provided in [115], where the authors present a timed automata-based model called *Cancer Hybrid Automata*, suitable to model the progression of cancer by discrete phenotypes (the states of the automaton) and the timed scheduling of drugs as control actions that can prevent the firing of discrete transition, i.e. the progression to a more critical state of the cancer.

State-of-the-art approaches in the control of hybrid non-linear models include *Multi-parametric Programming* [74], where the class of controllable models is limited to piecewise linear and piecewise affine systems; the methods proposed by Belta et al. [15, 68, 4] for the control with LTL-objectives of hybrid systems with multi-affine continuous dynamics, i.e. where non-linear terms are allowed only in the form of products of state variables. However, we will show that the above approaches cannot directly deal with the class of non-linear hybrid systems considered here. Hence, we opted for a method on the same line of [137, 147], based on transforming the hybrid control problem into a classical non-linear optimization problem.

The hybrid semantics we introduce for the D-CGF process-algebra was inspired by [26], where the authors extend the formal framework of CGF by defining a semantics in terms of hybrid automata [73], by identifying processes that can be treated as discrete control states, and keeping the usual continuous interpretation for the other processes. Several other methods for associating hybrid semantics to quantitative process algebras have been proposed, among which [61, 22, 29].

Differently from [112], where a stochastic process algebra and its continuous semantics are used to describe a classical epidemic model, we attempt to provide a formal framework for generic disease modelling, which supports multiple hybrid semantics and integrates with control-theoretical methods enabling the optimal scheduling of multiple drugs.

Structure of the chapter

SECTION 5.1 We give an overview of the CGF stochastic process algebra, together with the methods for deriving the CTMC and the ODE semantics. A closed population SIR model will serve as running example.

SECTION 5.2 We define D-CGF, a CGF extension for modelling disease and drug administration processes and we specify in D-CGF a open population SIR model with controls (vaccination and antiviral drugs).

SECTION 5.3 We provide a constructive procedure based on the stoichiometric matrix of the D-CGF to obtain the hybrid semantics in terms of Stochastic Hybrid Automata, and from the latter, in terms of Hybrid Dynamical Systems.

SECTION 5.4 We formulate the Model Predictive Control problem for the optimal scheduling of drugs over the hybrid semantics of the SIR epidemic model, and we briefly discuss the embedding approach, the technique we employ for the control of hybrid non-linear systems.

SECTION 5.5 We report and discuss the optimal therapy administration strategies computed for the SIR model of the influenza H1N1 occurred in the US in 2009, comparing different treatment scenarios obtained by assigning different costs/penalties to drugs.

5.1 CGF, A QUANTITATIVE EXTENSION TO CCS

Stochastic process algebras extend classical ones with quantitative information in form of action rates and have associated a Continuous Time Markov Chains (CTMC) semantics from which a continuous and less computationally demanding approximation in terms of ODE can be derived. The multiplicity of semantics it supports has made formal process-algebraic languages one of the most used tools in biological modelling.

In this section, we illustrate the *Chemical Ground Form (CGF)* [40, 41, 44], a subset of stochastic CCS conceived to represent the dynamics of chemical reactions. CGF provides a key example of how multiple semantics can be derived from an algebraic specification, since it can be encoded into systems of reactions, CTMC and ODEs. In [41], Cardelli also shows how to translate systems of chemical reactions back to stochastic processes and demostrates that the ODE and CTMC semantics of chemical reactions and CGF are equiv-

alent. In this section, we will just show the encoding from the process algebra to the different semantics, and we will employ a slightly different notation, closer to the one presented in [26].

A CGF model consists of a set of process definitions E, called *reagents*, and of an initial network configuration P, called *solution*. Process definitions in E are of the form $X = M$, where M, named *molecule*, is the summation (alternative composition) of action-prefixed terms. In the following, the notation $E.X$ will be used to indicate the molecule defined by X in E, and $M.i$ to indicate the i-th summand of a molecule M. We also refer to X as the *species name*. Below, we describe the formal syntax of a CGF model.

Definition 5.1.1 (CGF model)**.** *A CGF model* (E, P) *is defined by the following grammar*

$E ::=$	$\mathbf{0} \mid X = M, E$	*Reagents*
$M ::=$	$\mathbf{0} \mid \pi.P + M$	*Molecule*
$P ::=$	$\mathbf{0} \mid X \| P$	*Solution*
$\pi ::=$	$\tau^r \mid ?x^r \mid !x^r$	*Actions* ($r \in \mathbb{R}^+$)
$CGF ::=$	(E, P)	*Chemical Ground Form*

DELAYS, INTERACTIONS AND RATES We denote with Π_E be the set of stochastic actions occurring in a set of reagents E. From now on, we implicitly assume that Π is parametric with respect to E and we simply write Π. Any action $\pi \in \Pi$ is indexed by a stochastic rate $r \in \mathbb{R}^+$ (i.e. the rate of the exponential distribution determining its duration), and can be one of the following two types: τ, an *internal action* (or *delay*); or x, an *interaction* (or *synchronization/communication*) on a channel x. We equip our formal framework with a function $\rho : \Pi \to \mathbb{R}^+$, associating stochastic rates to actions. For $\pi \in \Pi$, we will often use the more succinct notation π^r, in place of $\pi^{\rho(\pi)}$. As usual, each interaction x is characterized by an *input action* $?x$ and by an *output action* $!x$. Therefore, the input and output actions associated to an interaction $x \in \Pi$ possess, by definition, the same stochastic rate $\rho(x)$. Technically, Π just contains delay actions and interactions, thus excluding input and output actions. Finally, the function $\mathit{actions}(X) \subseteq \Pi$ gives the set of actions occurring in the species X.

As in [26], we assume that any interaction $x \in \Pi$ occurs once in a list of reagents E, implying that there is at most one pair of actions $?x^r$ and $!x^r$. Moreover, we label every internal action with a unique index. In this way, any action in $\pi \in \Pi$ uniquely identifies the process term(s) prefixed by π in a list of reagents E.

Note that, differently from CCS, internal actions (fired independently) are explicitly distinguished from input and output actions (that require a syn-

chronization). This is one of the reason why the algebra does not have a restriction operator, most of the times used in CCS to force synchronizations.

5.1.1 Chemical Reaction System of a CGF

We discuss the procedure to derive a system of chemical reactions from a CGF specification. Due to the dyadic nature of the calculus, we will see that only unary and binary reactions are possible. However, this is not a major limitation in terms of biological and chemical meaningfulness. Indeed as pointed out in [66], in normal conditions, reactions involving three or more reagents can generally be reduced to a chain of bimolecular and monomolecular reactions, possibly involving additional reagents.

Let us provide a formal definition of a system of chemical reactions.

Definition 5.1.2 (Chemical reaction system)**.** *A* system of chemical reactions *is an indexed set of reactions* $C = \{j : react(j) \to_{r_j} prod(j)\}$*, with* $j = 1, \ldots, n$*, where:*

- $react(j)$ *is the* multiset of species consumed *by reaction* j*;*
- $prod(j)$ *is the* multiset of species produced *by reaction* j*;*
- $r_j \in \mathbb{R}^+$ *is the* reaction rate*.*

If a reaction j is unary, then $react(j) = \{X\}$, which is written in chemical notation simply as X. If j is instead binary, $react(j) = \{X_h, X_l\}$, written also $X_h + X_l$ (possibly with $h = l$).

The system of chemical reactions associated to a list of CGF reagents E is built by encoding internal actions as unary reactions and synchronizations as binary reactions. To this aim, we extend the $react$ and $prod$ functions to work with CFG actions. We recall that any action occurs only once in a list of reagents E. Then, given a delay action $\tau \in \Pi$, we are able to identify within E the only species $X = \ldots + \tau^r.(X_1 \| \ldots \| X_n) + \ldots$ with a term prefixed by τ ($\tau^r.(X_1 \| \ldots \| X_n)$). Then, the multisets of species consumed and produced by action τ are:

$$react(\tau) = \{X\} \qquad prod(\tau) = \{X_1, \ldots, X_n\} \qquad \text{(unary)}$$

Similarly, given an interaction $x \in \Pi$, let $X = \ldots + ?x^r.(X_1 \| \ldots \| X_n) + \ldots$ and $Y = \ldots + !x^r.(Y_1 \| \ldots \| Y_m) + \ldots$ be the species and the terms involved in the interaction x. In this case, $react(x)$ and $prod(x)$ are defined as:

$$react(x) = \{X, Y\} \qquad prod(x) = \{X_1, \ldots, X_n, Y_1, \ldots, Y_m\} \qquad \text{(binary)}$$

At this stage, the derivation of a set of chemical reactions comes in a straightforward way as follows.

Definition 5.1.3 (From CGF to chemical reaction systems)**.** *Let* (E, P) *be a CGF model. The system of chemical reactions associated to* E, C_E, *is defined as*

$$C_E = \{\pi : react(\pi) \rightarrow_{\rho(\pi)} prod(\pi) \mid \pi \in \Pi\}$$

5.1.2 CTMC Semantics

We illustrate how to derive a discrete semantics for CGF in terms of Continuous Time Markov Chains (CTMCs) through the following procedure: firstly, a labelled transition system is obtained from a CGF model by the application of operational semantics rules; secondly, the CTMC is extracted from the LTS.

Before discussing the procedure, some preliminary concepts and notation need to be introduced. Let P be a solution. We denote with $P^\dagger$ the solution P in *normal form*, which is obtained by sorting the variables in lexicographical order, possibly with repetitions. We denote with $\mathbb{P}^\dagger$ the *set of all the normalized solutions*. Normalized solutions will constitute the states of the LTS semantics and consequently, of the CTMC semantics.

Given a solution P, $P.m$ indicates the m-th variable occurring in P, and $P \setminus (m_1, \ldots, m_n)$ the solution obtained by removing from P the molecules at positions $m_1, \ldots, m_n$[1].

We now give a description of the LTS semantics. Let $P^\dagger$ be a normalized solution and its m-th and n-th molecule be defined by X and Y, respectively ($P^\dagger.m = X$ and $P^\dagger.n = Y$). We distinguish two possible transitions: those generated from unary reactions, formalized by the operational semantics rule UNARY in Table 13; and those generated from binary reactions, formalized by rule BINARY.

TRANSITIONS FROM UNARY REACTIONS Let $\tau \in \Pi$ and X be the species where action τ occurs (i.e. $\tau \in actions(X)$), implying that X can choose to perform an internal action with rate $\rho(\tau)$ and then evolve into the parallel composition of the species in $prod(\tau)$, written as $\|_{Q \in prod(\tau)} Q$. Then, in the LTS semantics there will be a transition from $P^\dagger$ to the normalized solution obtained from P by substituting X with the parallel composition of the products of action τ, which is denoted by $(P^\dagger \setminus m \|_{Q \in prod(\tau)} Q)^\dagger$. The transition

1 Even if the dotted notations above introduced could be confused with the action prefixing operator of the algebra, there is no ambiguity because of the different capitalization of the symbols

label will be given by $\{m\}, \tau, \rho(\tau)$, i.e. by a singleton identifying the term in the solution responsible for firing the transition, by the action fired, and by its rate.

TRANSITIONS FROM BINARY REACTIONS Let $x \in \Pi$ and X and Y be the pair of species involved in the synchronization x^r, i.e. $X = \ldots + ?x^r.Q + \ldots$ and $Y = \ldots !x^r.Q' + \ldots$ (or $X = \ldots + !x^r.Q + \ldots$ and $Y = \ldots + ?x^r.Q' + \ldots$). The resulting transition will be between $P^\dagger$ and $(P^\dagger \setminus (m, n) \|_{Q \in prod(x)} Q)^\dagger$, where the target solution is obtained from $P^\dagger$ by replacing X and Y with the parallel composition of the products of action x. In this case, the label is $\{m, n\}, x, \rho(x)$ and is composed of the 2-set identifying in the solution the involved pair of terms, the action fired and its rate.

TRANSITIONS LABELS Let L be the set of labels used to identify the position(s) in a solution of the term(s) involved in the execution of an action. Since only two forms are possible, $\{m\}$ and $\{m, n\}$, we define L as:

$$L = \{\{m\} \mid m \in \mathbb{N}\} \cup \{\{m, n\} \mid m, n \in \mathbb{N}\}$$

At this stage, we have the ingredients to formally define the semantics of a CGF model.

Definition 5.1.4 (LTS semantics of a CGF)**.** *The discrete semantics of a Chemical Ground Form* (E, P_0) *is a labelled transition system* $\Psi_{E,P_0} = (S, s_{init}, Act, \rightarrow)$ *where:*

- $S \subseteq \mathbb{P}^\dagger$ *is the set of states;*
- $s_{init} = P_0^\dagger \in S$ *is the initial state;*
- $Act \subseteq L \times \Pi \times \mathbb{R}^+$ *is the set of labels;*
- $\rightarrow \subseteq S \times Act \times S$ *is the transition relation, obtained by applying the rules in Table 13 to the initial state* s_{init}.

Finally, the Continuous Time Markov Chain associated to the LTS Ψ of a CGF model has the same set of states and initial state as Ψ, while the stochastic rate between any two states is calculated by summing up the rates of all the transitions of Ψ between the same two states.

Definition 5.1.5 (CTMC semantics of a CGF)**.** *Let* (E, P_0) *be a Chemical Ground Form and* $\Psi_{E,P_0} = (S, s_{init}, Act, \rightarrow)$ *be its LTS semantics. The CTMC semantics of*

$$\textsc{Unary}\ \frac{P.m = X \quad \tau \in actions(X)}{P \xrightarrow{\{m\},\tau,\rho(\tau)} (P \setminus m \|_{Q \in prod(\tau)} Q)^{\dagger}}$$

$$\textsc{Binary}\ \frac{P.m = X \quad P.n = Y \quad x \in actions(X) \cap actions(Y)}{P \xrightarrow{\{m,n\},x,\rho(x)} (P \setminus (m,n) \|_{Q \in prod(x)} Q)^{\dagger}}$$

Table 13: Inference rules for the LTS semantics of a CGF (P solution, $x, \tau \in \Pi$).

(E, P_0) *is a tuple* $(S, s_{init}, \mathbf{R})$ *where* $\mathbf{R} : S \times S \to \mathbb{R}^{\geqslant 0}$ *is the transition rate matrix, defined for each* $P, Q \in S$ *as follows:*

$$\mathbf{R}(P, Q) = \sum_{P \xrightarrow{L_i,\pi_i,r_i} Q} r_i$$

5.1.3 ODE Semantics

In this section we illustrate how to encode CGF processes into a system of differential equations following the *law of mass action*, by which the rate of a reaction is proportional to the concentration of its reactants.

Intuitively, the ODE system $\mathbf{X}$ associated to a CGF model (E, P) contains, for each species X defined in E, a state variable X representing the concentration of process X. Then, net change rate of X, denoted with $\dot{X}$, is increased by actions producing X and decreased by actions consuming X.

STOICHIOMETRIC MATRIX The procedure for extracting a system of ODEs requires to build the so-called *stoichiometric matrix* M_E, which has one row for each species in E and one column for each action. Let $\pi \in \Pi$ and let $\Delta(\pi, X) = \#(X, prod(\pi)) - \#(X, react(\pi))$ denote the net variation of X due to π, where with $\#(X, P)$ we denote the number of X occurring in the population P. Then, for each species X defined in E and action $\pi \in \Pi$, we define $M_E(X, \pi) = \Delta(\pi, X)$.

RATE VECTOR The *rate vector* ϕ_E has an element for each action $\pi \in \Pi$, so that $\phi_E(\pi)$ quantifies the mass action rate of π, obtained as the product

of the action rate $\rho(\pi)$ and the concentrations of the reactants in $react(\pi)$. Specifically, for each $\pi \in \Pi$, $\phi_E(\pi)$ is calculated as:

$$\phi_E(\pi) = \begin{cases} 0 & \text{if } react(\pi) = \emptyset \\ \rho(\pi) \prod_{X \in react(\pi)} X & \text{otherwise} \end{cases}$$

The formulation of ϕ_E presented here is based on [40], while in [26] a different version is proposed: if $react(\pi) = \{X, X\}$ that is, if π represents a *homeo binary reaction*, $\phi_E(\pi)$ is given by $\rho(\pi)X(X-1)$ and not by $\rho(\pi)X^2$, because the authors take into account the fact that one copy of X is involved in the reaction and therefore is subtracted in the second factor from the total concentration of X.

SYSTEM OF ODES Finally, the system of differential equations $\dot{\mathbf{X}}$ is given by the product of the stoichiometric matrix and of the rate vector, where the initial state $\mathbf{X}(0)$ follows from the multiplicity of the species in the initial solution P_0:

$$\dot{\mathbf{X}} = M_E \cdot \phi_E \qquad X(0) = \#(X, P_0), \text{ for all } X \text{ defined in } E$$

5.1.4 SIR Example

In this section we illustrate the CGF process algebra and its three semantics with the original version of the SIR (Susceptible → Infected → Recovered) epidemic model [84], introduced also in a qualitative version in Section 2.2.4. The dynamics of the model is described by the following rules:

- a susceptible individual (species S) can come into contact with an infected individual and become infected, with rate β;
- an infected individual (species I) can recover with rate ν; and
- a recovered individual (species R) does nothing since he/she cannot be infected anymore.

The corresponding CGF model (E, P) is defined as:

$$E: \begin{array}{ll} S = & ?i^{\beta}.I \\ I = & !i^{\beta}.I + \tau_r^{\nu}.R \\ R = & \mathbf{0} \end{array} \qquad P: P_0$$

where P_0 is the initial solution, at the moment left unspecified. The set of actions Π is composed by the action that turns an infected individual into

a recovered one, τ_r; and by i, the interaction representing the infection of a susceptible by an infected individual.

CHEMICAL REACTION SYSTEM SEMANTICS In order to derive the system of chemical reactions C_E associated to the SIR model (E, P), we just need to compute the species consumed (function $react$) and those produced (function $prod$) by every action $\pi \in \Pi$:

$$\begin{array}{ll} react(i) = \{I, S\} & prod(i) = \{I, I\} \\ react(\tau_r) = \{I\} & prod(\tau_r) = \{R\} \end{array} \qquad C_E = \left\{ \begin{array}{ll} i: & I + S \to_\beta I + I, \\ \tau_r: & I \to_\nu R \end{array} \right\}$$

CTMC SEMANTICS According to the method explained in Section 5.1.2, the CTMC of a CGF model (E, P) is derived from the LTS semantics of (E, P) by summing the rates of the transitions connecting the same pairs of states. We take as initial state the normalized solution $I \| I \| S$, corresponding to a population of two infected individuals and a susceptible one.

The resulting LTS and CTMC are shown in Figure 35, while Figure 36 (a) illustrates a path of the CTMC model simulated with the PRISM model checker [90].

ODE SEMANTICS The stoichiometric matrix M_E, the rate vector ϕ_E and the resulting system of differential equations for the SIR model are shown below. Figure 36 (b) displays the simulated trajectories for the SIR equations.

$$M_E = \begin{array}{c} \\ S \\ I \\ R \end{array} \begin{array}{c} \begin{array}{cc} i & \tau_r \end{array} \\ \begin{pmatrix} -1 & 0 \\ 1 & -1 \\ 0 & 1 \end{pmatrix} \end{array} \qquad \phi_E = \begin{array}{c} i \\ \tau_r \end{array} \begin{pmatrix} \beta IS \\ \nu I \end{pmatrix} \qquad \begin{array}{c} \dot{S} = -\beta IS \\ \dot{I} = \beta IS - \nu I \\ \dot{R} = \nu I \end{array}$$

5.2 D-CGF: A PROCESS ALGEBRA FOR DISEASE MODELLING

In this part we propose a variant of the CGF process algebra, suitable to describe models of complex diseases in a process-algebraic fashion, where the concepts of control and intervention over the disease have a primary role. We call this language the *Disease Chemical Ground Form (D-CGF)*. While keeping the syntax of D-CGF close to that of CGF, we provide a constructive procedure for deriving a semantics in terms of stochastic hybrid automata,

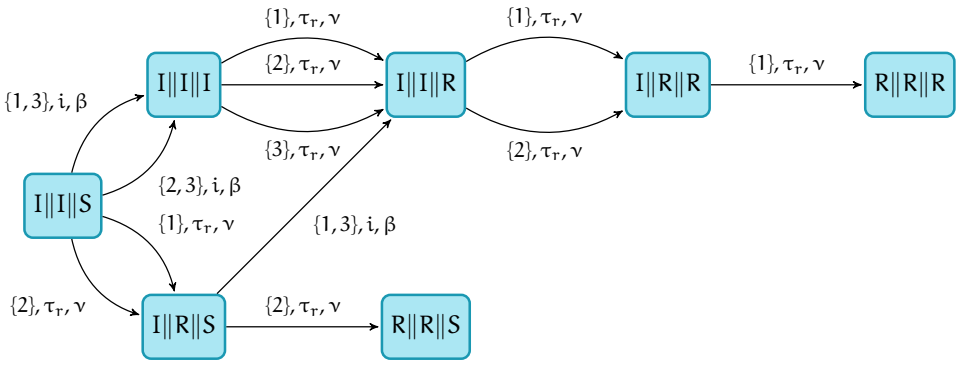

(a) LTS semantics

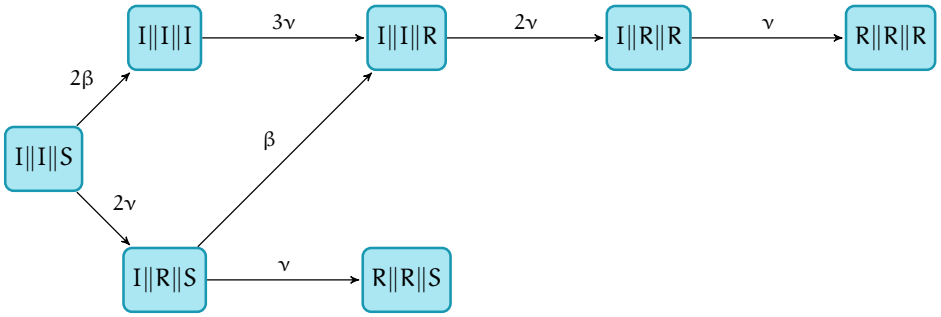

(b) CMTC semantics

Figure 35: LTS and CTMC semantics of the SIR model in CGF, with initial solution $P = I||I||S$.

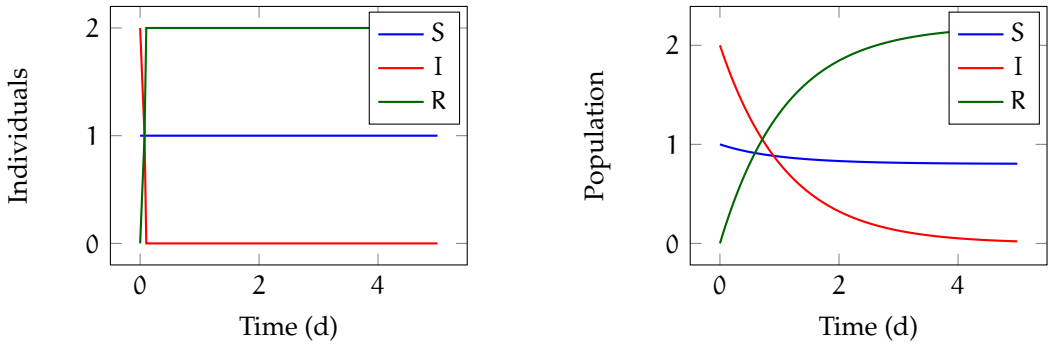

(a) CTMC simulation

(b) ODE simulation

Figure 36: Simulation of the CTMC and ODE versions of the SIR model ($S(0) = 1$, $I(0) = 2$, $R(0) = 0$, $\beta = 0.1$, $\nu = 1$).

from which a hybrid dynamical system that approximates the automata is built.

A D-CGF model is given by a CGF model, i.e. by a list of reagents E and an initial solution P, together with a list of *drug definitions* D and an *initial therapy* T. In the following definition, we highlight the additional terms that extend the CGF process algebra.

Definition 5.2.1 (D-CGF model)**.** *A D-CGF model* (E, P, D, T) *is defined by the following grammar*

$$
\begin{array}{rll}
E ::= & \mathbf{o} \mid X = M, E & \textit{Reagents} \\
M ::= & \mathbf{o} \mid \pi.P + M & \textit{Molecule} \\
P ::= & \mathbf{o} \mid X \| P & \textit{Solution} \\
\pi ::= & \tau^r \mid ?x^r \mid !x^r & \textit{Actions } (r \in \mathbb{R}^+) \\
D ::= & \mathbf{o} \mid Y = C, D & \textit{Drug definitions} \\
C ::= & \mathbf{o} \mid \pi.T + C & \textit{Therapy} \\
C ::= & \mathbf{o} \mid Y \| T & \textit{Combination of therapies} \\
D-CGF ::= & (E, P, D, T) & \textit{D-CGF model}
\end{array}
$$

Intuitively, processes defined in the CGF fragment of D-CGF are interpreted as continuous variables in the hybrid semantics. Indeed, they are used to describe species that collectively represent the population in the disease model. Different species can describe for instance the various compartments of an epidemic model, a pathogen, or a particular mutation.

On the other hand, drugs are processes that describe interventions on the disease scenario, and a therapy is defined as a particular combination of drugs. Drug processes could represent for instance the dosage of a drug or a change in the environment that *discretely* alter the disease dynamics. Therapy processes are subject to some restrictions (see Sect. 5.3) in order to be interpreted as *discrete elements*. In particular, they will constitute the *discrete locations* in the stochastic hybrid automata semantics, and the *discrete control inputs* in the hybrid dynamical systems semantics.

5.2.1 Epidemic Model with Controls

We illustrate D-CFG by means of an extension to the epidemic example presented in Section 5.1.4, even if this language is suitable to describe also models of virus infection, infectious cancers or other kinds of diseases where discrete intervention policies has to be modelled.

In particular, we consider a variant of the SIR model with open population (i.e. with births and deaths), and with two kinds of drugs, D1 and D2, that makes immune the susceptible population and increase the recovery rate of

infected individuals, respectively. $D1_{on}$ ($D2_{on}$) and $D1_{off}$ ($D2_{on}$) denote the drug being administered or not, respectively. Therefore, D1 can be thought as a *vaccination* that makes immune the susceptible individuals, while D2 as an *antiviral drug* for combating the course of the disease.

The resulting D-CGF model (E, P, D, T) is defined as follows:

$$E: \begin{array}{ll} S = & \tau^{b}_{b_S}.(S \| S) \ + \ \tau^{\mu}_{d_S}.\mathbf{o} + ?i^{\beta}.I + ?j^{\rho}.R \\ I = & \tau^{b}_{b_I}.(I \| S) \ + \ \tau^{\mu}_{d_I}.\mathbf{o} + !i^{\beta}.I \ + \ \tau^{\nu}_{r}.R + ?h^{k}.R \\ R = & \tau^{b}_{b_R}.(R \| S) \ + \ \tau^{\mu}_{d_R}.\mathbf{o} \end{array} \qquad P: \ P_0$$

$$D: \begin{array}{ll} D1_{off} = & \tau^{r1_{on}}_{1on}.D1_{on} \\ D1_{on} = & !j^{\rho}.D1_{on} \ + \ \tau^{r1_{off}}_{1off}.D1_{off} \\ D2_{off} = & \tau^{r2_{on}}_{2on}.D2_{on} \\ D2_{on} = & !h^{k}.D2_{on} \ + \ \tau^{r2_{off}}_{2off}.D2_{off} \end{array} \qquad T: \ D1_{off} \parallel D2_{off}$$

where the initial therapy T is the combination of $D1_{off}$ and $D2_{off}$; and P_0 is the initial solution, at the moment left unspecified. Here Π includes actions occurring in both molecule and drug processes (thus implicitly intended as $\Pi_{E,D}$) and is composed by:

- the internal actions τ_{b_S}, τ_{b_I} and τ_{b_R} which are responsible for the birth of new susceptible individuals from S, I and R, respectively;
- the delays τ_{d_S}, τ_{d_I} and τ_{d_R}, implementing the death of a susceptible, of an infected and of a recovered individual, respectively;
- the recovery action, τ_r;
- the infection action, i;
- the interaction j between S and the drug $D1_{on}$, describing the vaccination of a susceptible individual;
- the interaction h between I and the drug $D2_{on}$;
- the internal actions τ_{1on}, τ_{1off} and τ_{2on}, τ_{2off} used to turn on and turn off D1 and D2, respectively.

The corresponding system of chemical reactions $C_{E,D}$ is obtained by computing the processes consumed and produced by every action $\pi \in \Pi$ and is shown below:

$$C_{E,D} = \left\{ \begin{array}{ll} i: & I + S \to_{\beta} I + I, \\ \tau_r: & I \to_{\nu} R, \\ \tau_{b_S}: & S \to_{b} S + S, \\ \tau_{b_I}: & I \to_{b} I + S, \\ \tau_{b_R}: & R \to_{b} R + S, \\ \tau_{d_S}: & S \to_{\mu} \emptyset, \\ \tau_{d_I}: & I \to_{\mu} \emptyset, \\ \tau_{d_R}: & R \to_{\mu} \emptyset, \\ j: & D1_{on} + S \to_{\rho} D1_{on} + R, \\ h: & D2_{on} + I \to_{k} D2_{on} + R, \\ \tau_{1on}: & D1_{off} \to_{r1_{on}} D1_{on}, \\ \tau_{1off}: & D1_{on} \to_{r1_{off}} D1_{off}, \\ \tau_{2on}: & D2_{off} \to_{r2_{on}} D2_{on}, \\ \tau_{2off}: & D2_{on} \to_{r2_{off}} D2_{off} \end{array} \right\}$$

In the following, we will omit the purely discrete and the purely continuous semantics of a generic D-CGF model (E, P, D, T), which is the same as the CGF model $(E \cup D, P \| T)$, obtained by combining the CGF components with the therapy components of the D-CGF model.

5.3 HYBRID SEMANTICS OF D-CGF

In order to interpret drug terms in D as discrete components, we need to identify collections of terms in which exactly one term is active in every therapy reachable from the initial one. We call such a collection a *Switching Drug (SD)*, described in Definition 5.3.1. Intuitively, a switching drug models a discrete component whose terms represent its internal states, since exactly one of them is active at each step.

Let D' be a SD. Condition 1 of Def. 5.3.1 states that every action has to conserve the number of terms in D'. We also exclude synchronizations between drug terms within D' (condition 2 of Def. 5.3.1). Clearly, if just one term of D' is allowed to be active at each time, no synchronizations can occur between any two terms in D'. Let $Y, Y' \in D'$. We also require any action making term Y evolve into Y' to be internal and not to involve other processes (condition 3). Such an action is also called a *switch*.

Then, we say that a set of drug definitions D is well formed if it can be partitioned into a set of switching drugs each of them having only one term active in the initial therapy (Def. 5.3.2). We provide a constructive procedure to calculate the set of switching drugs of a D-CGF model, based on

its stoichiometric matrix and on an automata-like structure called SD-graph. Finally, the method presented in Sect. 5.1.3 for deriving the ODE semantics of a CGF model is adapted with the notion of SD-graph in order to distil multiple hybrid semantics, namely Stochastic Hybrid Automata and Hybrid Dynamical Systems.

Definition 5.3.1 (Switching Drug)**.** *Let* (E, P, D, T) *be a D-CGF model, and* $D' \subseteq D$ *a set of drug terms*[2]*.* D' *is a* Switching Drug (SD) *if for each action* $\pi \in \Pi$ *the following conditions hold:*

1. π *conserves the number of terms in* D'*:* $\#(D', \mathtt{react}(\pi)) = \#(D', \mathtt{prod}(\pi))$*;*
2. π *involves at most one reagent in* D'*:* $\#(D', \mathtt{react}(\pi)) \leqslant 1$*; and*
3. *for any drug term* Y *of* D' *in* $\mathtt{react}(\pi)$*, if there exists a term* $Y' \in D'$ *different from* Y *and in* $\mathtt{prod}(\pi)$*, then* Y *and* Y' *are the only reactant and product of* π*, respectively:*

$$\forall Y \in D'.\, (Y \in \mathtt{react}(\pi) \;\wedge\; \exists Y' \in D'.(Y \neq Y' \wedge Y' \in \mathtt{prod}(\pi)) \implies \mathtt{react}(\pi) = \{Y\} \;\wedge\; \mathtt{prod}(\pi) = \{Y'\})$$

Note that conditions 1+2 of the definition of switching drug additionally imply that π involves at most one product in D'. Stated differently, condition 1 tells that there are no actions able to modify the number of active terms in D', and thus that the internal state of the SD D' can be changed only by actions having in its reactants a term in D'. Finally, condition 3 requires that every action causing the switch from Y to Y' has to be an internal action of Y, by the constraint $\mathtt{react}(\pi) = \{Y\}$ on the right-hand side of the implication.

Definition 5.3.2 (Well-formed drug definitions)**.** *Let* (E, P, D, T) *be a D-CGF model.* D *is* well-formed *if there exists a partition* $\mathcal{D} = \{D_1, \ldots, D_n\}$ *of* D *such that, for all* $i = 1, \ldots, n$*:*

1. D_i *is a switching drug; and*
2. *exactly one term of* D_i *is active in the initial therapy* T*:*

$$\#(D_i, T) = \sum_{Y \in D_i} \#(Y, T) = 1$$

2 With abuse of notation, we treat the list of drug definitions D as a set.

In other words, D is a well-formed set of drug definitions if it can be partitioned into a set of switching drugs $\mathcal{D}$, and each $D_i \in \mathcal{D}$ is such that exactly one term of D_i is active in the initial therapy. This in turn implies that exactly one term of D_i is active in every reachable configuration, because actions of a SD conserve the number of active terms in that SD.

As pointed out also in [26], Petri Nets could have been similarly applied in order to study the conservation properties in a switching drug. In particular, a set of switching drugs could be seen as a set of *strictly conservative* (i.e. with a constant number of tokens) and *1-bounded* (i.e. the maximum number of token is 1) Petri Nets.

Proposition 5.3.3. *Let* (E, P, D, T) *be a D-CGF model,* $M_{E,D}$ *be the associated stoichiometric matrix,* M_D *be the elements of* $M_{E,D}$ *restricted to* D *and* M_E *be those restricted to* E. D *is a switching drug if the following conditions hold for any* $\pi \in \Pi$*:*

1. *Conservation of terms in* D*:* $\sum_{Y \in D} M_D(Y, \pi) = 0$*;*
2. $\sum_{Y \in D} M_D(Y, \pi)^2 \leqslant 2$*;*
3. *Exclusive switch:* $\forall Y \in D.\ (M_D(Y, \pi) = -1 \implies (\forall X \in E.\ M_E(X, \pi) = 0 \wedge \pi$ *internal*$))$.

Proof. See Appendix A.1. □

Corollary 5.3.4 (Admissible values of stoichiometric matrix)**.** *Let* (E, P, D, T) *be a D-CGF model and* M_D *be the associated stoichiometric matrix restricted to* D. *If conditions 1 and 2 of Prop. 5.3.3 hold, then for any action* $\pi \in \Pi$ *and any term* $Y \in D$,

$$M_D(Y, \pi) \in \{-1, 0, 1\}$$

Proof. If for any action $\pi \in \Pi$, the sum of the squared elements of the π-th column of M_D is less than or equals to 2, then there are at most two terms, Y and Y', such that $M_D(Y, \pi) \in \{-1, 1\}$ and $M_D(Y', \pi) \in \{-1, 1\}$, and for every other Y'' different from Y and Y', $M_D(Y'', \pi) = 0$. Moreover, by the conservation property, the values $M_D(Y, \pi)$ and $M_D(Y', \pi)$ are necessarily different. □

Note that such conditions on the stoichiometric matrix are not sufficient to ensure that D is well-formed. Recalling that D is well-formed if it can be partitioned into a set of switching drugs, such conditions consider only the trivial partition $\{D\}$, and we cannot show just from the stoichiometric matrix that exactly one term in D is active in the initial configuration.

The algorithm for extracting the SDs consists in building a graph called *SD-graph*, whose nodes are process terms in D and whose arcs connect pairs (Y_1, Y_2) of terms that are involved in a *switch*, i.e. such that $M_D(Y_1, \pi) = -1$ and $M_D(Y_2, \pi) = 1$ for some action π. Arcs are labelled with the action and its rate.

Definition 5.3.5 (SD-graph)**.** *Let* (E, P, D, T) *be a D-CGF model and* M_D *be the stoichiometric matrix restricted to* D*. The* SD-graph $\mathcal{G}_{M_D} = (D, \rightarrow)$ *associated to* M_D *is a directed graph where vertices are the terms in* D *and the set of edges is defined as follows:*

$$\rightarrow = \{(Y_1, \pi, r, Y_2) \in D \times \Pi \times \mathbb{R}^+ \times D \mid M_D(Y_1, \pi) = -1,\ M_D(Y_2, \pi) = 1,\ r = \rho(\pi)\} \quad (12)$$

We show how to check the well-formedness of D by considering the set of connected components of $\mathcal{G}_{M_D}$, denoted by $C(\mathcal{G}_{M_D}) = \{G_1, \ldots, G_n\}$. Note that the sets of nodes of the connected components in the SD-graph $\mathcal{G}_{M_D}$ form, by definition, a partition of D. The strategy will consist in showing that if D is a switching drug, or equivalently the stoichiometric matrix $M_{E,D}$ meets the conditions at Prop. 5.3.3, then the sets of nodes of $G_1, \ldots, G_n$ are also switching drugs. This will be shown in Lemma 5.3.6. At that stage, for ensuring that D is well-formed, we would just need to impose that exactly one term in each set of nodes in $C(\mathcal{G}_{M_D})$ is active in the initial therapy T, as illustrated in Theorem 5.3.7.

Lemma 5.3.6. *Let* (E, P, D, T) *be a D-CGF model,* M_D *be the stoichiometric matrix restricted to* D*,* $C(\mathcal{G}_{M_D}) = \{G_1 = (D_1, \rightarrow_1), \ldots, G_n = (D_n, \rightarrow_n)\}$ *be the set of connected components of the associated SD-graph* $\mathcal{G}_{M_D}$*. Then, if* D *is a switching drug, every set of nodes* D_i *in* $C(\mathcal{G}_{M_D})$ *is a switching drug.*

Proof. See Appendix A.2. □

Theorem 5.3.7. *Let* (E, P, D, T) *be a D-CGF model,* $M_{E,D}$ *be the associated stoichiometric matrix and* $C(\mathcal{G}_{M_D}) = \{G_1 = (D_1, \rightarrow_1), \ldots, G_n = (D_n, \rightarrow_n)\}$ *be the connected components of the corresponding SD-graph. Then,* D *is well formed if the following conditions hold:*

1. $M_{E,D}$ *meets the conditions at Prop. 5.3.3;*
2. *for each set of nodes* D_i *in* $C(\mathcal{G}_{M_D})$*, there is exactly one term in* D_i *active in the initial therapy:* $\#(D_i, T) = 1$*.*

Proof. According to Lemma 5.3.6, condition 1 implies that every set of nodes D_i in the connected components of $\mathcal{G}_{M_D}$ is a switching drug. Considering

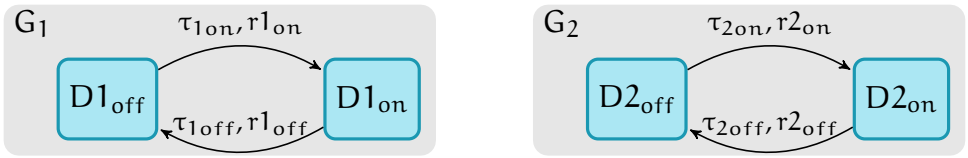

Figure 37: SD-graph for the SIR epidemic example with controls.

that the set $\{D_i \mid i = 1, \ldots, n\}$ is a partition of D, condition 2 is enough to ensure that D is well-formed. □

The stoichiometric matrix $M_{E,D}$ associated to the SIR example with therapies is given below.

$$
\begin{array}{c}
\\
S \\ I \\ R \\ \\ D1_{off} \\ D1_{on} \\ D2_{off} \\ D2_{on}
\end{array}
\begin{array}{c}
\begin{array}{ccccccccccccc}
\tau_{b_S} & \tau_{b_I} & \tau_{b_R} & \tau_{d_S} & \tau_{d_I} & \tau_{d_R} & \tau_r & \tau_{1on} & \tau_{1off} & \tau_{2on} & \tau_{2off} & i & j & h
\end{array} \\
\begin{pmatrix}
1 & 1 & 1 & -1 & 0 & 0 & 0 & 0 & 0 & 0 & 0 & -1 & -1 & 0 \\
0 & 0 & 0 & 0 & -1 & 0 & -1 & 0 & 0 & 0 & 0 & 1 & 0 & -1 \\
0 & 0 & 0 & 0 & 0 & -1 & 1 & 0 & 0 & 0 & 0 & 0 & 1 & 1 \\
 & & & & & & & & & & & & & \\
0 & 0 & 0 & 0 & 0 & 0 & 0 & -1 & 1 & 0 & 0 & 0 & 0 & 0 \\
0 & 0 & 0 & 0 & 0 & 0 & 0 & 1 & -1 & 0 & 0 & 0 & 0 & 0 \\
0 & 0 & 0 & 0 & 0 & 0 & 0 & 0 & 0 & -1 & 1 & 0 & 0 & 0 \\
0 & 0 & 0 & 0 & 0 & 0 & 0 & 0 & 0 & 1 & -1 & 0 & 0 & 0
\end{pmatrix}
\end{array}
$$

It is immediate to check that the conditions at Prop. 5.3.3 are met in $M_{E,D}$. The SD-graph for the SIR example is given in Fig. 37. Its connected components G_1 and G_2 are such that exactly one term in each G_i is active in the initial therapy $T = D1_{off} \mid D2_{off}$. Therefore the set of drug definitions D of the SIR example is well-formed and $\mathcal{D} = \{\{D1_{off}, D1_{on}\}, \{D2_{off}, D2_{on}\}\}$ is the set of switching drugs.

5.3.1 Stochastic Hybrid Automata Semantics

In this section, we illustrate the model of *stochastic hybrid automata (SHA)* and we present the method to derive a SHA semantics from a well-formed D-CGF model.

Stochastic hybrid automata are a quite powerful formalism combining nondeterministic choices, continuous dynamics, stochasticity and real-time behaviour, thus generalizing a variety of automata-based models like Continuous Time Markov Chains, Discrete Time Markov Chains, Labelled Transition Systems, Timed and Hybrid Automata, Markov Decision Processes and Probabilistic Timed Automata.

In the following we will give just a brief account of SHA, in a symbolic fashion as in [69]. For a more complete treatment of the topic, we refer the interested reader to [69].

VARIABLES We consider a set Var of *typed variables*, and we denote with D_v the domain of variable $v \in \mathsf{Var}$. Then, v can be of the following types: Boolean ($D_v = \mathbb{B}$); integer ($D_v \subseteq \mathbb{Z}$); continuous ($D_v = \mathbb{R}$); or a clock variable ($D_v = \mathbb{R}^{\geqslant 0}$).

EXPRESSIONS Let Exp be the set of *expressions* containing variables in Var. Expressions in Exp may contain references to the first derivative of continuous variables, sampling of values according to probability distributions, non-deterministic choice of values, or comparison and arithmetic operators on sub-expressions.

ASSIGNMENTS A variable *assignment* is a function $f = \{v_1 \mapsto e_1, \ldots, v_n \mapsto e_n\}$, mapping any variable v_i to the expression $e_i \in \mathsf{Sxp}$, and any other variable v_j, $j \neq 1, \ldots, n$ to its original value. With $\mathsf{Sxp} \subseteq \mathsf{Exp}$, we denote the set of expressions not containing derivatives. The set of all variable assignments is $\mathsf{Asgn} = \mathsf{Var} \to \mathsf{Sxp}$.

INVARIANTS *Invariants* are Boolean expressions that cannot contain sampling of values. Invariants are employed, as usual, to control the passage of time, or to specify the continuous dynamics in each discrete location of the SHA. The set of invariant expressions is denoted by Ixp.

BOOLEAN AND ARITHMETIC EXPRESSIONS We denote with $\mathsf{Bxp} \subseteq \mathsf{Ixp}$ the set of simple Boolean expressions and with Axp the set of the arithmetic ones (that evaluate to $\mathbb{R}$). Expressions in Bxp and Axp cannot contain derivatives, sampling and non-deterministic values.

Definition 5.3.8 (Stochastic Hybrid Automaton [69])**.** *A* stochastic hybrid automaton (SHA) *is a tuple* $(\mathsf{Loc}, \mathsf{Var}, \mathsf{Inv}, l_0, \mathsf{Act}, v_0, \to)$*, where:*

- Loc *is a finite set of* locations*;*
- Var *is a finite set of* typed variables*;*
- $\mathsf{Inv} : \mathsf{Loc} \to \mathsf{Ixp}$ *maps each location to an* invariant*;*
- $l_0 \in \mathsf{Loc}$ *is the* initial location*;*
- Act *is a finite set of* actions*;*
- $v_0 : \mathsf{Var} \to \mathsf{Sxp}$ *maps each variable to an expression representing its* initial value*;*
- $\to \subseteq \mathsf{Loc} \times \mathsf{Act} \times \mathsf{Bxp} \times \mathsf{Bxp} \times \mathsf{Wxp}$ *is the finite* transition relation*, with* $\mathsf{Wxp} = \mathsf{Asgn} \times \mathsf{Loc} \to \mathsf{Axp}$.

A transition $(s, a, g, u, w) \in \rightarrow$ (or more compactly, $s \xrightarrow{a,g,u} w$) consists of a *source location* s; an action label a; a guard g, determining when the transition is enabled; a urgency constraint u, that avoids the passage of time when u is satisfied; and a target $w \in \mathsf{Wxp}$, that represents a distribution over assignments (variable updates) and target locations. w is used to model a probabilistic choice, but if it exist an assignment A and a target location t s.t. $w(A, t) = 1$ and $w(A', t') = 0$ for any $(A', l') \neq (A, l)$ - that is to say, w is a Dirac distribution - then we write $s \xrightarrow{a,g,u,A} t$ in place of $s \xrightarrow{a,g,u} w$.

STOCHASTIC TRANSITIONS Even if they are not explicitly mentioned in the formalism of SHA, stochastic transitions can be implemented through a combination of clocks, guards, urgency constraints, and exponentially distributed values. The idea is to make the stochastic rate of each transition correspond to a continuous variable used to store the random duration of the action, and to consider a clock variable c.

Starting from a source location s, we consider stochastic transitions of the form $s \xrightarrow{a,r} t$, where a and r are the transition label and rate, respectively. Let $\mathsf{Var}_s = \{v_{s,a,r,t} \mid \exists t.\ s \xrightarrow{a,r} t\}$ be the set of continuous variables used to keep the durations of the transitions exiting location s. Then, we need to add an additional location s' and a SHA transition $s \xrightarrow{\tau,\top,\bot,A} s'$ whose only task is to update the values of the variables in Var_s with exponentially distributed random values: $A = \{v_{s,a,r,t} \mapsto \mathsf{Exp}(r) \mid v_{s,a,r,t} \in \mathsf{Var}_s\}$. Finally, for each outgoing transition $s \xrightarrow{a,r} t$, we add the SHA transition $s' \xrightarrow{a,g,u,A'} t$, where:

- the guard g and the urgency constraint u are set in a way that the transition is taken exactly at time $v_{s,a,r,t}$: $g = c \geqslant v_{s,a,r,t}$ and $u = c \leqslant v_{s,a,r,t}$; and
- the assignment A' is responsible for resetting the clock c: $A' = \{c \mapsto 0\}$.

In the following, we will write $s \xrightarrow{a,r} t$ as a shorthand for the pair of SHA transitions $s \xrightarrow{\tau,\top,\bot,A} s'$ and $s' \xrightarrow{a,g,u,A'} t$ used to implement the stochastic transition.

SHA SEMANTICS OF D-CGF We define the semantics of a well-formed D-CGF model (E, P, D, T) as a stochastic hybrid automaton, whose locations and transitions correspond to the product automaton of the connected components of the SD-graph $\mathcal{G}_{M_D}$; and the continuous dynamics of the species in E are set as location invariants. In this way, the discrete locations of the

automaton would be identified by the set of active drug terms, i.e. by the therapy being administered.

In order to properly set up the continuous dynamics at each location, we need to introduce a slightly modified definition of rate vector, introduced in the ODE semantics of CGF (Sect. 5.1.3), that takes into account the currently active combination of discrete drugs. Clearly, if the mass action rate of an action π, $\phi_{E,D}(\pi)$, depends on a drug term Y being active, but Y does not occur in the given therapy, then $\phi_{E,D}(\pi) = 0$.

Definition 5.3.9 (D-CGF rate vector)**.** *Let* (E, P, D, T) *be a well-formed D-CGF model and* $D' \subseteq D$ *be a set of drug terms representing the therapy being administered. Then, the rate vector at* D'*, written* $\phi_{E,D}(D')(\pi)$*, is defined for each action* $\pi \in \Pi$ *as:*

$$\phi_{E,D}(D')(\pi) = \begin{cases} 0 & \text{if } \mathtt{react}(\pi) \cap E = \emptyset \\ 0 & \text{if } \exists Y \in \mathtt{react}(\pi) \cap D.\ Y \notin D' \\ \rho(\pi) \prod_{X \in \mathtt{react}(\pi) \cap E} X & \text{otherwise} \end{cases}$$

Note that we are allowed to consider a set D' of drugs, instead of a multiset, because the well-formedness property implies that multiple copies of the same drug term cannot occur.

Let us remind that each species X defined in E corresponds to a state variable X in the continuous fragment of the hybrid semantics of D-CGF. Given a set of active drugs D', the continuous dynamics at D' results from the product of the stoichiometric matrix restricted to the set of species E, M_E, and the rate vector at D':

$$\mathbf{f}_{D'}(\mathbf{X}) = M_E \cdot \phi_{E,D}(D')$$

At this point, we are ready to define the stochastic hybrid automata semantics of D-CGF.

Definition 5.3.10 (SHA semantics of D-CGF)**.** *Let* (E, P, D, T) *be a D-CGF model and* $C(\mathcal{G}_{M_D}) = \{G_1 = (D_1, \to_1), \ldots, G_n = (D_n, \to_n)\}$ *be the set of connected components of the associated SD-graph* $\mathcal{G}_{M_D}$*. The* stochastic hybrid automata semantics *of* (E, P, D, T) *is a tuple* $\mathcal{A}_{E,P,D,T} = (\mathsf{Loc}, \mathsf{Var}, \mathsf{Inv}, l_0, \mathsf{Act}, \nu_0, \to)$*, where:*

- *the set of locations is given by the product of the nodes of the components in* $C(\mathcal{G}_{M_D})$*:*

$$\mathsf{Loc} = D_1 \times \ldots \times D_n$$

- Var *contains a continuous variable for each species in* E*:*

$$\mathsf{Var} = \{X \mid X \textit{ defined in } \mathsf{E}\}$$

- Inv *maps each location* $l = (Y_1, \ldots, Y_n)$ *to the invariant constraining the continuous dynamics at* l*:*

$$\mathsf{Inv}(Y_1, \ldots, Y_n) = \bigwedge_{X \in \mathsf{Var}} \dot{X} = \mathbf{f}_{\{Y_1,\ldots,Y_n\}}(X)$$

- *the initial location* l_0 *is the only location whose underlying drug terms are active in the initial therapy* T*:*

$$l_0 = (Y_1, \ldots, Y_n) \textit{ s.t. } \#(Y_i, \mathsf{T}) = 1, i = 1, \ldots, n$$

- Act *is the set of switching actions occurring in the SD-graph;*
- ν_0 *assigns an initial value to each variable* $X \in \mathsf{Var}$*, according to the multiplicity of the species* X *in the initial solution* P*:*

$$\nu_0(X) = \#(X, \mathsf{P})$$

- *the set of stochastic transitions* $\rightarrow \subseteq \mathsf{Loc} \times \mathsf{Act} \times \mathbb{R}^+ \times \mathsf{Loc}$ *are derived from the product of the connected components* $(D_1, \rightarrow_1), \ldots, (D_n, \rightarrow_n)$ *of* $\mathcal{G}_{M_D}$ *as follows:*

$$\rightarrow = \bigcup_{i=1}^{n} \bigcup_{Y_i \xrightarrow{a,r}_i Y_i'} (Y_1, \ldots, Y_i, \ldots, Y_n) \xrightarrow{a,r} (Y_1, \ldots, Y_i', \ldots, Y_n)$$

In this definition, we directly refer to stochastic transitions of the form $(Y_1, \ldots, Y_i, \ldots, Y_n) \xrightarrow{a,r} (Y_1, \ldots, Y_i', \ldots, Y_n)$, omitting the SHA implementation previously introduced. Clearly, such a transition is defined in the SHA semantics only if there exist the transition $Y_i \xrightarrow{a,r}_i Y_i'$ in the i-th connected component G_i of $\mathcal{G}_{M_D}$.

We illustrate the SHA semantics of the SIR epidemic model with therapies. According to its SD-graph (Fig. 37), the set of locations identifies the possible combinations of discretely-dosed drugs:

$$\begin{aligned}\mathsf{Loc} = \{&l_0 = (D1_{off}, D2_{off}), l_1 = (D1_{on}, D2_{off}),\\ &l_2 = (D1_{off}, D2_{on}), l_3 = (D1_{on}, D2_{on})\}\end{aligned}$$

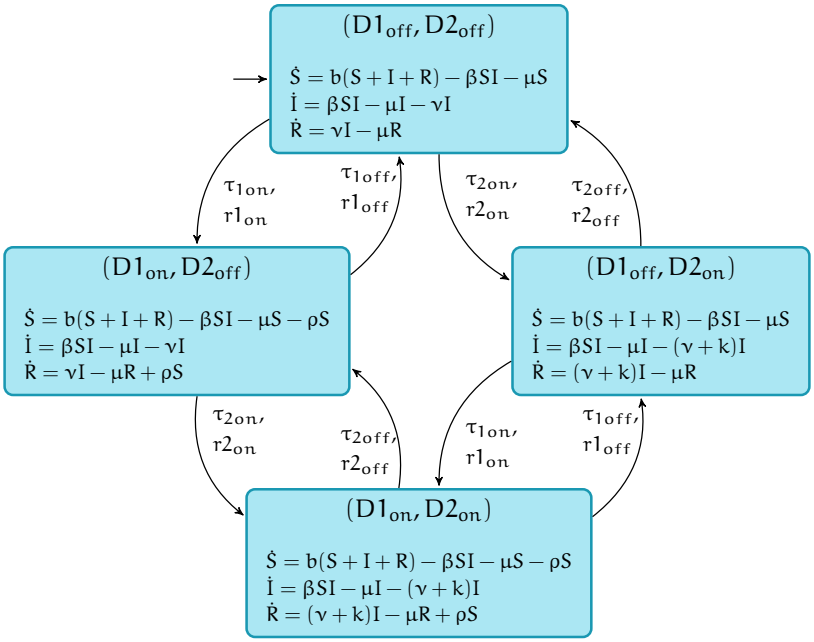

Figure 38: Stochastic Hybrid Automata semantics of the SIR model with therapies. Discrete locations identify the therapy administered and invariants determine the continous dynamics.

Given that in the initial therapy no drugs are being administered ($T = D1_{off} \| D2_{off}$), the initial location would be $l_0 = (D1_{off}, D2_{off})$.

The rate vectors at each location are shown below, and the resulting SHA is depicted in Fig. 38.

$$\phi_{E,D}(l) = \begin{array}{c} \\ i \\ \tau_r \\ \tau_{b_S} \\ \tau_{b_I} \\ \tau_{b_R} \\ \tau_{d_S} \\ \tau_{d_I} \\ \tau_{d_R} \\ j \\ h \\ \tau_{1on} \\ \tau_{1off} \\ \tau_{2on} \\ \tau_{2off} \end{array} \begin{array}{c} \{D1_{off}, D2_{off}\} \\ \begin{pmatrix} \beta IS \\ \nu I \\ bS \\ bI \\ bR \\ \mu S \\ \mu I \\ \mu R \\ 0 \\ 0 \\ 0 \\ 0 \\ 0 \\ 0 \end{pmatrix} \end{array} \begin{array}{c} \{D1_{on}, D2_{off}\} \\ \begin{pmatrix} \beta IS \\ \nu I \\ bS \\ bI \\ bR \\ \mu S \\ \mu I \\ \mu R \\ \rho S \\ 0 \\ 0 \\ 0 \\ 0 \\ 0 \end{pmatrix} \end{array} \begin{array}{c} \{D1_{off}, D2_{on}\} \\ \begin{pmatrix} \beta IS \\ \nu I \\ bS \\ bI \\ bR \\ \mu S \\ \mu I \\ \mu R \\ 0 \\ kI \\ 0 \\ 0 \\ 0 \\ 0 \end{pmatrix} \end{array} \begin{array}{c} \{D1_{on}, D2_{on}\} \\ \begin{pmatrix} \beta IS \\ \nu I \\ bS \\ bI \\ bR \\ \mu S \\ \mu I \\ \mu R \\ \rho S \\ kI \\ 0 \\ 0 \\ 0 \\ 0 \end{pmatrix} \end{array}$$

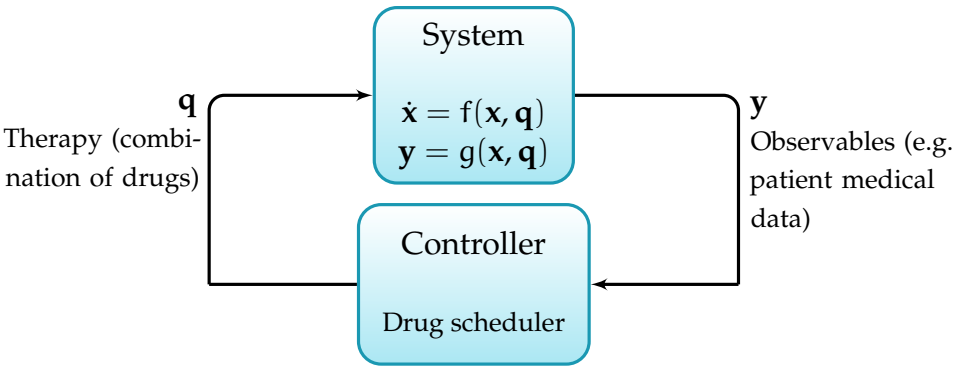

Figure 39: Control loop in a controlled switched system. The plant defines the piecewise smooth dynamics of the system $\dot{\mathbf{x}}$ and the observable output $\mathbf{y}$. The output could represent patient's medical data obtained after a visit. Depending on $\mathbf{y}$, the controller acts as therapy scheduler and determines the operation mode $\mathbf{q}$ (a therapy, e.g. a particular combination of drugs) of the plant.

5.3.2 Hybrid Dynamical Systems Semantics

Here we describe the semantics of a D-CGF model in terms of a particular class of hybrid dynamical systems, called *controlled switched systems (CSS)* [102]. While in the general formulation of hybrid dynamical system the external control input and the discrete operation mode are distinct, in a CSS the external controller produces a switching signal (i.e. the discrete mode) that is given in input to the plant (i.e. the controlled system). The state-space form of a controlled switched system is the following:

$$\begin{aligned}\dot{\mathbf{x}} &= f(\mathbf{x}, \mathbf{q}) \\ \mathbf{y} &= g(\mathbf{x}, \mathbf{q}),\end{aligned}$$

where $\mathbf{x} \in \mathbb{R}^n$ is the continuous state vector; f is a vector-valued smooth function determining the continuous dynamics of $\mathbf{x}$ according to the discrete operation mode $\mathbf{q}$; and g is the output function. The above equations are often written with the form $\dot{\mathbf{x}} = f_{\mathbf{q}}(\mathbf{x}) \quad \mathbf{y} = g_{\mathbf{q}}(\mathbf{x})$, stressing the different dynamics and outputs under different operation modes. Note that a controlled switched system can also be seen as a hybrid dynamical system with controlled discrete inputs. Figure 39 shows the control loop in a CSS.

APPROXIMATION FROM SHA TO CSS Recalling that each location of the stochastic hybrid automata semantics represents a possible combination of drugs, ideally, we aim to derive a system where therapies can be externally controlled by a (automated) therapist. To this aim, the proposed encoding

makes SHA locations correspond to the discrete modes in the CSS; and the continuous dynamics specified in a location invariant, to the continuous dynamics at the corresponding mode in the CSS.

Note that with this approximation we relax the SHA transition relation, by allowing arbitrary sequences of control moves in the CSS. We also assume instantaneous transitions, discarding the stochastic delays determined by the transition rates. Note that the CSS encoding represents an *over - approximation* of the original SHA, because any timed sequence of control moves (i.e. SHA locations) is permitted. W.l.o.g., we omit the observation function g of a CSS, assuming that every state variable is observable ($\mathbf{y} = \mathbf{x}$), even if our framework potentially supports also features like partial observability or output disturbances.

Definition 5.3.11 (CSS semantics of D-CGF)**.** *Let* (E, P, D, T) *be a D-CGF model and* $\mathcal{A}_{E,P,D,T} = (\mathsf{Loc}, \mathsf{Var}, \mathsf{Inv}, l_0, \mathsf{Act}, \nu_0, \rightarrow)$ *be its stochastic hybrid automata semantics. Then the* hybrid dynamical systems semantics *of* (E, P, D, T) *is a* Controlled Switched System (CSS)

$$\begin{aligned}\dot{\mathbf{x}} &= f(\mathbf{x}, \mathbf{q})\\ \mathbf{y} &= \mathbf{x}\end{aligned}$$

where

- *the vector of controlled discrete modes* $\mathbf{q} = [q_1, \ldots, q_n]^T$ *has as many elements as the discrete locations of the SHA; thus we can consider a bijection* $b_{\mathsf{Loc}} : \mathsf{Loc} \rightarrow \{q_1, \ldots, q_n\}$*;*
- *the continuous state vector* $\mathbf{x} = [x_1, \ldots, x_m]^T$ *has as many elements as the continuous variables in* Var*, related by the following bijection:* $b_{\mathsf{Var}} : \mathsf{Var} \rightarrow \{x_1, \ldots, x_m\}$*; and*
- *the continuous dynamics of the CSS,* f*, are extracted from the location invariant, for each state* x *and mode* q*, as follows:*

$$f(b_{\mathsf{Var}}^{-1}(x), q) = \mathsf{Inv}(b_{\mathsf{Loc}}(q))$$

Below, we illustrate the CSS semantics of the SIR epidemic model, where we use $\mathbf{q}_i$ to denote the i-th element of $\mathbf{q}$.

$$\mathbf{q} = \begin{bmatrix} (D1_{off}, D2_{off}) \\ (D1_{on}, D2_{off}) \\ (D1_{off}, D2_{on}) \\ (D1_{on}, D2_{on}) \end{bmatrix} \qquad \mathbf{x} = \begin{bmatrix} S \\ I \\ R \end{bmatrix}$$

$$f_{q_1} = \begin{cases} \dot{S} = b(S+I+R) - \beta SI - \mu S \\ \dot{I} = \beta SI - \mu I - \nu I \\ \dot{R} = \nu I - \mu R \end{cases} \qquad f_{q_2} = \begin{cases} \dot{S} = b(S+I+R) - \beta SI - \mu S - \rho S \\ \dot{I} = \beta SI - \mu I - \nu I \\ \dot{R} = \nu I - \mu R + \rho S \end{cases}$$

$$f_{q_3} = \begin{cases} \dot{S} = b(S+I+R) - \beta SI - \mu S \\ \dot{I} = \beta SI - \mu I - (\nu + k)I \\ \dot{R} = (\nu + k)I - \mu R \end{cases} \qquad f_{q_4} = \begin{cases} \dot{S} = b(S+I+R) - \beta SI - \mu S - \rho S \\ \dot{I} = \beta SI - \mu I - (\nu + k)I \\ \dot{R} = (\nu + k)I - \mu R + \rho S \end{cases}$$

5.4 OPTIMAL CONTROL PROBLEM DEFINITION

In this section we define the optimal control law for therapy scheduling in the SIR model by means of *Model Predictive Control (MPC)* [38], and we illustrate the embedding approach for the optimal control of non-linear hybrid models generated from D-CGF specifications.

MODEL PREDICTIVE CONTROL MPC is based on iterative, finite horizon optimization of a system model or, in the vocabulary of Control Theory, a *plant*. The plant model is used to predict the behaviour of the future output of the system on the basis of the inputs and the possible disturbances applied to it. In particular, at each time t, the current plant state $\mathbf{x}(t)$ is sampled and a *control strategy* $\mathbf{v}(\cdot)$, i.e. a sequence of control actions for each controlled input, is computed that minimizes an objective function $J(t)$ for a relatively short time horizon in the future: $[t, t + T_p]$. T_p is referred to as the *prediction horizon*. At this stage, only the first element $\mathbf{v}(t)$ of the optimal control strategy at t is applied to the system, then the horizon is shifted, and the optimization problem is posed again at time $t + 1$, thus yielding a new control and new predicted state path. Therefore the prediction horizon keeps being shifted forward till the end of simulation, and for this reason MPC is also called *receding horizon control*.

The cost function (also called *performance index*) at t, $J(t)$, is based on assigning weights/penalties to the state variables and control actions through the functions f and g, respectively. Generic continuous-time and discrete-time cost functions are of the following form:

$$J(t) = \int_t^{t+T_p} \{f(\mathbf{x}(k)) + g(\mathbf{v}(k))\}\, dk \qquad \text{(continuous-time)}$$

$$J(t) = \sum_{k=t}^{t+T_p} f(\mathbf{x}(k)) + g(\mathbf{v}(k)) \qquad \text{(discrete-time)}$$

A MPC problem typically takes into account additional constraints, like equality constraints that set the *initial state* of the system; inequality constraints indicating the *allowed values* for state variables and control inputs; or *terminal constraints*, imposing the system to reach a state within a given set of terminal states.

5.4.1 Problem Formulation

We formulate a STI (Structured Therapy Interruption) problem for the optimal scheduling of multiple drugs in the SIR model, by the following MPC problem:

$$\begin{aligned} & \min_{\mathbf{q}} \int_{t}^{t+T_p} \{\|R\mathbf{q}(k)\|_1 + \|Q\mathbf{x}(k)\|_1\}\, dk \\ \text{subj. to } & \dot{\mathbf{x}}(t) = f(\mathbf{x}(t), \mathbf{q}(t)) \\ & \mathbf{x}(t) \in [0,1]^3 \\ & \mathbf{q}(t) \in \{0,1\}^4 \text{ and } \textstyle\sum_i q_i(t) = 1 \\ & \forall t \in [0, T_f] \\ & \mathbf{x}(0) = \mathbf{x}_0 \text{ and } \mathbf{x}(T_f) \in \mathcal{X}_f \end{aligned}$$

where T_p is the prediction horizon; T_f is the end of simulation time; $\|\mathbf{v}\|_1 = \sum_i |v_i|$ denotes the 1-norm of a vector $\mathbf{v}$; the vector of controlled modes $\mathbf{q}$ is constrained to discrete values; $\mathbf{x}_0 = [S_0\ I_0\ R_0]^T$ is the initial state; $\mathcal{X}_f = \{[S\ I\ R]^T \in [0,1] \times [0, I_0] \times [0,1]\}$ represents the terminal constraints, imposing that the number of infected individuals at the final step has to be less or equal to the initial one [3]; the state vector $\dot{\mathbf{x}}$ is subject to the piecewise continuous dynamics determined by the CSS semantics of the SIR model, and is bounded by the interval $[0,1]$ [4]; and R and Q are the weights on the controlled inputs and on the system state, respectively.

5.4.2 Control of Hybrid Nonlinear Systems through the Embedding Approach

Let us remark that we are aiming to synthesize optimal control strategies over the *non-linear hybrid systems* semantics that can be derived from D-CGF specifications. Clearly, classical non-linear optimization techniques do not

3 Note that we cannot impose that the infected population is completely extinct in the final step, because all negative terms in the equation of I are density-dependent, thus it would be possible to get a null concentration only asymptotically.

4 Variables in the SIR model are constrained in the interval $[0,1]$ because their initial values sum to 1 and the equations are balanced

apply in our case, since they require certain smoothness conditions to be met. Moreover, the methods by Belta et al. [15, 68, 4] for the LTL-based control of rectangular (i.e. multi-affine, see Sect. 4.3) hybrid systems, could be applied in our case only if we exclude homeo-synchronizations, i.e. those reactions occurring between the same process and thus leading to a term in the mass-action equation containing a squared state variable.

On the other hand, a method that supports general non-linear hybrid dynamics is called *Finite Set Control Transcription (FSCT)* [137, 147], and consists in transforming the hybrid control problem into a parameter optimization problem that can be solved with classical non-linear programming techniques. Specifically, FSCT divides the time-line into a fixed number of segments, whose boundaries represents the points in time where the discrete control switches from one value to another. Then, the transcribed problem is formulated to optimize the length of each segment.

In this section, we will adopt a method in the same spirit as FSCT, called the *embedding approach* [17, 107, 108], where the original hybrid system is embedded into a larger class of systems without discontinuities, and the optimization problem is formulated for the latter. The advantage of the embedding approach is that no assumptions about the number of switches nor about the mode sequence have to be made in order to solve the problem, due to some theoretical relationships between the original problem, hereafter called *Switched Optimal Control Problem (SOCP)*, and the *Embedded Optimal Control Problem (EOCP)*.

The embedded problem is defined by relaxing the discreteness constraint on the mode vector $\mathbf{q}$, by allowing real values in the interval $[0, 1]$ and imposing the sum of the embedded modes to be equals to 1. The nonlinear optimization problem resulting from the embedding of the hybrid control problem shown in Sect. 5.4.1 is:

$$
\begin{aligned}
& \min_{\tilde{\mathbf{q}}} \int_{t}^{t+T_p} \{\tilde{q}_i(k)(\|R_{\cdot,i}\|_1 + \|Q\tilde{\mathbf{x}}(k)\|_1)\}\, dk \\
\text{subj. to} \quad & \dot{\tilde{\mathbf{x}}}(t) = \textstyle\sum_i \tilde{q}_i(t) \cdot f_{q_i}(\tilde{\mathbf{x}}(t)) \\
& \tilde{\mathbf{x}}(t) \in [0, 1]^3 \\
& \tilde{\mathbf{q}}(t) \in [0, 1]^4 \text{ and } \textstyle\sum_i \tilde{q}_i(t) = 1 \\
& \forall t \in [0, T_f] \\
& \tilde{\mathbf{x}}(0) = \mathbf{x}_0 \text{ and } \tilde{\mathbf{x}}(T_f) \in \mathcal{X}_f
\end{aligned}
$$

where $\tilde{\mathbf{x}}$ and $\tilde{\mathbf{q}}$ denotes the state vector and the relaxed mode vector of the EOCP; $R_{\cdot,i}$ denotes the i-th column of the therapy-weighting matrix R; and the continuous dynamics is now defined as the sum of the dynamics at each mode q_i, $f_{q_i}(\tilde{\mathbf{x}}(t))$, weighted by the value of the relaxed mode $\tilde{q}_i$. Similarly,

the integrand of the cost function results from the combination of the cost at each q_i weighted by $\tilde{q}_i$: $\tilde{q}_i(k)(\|R_{\cdot,i}\|_1 + \|Q\tilde{\mathbf{x}}(k)\|_1)$. It is immediate to see that this quantity is equals to the cost in the SOCP where $\mathbf{q}$ and $\mathbf{x}$ are replaced by their relaxed versions: $\|R\tilde{\mathbf{q}}(k)\|_1 + \|Q\tilde{\mathbf{x}}(k)\|_1$.

Specifically, the dynamics of the SIR model would become:

$$\begin{aligned}\dot{\tilde{\mathbf{x}}}(t) = &\tilde{q}_1 \begin{bmatrix} b(S+I+R) - \beta SI - \mu S \\ \beta SI - \mu I - \nu I \\ \nu I - \mu R \end{bmatrix} + \tilde{q}_2 \begin{bmatrix} b(S+I+R) - \beta SI - \mu S - \rho S \\ \beta SI - \mu I - \nu I \\ \nu I - \mu R + \rho S \end{bmatrix} + \\ &\tilde{q}_3 \begin{bmatrix} b(S+I+R) - \beta SI - \mu S \\ \beta SI - \mu I - (\nu+k) I \\ (\nu+k) I - \mu R \end{bmatrix} + \tilde{q}_4 \begin{bmatrix} b(S+I+R) - \beta SI - \mu S - \rho S \\ \beta SI - \mu I - (\nu+k) I \\ (\nu+k) I - \mu R + \rho S \end{bmatrix}\end{aligned}$$

At this stage, we give an overview of the theoretical framework developed in [17] and we show that the SIR model with controls and more generally, the hybrid non-linear models generated from D-CGF specifications are amenable to be analysed with the embedding approach.

SUFFICIENT CONDITIONS FOR EOCP SOLUTIONS We first illustrate the sufficient conditions for the existence of an optimal solution to the EOCP (Theorem 9 of [17]). Note that the embedding approach is designed to work with problems possibly including also a vector $\mathbf{z}$ of continuous control variables. Since we are dealing with controlled switched systems where the discrete modes are the only controllable elements, most of the following requirements straightforwardly hold.

1. *For every mode* q_i*, the cost function at* q_i*,* $c_{q_i}(t, \mathbf{x}, \mathbf{z})$*, is affine in the continuous control input* $\mathbf{z}$*, i.e.* $c_{q_i}(t, \mathbf{x}, \mathbf{z}) = A(t, \mathbf{x}) + B(t, \mathbf{x}) \cdot \mathbf{z}$*. Moreover,* $c_{q_i}(t, \mathbf{x}, \mathbf{z})$ *is a convex function of* $\mathbf{z}$*.*

   Since we do not consider continuous controlled inputs, this condition does clearly hold in the hybrid semantics of any D-CGF model.

2. *The terminal set* $\mathcal{X}_f$ *is compact, i.e. it is bounded and closed.*

   In the SIR model, $\mathcal{X}_f = \{[S\ I\ R]^T \in [0,1] \times [0, I_0] \times [0,1]\}$ is compact, because closed intervals are compact sets. This requirement is not met a priori by a generic D-CGF model, because the terminal set is only defined in a second stage. For instance, if no terminal constraints are specified, this requirement is trivially met if the domains of the state variables are given as closed intervals.

3. *The set of admissible continuous controlled inputs is compact and convex.*

As pointed out before, this condition is met by the semantics of any D-CGF model, because we do not consider continuous controlled inputs.

As a consequence, the control problem defined over the hybrid semantics of D-CGF admits an optimal solution as long as the set of terminal states is compact.

RELATIONSHIPS BETWEEN EOCP AND SOCP In Theorem 1 of [17], the authors demonstrate that *the set of trajectories of the switching system is dense in the set of trajectories of the embedded system*, meaning that the solution of the embedded optimal control problem can be approximated arbitrarily close by the trajectory of a switched system.

More formally, if the EOCP admits a solution with a real-valued trajectory $\psi(\cdot)$ and relaxed control inputs $\tilde{\mathbf{q}}(\cdot)$, then for each $\epsilon > 0$, there exists a solution of the SOCP, given by sequence of discrete control inputs $\mathbf{q}_\epsilon(\cdot)$ and by a trajectory $\phi_\epsilon(\cdot)$ such that, for all $t \in [0, T_f]$, $|\phi_\epsilon(t) - \psi(t)| < \epsilon$.

This result is used to prove that *if the SOCP has a solution, then it is also a solution of the EOCP* (Proposition 5 of [17]), apart from isolated cases that can be fixed by enlarging the set of terminal states, as discussed in [108].

Reminding that the embedded problem over a D-CGF model always admits a solution under mild constraints on the terminal states, if the associated SOCP has a solution, then the SOCP solution is one of the possibly non-unique solutions given by the optimal solution space of the EOCP. Conversely, if the EOCP has a solution but there does not exist a SOCP solution, by Theorem 1 of [17], it is possible to approximate the EOCP solution with arbitrary precision to obtain a suboptimal solution of the SOCP.

MODE PROJECTIONS A method to derive a switched solution from the embedded one consists in projecting the vector relaxed modes $\tilde{\mathbf{q}}$ back into a vector of discrete modes $\mathbf{q}$. Naturally, we need to perform a mode projection only if none of the relaxed modes takes values in $\{0, 1\}$, otherwise we would already have an admissible mode of the switched system.

Therefore, suppose $\tilde{\mathbf{q}}(t) \in (0, 1)^n$, with $t \in [0, T_f]$. In practice, the projected mode vector is calculated so that the only active mode corresponds to the relaxed mode with the highest value. This is formalized as follows:

$$q_i(t) = \begin{cases} 1 & \text{if } i = \arg\max_j \tilde{q}_i(t) \\ 0 & \text{otherwise} \end{cases}$$

For more details on the adequacy of the mode projection technique to obtain a (sub-)optimal solution of the SOCP, see [17, 107, 108].

5.5 OPTIMAL THERAPY SCHEDULING: THE CASE OF H1N1 INFLUENZA

In this section, we apply our methodology and the above defined hybrid control problem over the SIR model with therapies to the case study of the pandemic influenza A(H1N1), occurred in the US in 2009. The optimal control problem was realized in MATLAB using the implementation of the embedding approach provided in [108]. The result will consist in an optimal STI (Structured Therapy Interruption) strategy for the scheduling of vaccination and antiviral treatments. We follow the work by Towers and Feng [148], where the authors parametrize a SIR model on the basis of the influenza data collected by the *Centers for Disease Control and Prevention (CDC)* during the early months of 2009.

The model presented in [148] is a closed-population SIR model with seasonal (i.e. periodic) variation in the contact rate β. Our model is slightly different since it takes into account births and death, but do not consider seasonal variations of the infection rate. In [58], the same SIR model for H1N1 is enriched with (continuous) therapies, in order to analyse the impact of vaccination and antiviral drug treatment on the spread and control of the disease, through simple parametric analyses. Here, we consider vaccination (drug 1) and antiviral treatment (drug 2) as well, but we focus on the automatic synthesis of dosing strategies that seek to optimize an objective function, trading-off between the impact of the administered drugs and the need to control and counteract the spread of the influenza. Model parameters are listed in Table 14.

5.5.1 Penalties and treatment scenarios

Let us recall that the cost function of our optimal control problem assigns weights (penalties) to state variables (matrix Q) and to controlled modes (matrix R). Q has been set so that the state variable I (infected population) has associated a weight equals to 100 and thus is heavily penalized over variables S (susceptible, weight 0.1) and R (recovered, weight 0):

$$Q = \begin{bmatrix} 0.1 & 0 & 0 \\ 0 & 100 & 0 \\ 0 & 0 & 0 \end{bmatrix}$$

Matrix R allows us to implement different therapy administration strategies. The higher R, the higher penalty is given to a drug dosage. In particu-

Parameter	Description	Value
S_0	Initial susceptible population	$1 - I_0$
I_0	Initial infected population	3.05×10^{-8}
R_0	Initial recovered population	0
β	Contact rate	0.52
ν	Recovery rate	$\frac{1}{3}$
b	Birth rate	0.02
μ	Death rate	0.02
ρ	Vaccination rate under drug 1	1
k	Recovery rate under drug 2	0.5
T_p	Prediction horizon	10 d
T_f	Simulation time	365 d

Table 14: Parameters of the SIR model for H1N1 influenza as reported in [148]. Initially, we consider just one infected individual over the total US population (3.05×10^8).

lar if $R[i, i]$ is assigned a large value, then the strategy is to avoid the therapy i as much as possible. This can be the case of a treatment with severe side effects or of a patient in an early stage of the disease that can be treated even with a small dosage. On the contrary, a low value to R_{ii} leads to a strategy where the dosage of the i-th combination of drugs is much more prominent (e.g. little side effects or mature stage of disease). Additionally we can assign different weights to different drugs according to their therapeutic impact on the patient, thus possibly enabling a wider spectrum of control strategies.

The optimally controlled solutions will be computed according to four different scenarios obtained by varying the weights on the controlled therapies. We clearly assign no penalty to the first therapy, which corresponds to the absence of both drugs, and the weight of the last therapy $(D1_{on}, D2_{on})$ takes the sum of the weights of therapies $(D1_{on}, D2_{off})$ and $(D1_{off}, D2_{on})$, except for the fourth scenario:

1. Low penalties to D1 and D2: $R = \begin{bmatrix} 0 & 0 & 0 & 0 \\ 0 & 0.1 & 0 & 0 \\ 0 & 0 & 0.1 & 0 \\ 0 & 0 & 0 & 0.2 \end{bmatrix}$
2. High penalty to D1, meaning that the antiviral treatment is favoured over the vaccination: $R = \begin{bmatrix} 0 & 0 & 0 & 0 \\ 0 & 100 & 0 & 0 \\ 0 & 0 & 0.1 & 0 \\ 0 & 0 & 0 & 100.1 \end{bmatrix}$.

3. High penalty to D2, meaning that the vaccination is preferred to the antiviral treatment: $R = \begin{bmatrix} 0 & 0 & 0 & 0 \\ 0 & 0.1 & 0 & 0 \\ 0 & 0 & 100 & 0 \\ 0 & 0 & 0 & 100.1 \end{bmatrix}$.
4. High penalty to their combination: $R = \begin{bmatrix} 0 & 0 & 0 & 0 \\ 0 & 0.1 & 0 & 0 \\ 0 & 0 & 0.1 & 0 \\ 0 & 0 & 0 & 100 \end{bmatrix}$

5.5.2 Results

Table 15 reports the optimal trajectories and the synthesized treatment strategies under the previously introduced four scenarios. At the top of each scenario-specific plot, we directly reported the discrete dosage sequence of drugs D1 and D2, extracted from the sequence of discrete modes in the obvious way: $D1 = 1$ in mode $q_2 = (D1_{on}, D2_{off})$ and $q_4 = (D1_{on}, D2_{on})$; $D2 = 1$ in q_4 and in $q_3 = (D1_{off}, D2_{on})$.

Firstly, we observe that the vaccination (D1) and the antiviral treatment (D2) are never administered simultaneously, indicating that optimal intervention strategies are based on the exclusive application of D1 and D2.

Moreover, the optimal trajectories and the control moves in Scenarios 1, 3 and 4 are practically identical, meaning that when D1 and D2 are assigned the same penalty (Scenarios 1 and 4), the optimal solution would consist in choosing only D1, that corresponds to the same strategy applied when D2 is penalized over D1 (Scenario 3). In other words, the vaccination of susceptible individuals proves to be a much more efficient strategy in the overall control of the H1N1, than the administration of antiviral drugs to infected individuals.

In these three scenarios, the strategy consists in a continuous vaccination policy, repeated at mostly regular time-intervals (with an approximate frequency of 3 vaccinations each 10 days). Since we consider a open population model where newborns enter the susceptible compartment (there is no maternal-derived immunity), repeated vaccinations are necessary to keep as lowest as possible the number of individuals that can be affected by H1N1. The same frequency of intervention can be observed for the antiviral treatment in Scenario 2, where repeated and short-term dosages are preferred to longer and less frequent treatments. This behaviour has to be ascribed also to the fact that we do not assume in our model any penalty to frequent mode changes.

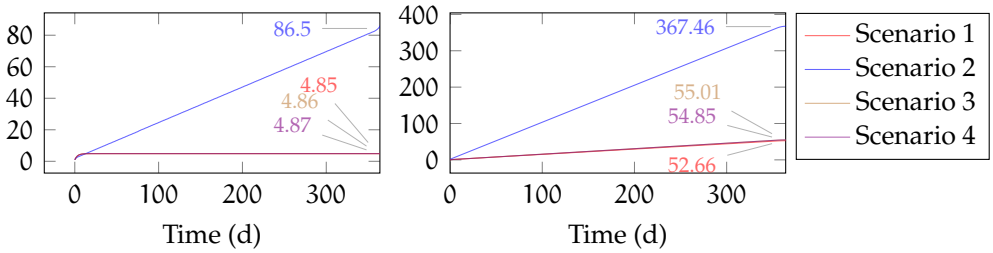

(a) Cumulated infections **(b)** Cumulated cost

Figure 40: Cumulated cases of infection (a) and corresponding costs (b) under the four treatment scenarios. Infections are computed according to the total US population estimated in 2009 (3.05×10^8 individuals).

On the other hand, in Scenario 2 the populations of susceptible and recovered individuals remains approximately the same as in the initial state, because the policy of the exclusive application of D2 affects only the compartment of infected individuals.

The disease outcomes under the four scenarios are depicted in Fig. 40 a), where the cumulative number of infection cases is reported by considering the total US population in 2009, as previously done in the parametrization of the initial concentration of infected individuals. We immediately note that Scenarios 1, 3 and 4 produce virtually identical infection curves, with a total number of infected individuals close to 5 at the end of simulation, which is consistently lower than the number of infections reported for Scenario 2: 86.5 at the end of the first year. Interestingly, the strategy based on pulse vaccinations (resulting from Scenarios 1, 3 and 4) succeeds in stopping the epidemics at the first days of simulation. Contrarily, the strategy based on the pulse dosage of antiviral drugs (resulting from Scenario 2) is not able to effectively counteract the H1N1 infection, which linearly increases despite of the frequent drug administrations. This can be explained by the fact that the absence of vaccination actions in Scenario 2 lead to a high susceptible population and in turn, to a continuous inflow of potential infected individuals.

Finally, Figure 40 b) compares the cumulative cost associated with the optimal control strategy in each scenario. Similarly to the results on the infection curves, Scenario 2 has a notably higher cost than the other scenarios, due to the high penalty associated to the infected population in the objective function. However, in this case the cost of Scenarios 1, 3 and 4 does not reach a plateau here because, albeit very small, it is increased by the penalty associated to the susceptible population.

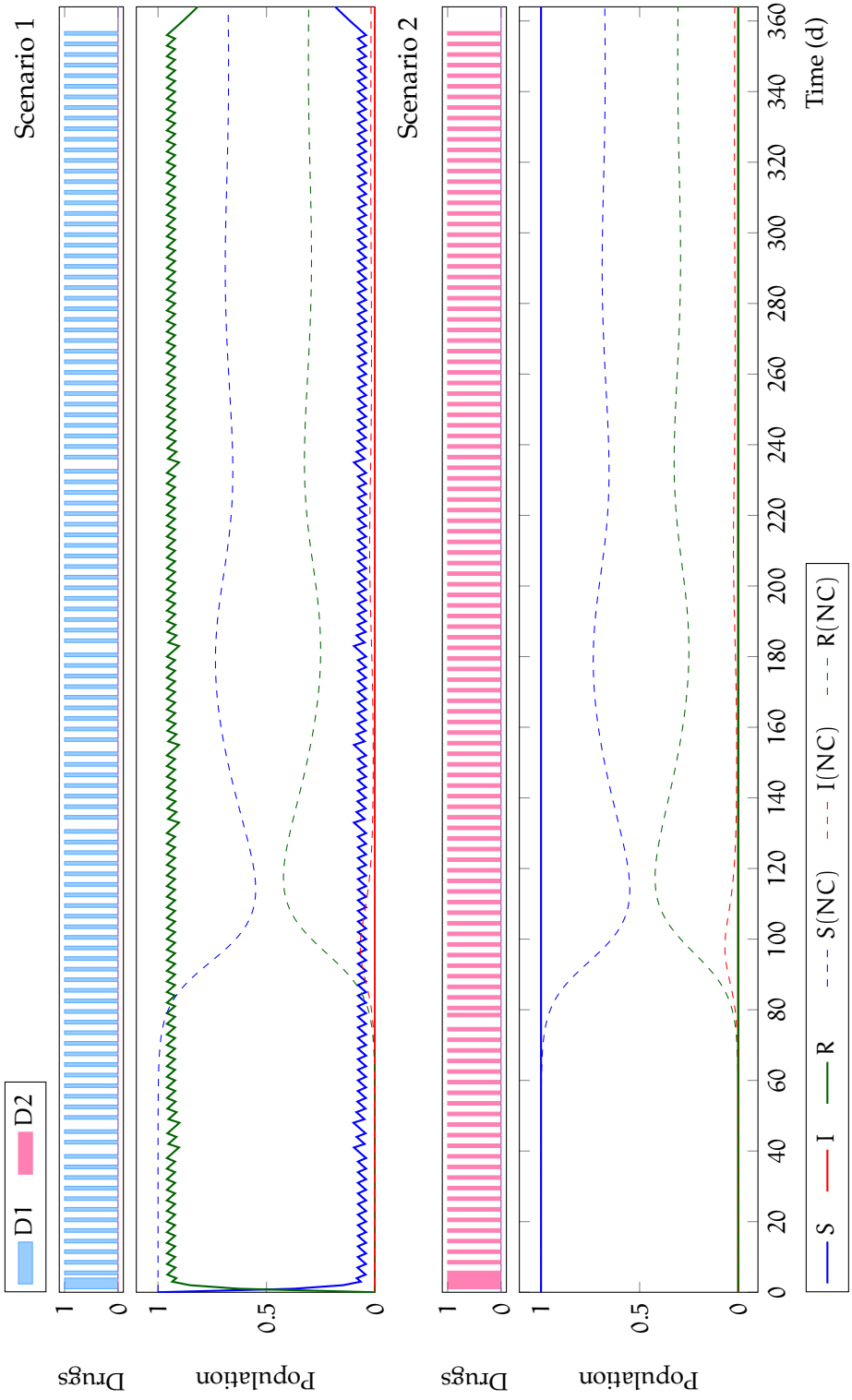
Scenario 1
Scenario 2
D1
D2
Drugs
Population
S
I
R
S(NC)
I(NC)
R(NC)
Time (d)
0
20
40
60
80
100
120
140
160
180
200
220
240
260
280
300
320
340
360
0.5
1

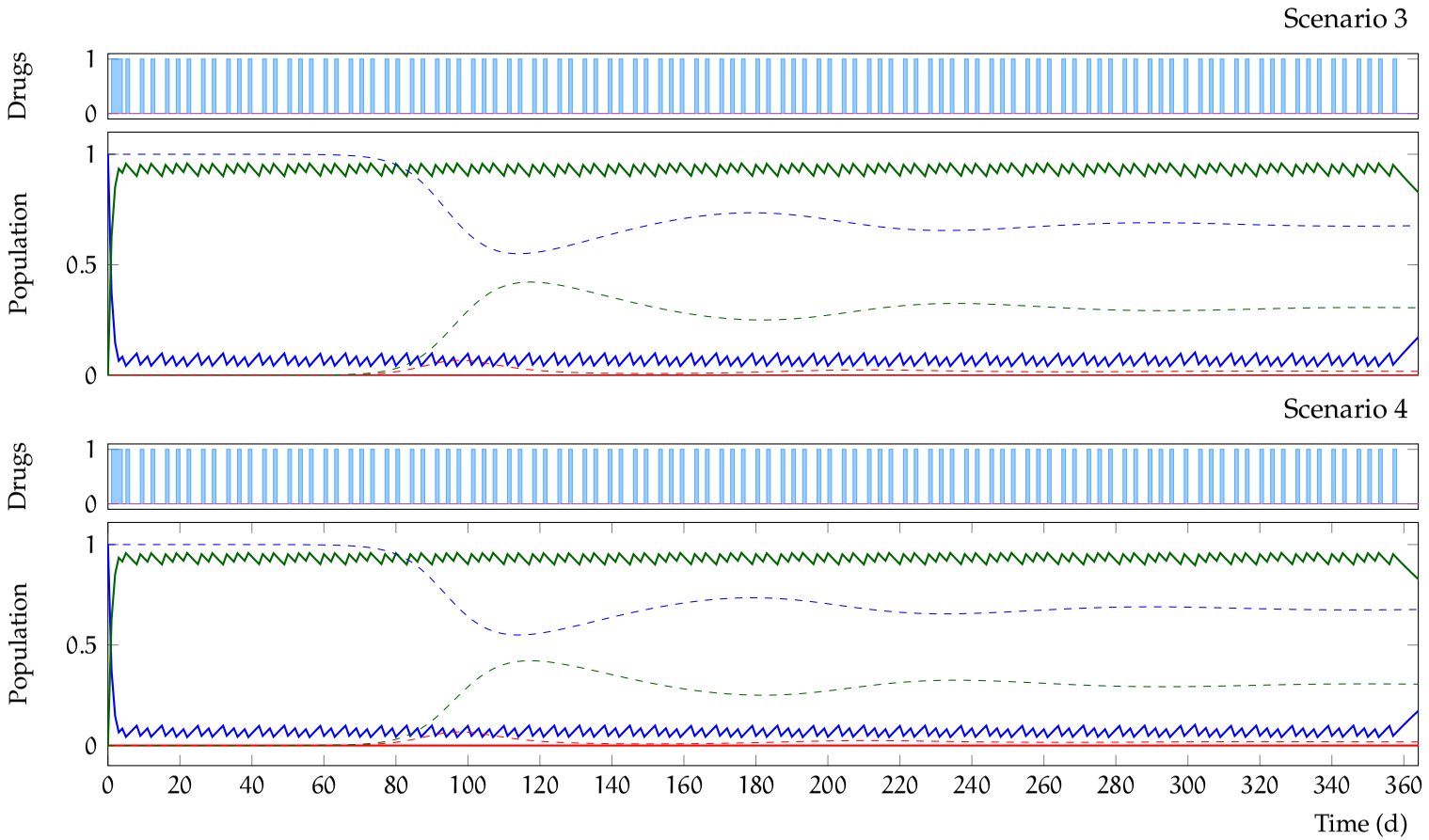

Table 15: Optimal solutions and therapy administration strategies in the SIR model for H1N1 influenza, under different treatment scenarios. Plain lines depicts the optimally controlled trajectories; dashed lines illustrate the evolution of the influenza without the application of disease control. On top of each scenario-specific plot, the discrete drug dosage is reported.

5.6 SUMMARY

The field of predictive models in biomedicine is challenged by the need of a better comprehension of the phenomenon of scales in the biological organisation, particularly their role in the transition between health and disease conditions. The multiscale modelling of molecules-cell-tissue-organ-body interactions is a key step in the process of identifying the most important parameters acting in a disease state and their calibration, linking basic research and clinical practice (therapies).

Here we discuss how a description based on hybrid systems is beneficial to the formulation of a multiscale modelling in macro-biological processes like an epidemics. A second instance of the utility of hybrid dynamics approach stems from the presence of multiple controls in biological systems. These controls could be framed as occurring naturally (the immune system response) or induced after the administration of a therapy. It is very often the case of multiple treatments, i.e. switching between therapies or combination of therapies which is the case considered in this study. In particular, we show the suitability of the introduced D-CGF process algebra to accomplish the task: here, its semantics is given in terms of a stochastic hybrid automaton and of a hybrid dynamical system where the large number of individuals in a population provides the basis for a continuous modelling approach and the dosage of multiple drugs is implemented as discrete transitions/switches.

The presented approach could open several interesting directions not just in the field of epidemics control, but also in clinical and biomedical research. First, it is general and could be used for different tissues and organs or multiorgan diseases. Second, it is possible to extend the mathematical formulation to all the scales of biological organisation involved in the infection and recovery conditions. Third, the therapy could be complex and built on several nested and hierarchical protocols.

One final comment: given the richness of examples provided by biological processes and medical therapies, there is basis for deriving interesting theories. We remind the *bon mot* of Stan Ulam: Ask not what mathematics can do for biology. Ask what biology can do for Mathematics.

REFERENCES

[1] L. Aceto, A. Ingólfsdóttir, K. G. Larsen, and J. Srba. *Reactive Systems: Modelling, Specification and Verification*. Cambridge University Press, 2007.

[2] M. Ardura, R. Banchereau, A. Mejias, T. Di Pucchio, C. Glaser, F. Allantaz, V. Pascual, J. Banchereau, D. Chaussabel, and O. Ramilo. Enhanced monocyte response and decreased central memory T cells in children with invasive Staphylococcus aureus infections. *PLoS One*, 4(5):e5446, 2009.

[3] B. Ayati, C. Edwards, G. Webb, and J. Wikswo. A mathematical model of bone remodeling dynamics for normal bone cell populations and myeloma bone disease. *Biology Direct*, 5(1):28, 2010.

[4] E. Aydin Gol and C. Belta. Time-constrained temporal logic control of multi-affine systems. *Nonlinear Analysis: Hybrid Systems*, 2013.

[5] A. Aziz, K. Sanwal, V. Singhal, and R. Brayton. Model-checking continuous-time Markov chains. *ACM Transactions on Computational Logic*, 1(1):162–170, 2000.

[6] J. C. Baeten. A brief history of process algebra. *Theoretical Computer Science*, 335(2):131–146, 2005.

[7] F. Bagnoli, P. Liò, and L. Sguanci. Risk perception in epidemic modeling. *Physical Review E*, 76(6):061904, 2007.

[8] R. Barbuti, S. Cataudella, A. Maggiolo-Schettini, P. Milazzo, and A. Troina. A probabilistic model for molecular systems. *Fundamenta Informaticae*, 67(1-3):13–27, 2005.

[9] E. Bartocci, D. Cacciagrano, M. Di Berardini, E. Merelli, and L. Tesei. Timed operational semantics and well-formedness of Shape Calculus. *Scientific Annals of Computer Science*, 20, 2010.

[10] E. Bartocci, D. R. Cacciagrano, M. R. D. Berardini, E. Merelli, and L. Tesei. Shape calculus: Timed operational semantics and well-formedness. *CoRR*, abs/1011.2488, 2010.

[11] E. Bartocci, F. Corradini, M. Di Berardini, E. Merelli, and L. Tesei. Shape Calculus. A spatial mobile calculus for 3D shapes. *Scientific Annals of Computer Science*, 20, 2010.

[12] G. Batt, C. Belta, and R. Weiss. Temporal logic analysis of gene networks under parameter uncertainty. *IEEE Transactions on Automatic Control*, 53:215–229, 2008.

[13] G. Batt, D. Ropers, H. De Jong, J. Geiselmann, M. Page, and D. Schneider. Qualitative analysis and verification of hybrid models of genetic regulatory networks: Nutritional stress response in Escherichia coli. *Hybrid Systems: Computation and Control*, pages 134–150, 2005.

[14] G. Batt, B. Yordanov, R. Weiss, and C. Belta. Robustness analysis and tuning of synthetic gene networks. *Bioinformatics*, 23(18):2415–2422, 2007.

[15] C. Belta and L. Habets. Controlling a class of nonlinear systems on rectangles. *Automatic Control, IEEE Transactions on*, 51(11):1749–1759, 2006.

[16] C. Belta, L. Habets, and V. Kumar. Control of multi-affine systems on rectangles with application to hybrid biomolecular networks. In *Proceedings of the 41st IEEE Conference on Decision and Control*, pages 534–539. IEEE, 2002.

[17] S. C. Bengea and R. A. DeCarlo. Optimal control of switching systems. *automatica*, 41(1):11–27, 2005.

[18] J. A. Bergstra and J. W. Klop. Process algebra for synchronous communication. *Information and control*, 60(1):109–137, 1984.

[19] S. Berman, A. Halász, and V. Kumar. MARCO: A reachability algorithm for multi-affine systems with applications to biological systems. In *Proceedings of the 10th International Conference on Hybrid Systems: Computation and Control (HSCC 2007)*, pages 76–89. Springer, 2007.

[20] M. Bernardo and R. Gorrieri. A tutorial on EMPA: A theory of concurrent processes with nondeterminism, priorities, probabilities and time. *Theoretical Computer Science*, 202(1-2):1–54, 1998.

[21] A. T. Bittig and A. M. Uhrmacher. Spatial modeling in cell biology at multiple levels. In *Proceedings of the 2010 Winter Simulation Conference*, pages 608–619. IEEE, 2010.

[22] L. Bortolussi, V. Galpin, J. Hillston, and M. Tribastone. Hybrid semantics for PEPA. In *Quantitative Evaluation of Systems (QEST), 2010 Seventh International Conference on the*, pages 181–190. IEEE, 2010.

[23] L. Bortolussi and A. Policriti. Connecting process algebras and differential equations for Systems Biology. In *Process Algebra and Stochastically Timed Activities: Proc. 6th PASTA workshop*, 2006.

[24] L. Bortolussi and A. Policriti. Stochastic concurrent constraint programming and differential equations. *Electronic Notes in Theoretical Computer Science*, 190(3):27–42, 2007.

[25] L. Bortolussi and A. Policriti. Modeling biological systems in stochastic concurrent constraint programming. *Constraints*, 13(1-2):66–90, 2008.

[26] L. Bortolussi and A. Policriti. Hybrid dynamics of stochastic π-calculus. *Mathematics in Computer Science*, 2(3):465–491, 2009.

[27] L. Bortolussi and A. Policriti. The importance of being (a little bit) discrete. *Electronic Notes in Theoretical Computer Science*, 229(1):75–92, 2009.

[28] L. Bortolussi and A. Policriti. Hybrid dynamics of stochastic programs. *Theor. Comput. Sci.*, 411(20):2052–2077, 2010.

[29] L. Bortolussi and A. Policriti. (Hybrid) automata and (stochastic) programs. The hybrid automata lattice of a stochastic program. *Journal of Logic and Computation*, 2011.

[30] L. Bortolussi and A. Policriti. Studying cancer-cell populations by programmable models of networks. *Network Modeling Analysis in Health Informatics and Bioinformatics*, 1(3):117–133, 2012.

[31] L. Bortolussi and A. Policriti. (hybrid) automata and (stochastic) programs*The hybrid automata lattice of a stochastic program. J. Log. Comput.*, 23(4):761–798, 2013.

[32] P. Buchholz. Markovian process algebra: Composition and equivalence. In *Proc. of PAPM*, pages 11–30. Citeseer, 1994.

[33] F. Buti. *Spatial Modelling, Simulation and Verification for Biological Systems*. PhD thesis, School of Science and Technology, University of Camerino, 2011.

[34] F. Buti, M. Callisto De Donato, F. Corradini, M. R. Di Berardini, E. Merelli, and L. Tesei. Towards abstraction-based verification of Shape Calculus. *Electronic Notes in Theoretical Computer Science*, 284:23–34, 2012.

[35] F. Buti, F. Corradini, E. Merelli, and L. Tesei. A Geometrical Refinement of Shape Calculus Enabling Direct Simulation. In *SIMULTECH*, pages 218–227, 2012.

[36] D. Cacciagrano, F. Corradini, E. Merelli, and L. Tesei. Multiscale Bone Remodelling with Spatial P Systems. In *Proceedings Compendium of the Fourth Workshop on Membrane Computing and Biologically Inspired Process Calculi*, 2010.

[37] M. Calder, V. Vyshemirsky, D. Gilbert, and R. Orton. Analysis of signalling pathways using continuous time Markov chains. *Transactions on Computational Systems Biology VI*, pages 44–67, 2006.

[38] E. F. Camacho, C. Bordons, E. F. Camacho, and C. Bordons. *Model predictive control*, volume 2. Springer London, 2004.

[39] L. Cardelli. Brane calculi. In *Computational methods in Systems Biology*, pages 257–278. Springer, 2005.

[40] L. Cardelli. From processes to ODEs by chemistry. In *Fifth Ifip International Conference On Theoretical Computer Science–Tcs 2008*, pages 261–281. Springer, 2008.

[41] L. Cardelli. On process rate semantics. *Theoretical Computer Science*, 391(3):190–215, 2008.

[42] L. Cardelli and P. Gardner. Processes in space. In *Programs, Proofs, Processes*, volume 6158 of *Lecture Notes in Computer Science*, pages 78–87. Springer, 2010.

[43] L. Cardelli and A. D. Gordon. Mobile ambients. In *Foundations of Software Science and Computation Structures*, pages 140–155. Springer, 1998.

[44] L. Cardelli and G. Zavattaro. On the computational power of biochemistry. In *Algebraic Biology*, pages 65–80. Springer, 2008.

[45] H. Chang and A. Astolfi. Immune response's enhancement via controlled drug scheduling. In *Decision and Control, 2007 46th IEEE Conference on*, pages 3919–3924. IEEE, 2007.

[46] H. Chang and A. Astolfi. Control of HIV infection dynamics. *Control Systems, IEEE*, 28(2):28–39, 2008.

[47] D. Chaussabel, C. Quinn, J. Shen, P. Patel, C. Glaser, N. Baldwin, D. Stichweh, D. Blankenship, L. Li, I. Munagala, et al. A modular analysis framework for blood genomics studies: application to systemic lupus erythematosus. *Immunity*, 29(1):150–164, 2008.

[48] F. Ciocchetta and M. L. Guerriero. Modelling biological compartments in Bio-PEPA. *Electronic Notes Theoretical Computer Science*, 227:77–95, January 2009.

[49] F. Ciocchetta and J. Hillston. Bio-PEPA: A framework for the modelling and analysis of biological systems. *Theor. Comput. Sci.*, 410(33-34):3065–3084, 2009.

[50] T. Claro, A. Widaa, M. O'Seaghdha, H. Miajlovic, T. Foster, F. O'Brien, and S. Kerrigan. Staphylococcus aureus Protein A Binds to Osteoblasts and Triggers Signals That Weaken Bone in Osteomyelitis. *PloS one*, 6(4):e18748, 2011.

[51] B. Cook, J. Fisher, E. Krepska, and N. Piterman. Proving stabilization of biological systems. In *Proceedings of 12th International Conference on Verification, Model Checking, and Abstract Interpretation (VMCAI 2011)*, pages 134–149. Springer, 2011.

[52] R. De Nicola, J. Katoen, D. Latella, and M. Massink. STOKLAIM: A stochastic extension of KLAIM. Technical report, TR 2006-TR-01, ISTI, 2006, 2006.

[53] D. Dingli and M. Nowak. Cancer biology: infectious tumour cells. *Nature*, 443(7107):35–36, 2006.

[54] A. Donzé. Breach, a toolbox for verification and parameter synthesis of hybrid systems. In *Computer Aided Verification*, pages 167–170. Springer, 2010.

[55] J. E. Dumont, F. Pécasse, and C. Maenhaut. Crosstalk and specificity in signalling: Are we crosstalking ourselves into general confusion? *Cellular signalling*, 13(7):457–463, 2001.

[56] A. Edelstein and N. Agmon. Brownian simulation of many-particle binding to a reversible receptor array. *Journal of Computational Physics*, 132(2):260–275, 1997.

[57] F. Fages, S. Soliman, and N. Chabrier-Rivier. Modelling and querying interaction networks in the biochemical abstract machine BIOCHAM. *Journal of Biological Physics and Chemistry*, 4(2):46–73, 2004.

[58] Z. Feng, S. Towers, and Y. Yang. Modeling the effects of vaccination and treatment on pandemic influenza. *The AAPS journal*, 13(3):427–437, 2011.

[59] J. Fisher, D. Harel, and T. A. Henzinger. Biology as reactivity. *Communications of the ACM*, 54(10):72–82, 2011.

[60] J. Fisher and T. A. Henzinger. Executable cell biology. *Nature biotechnology*, 25(11):1239–1249, 2007.

[61] V. Galpin, L. Bortolussi, and J. Hillston. HYPE: a process algebra for compositional flows and emergent behaviour. *CONCUR 2009-Concurrency Theory*, pages 305–320, 2009.

[62] S. Gao, S. Kong, and E. M. Clarke. dreal: An smt solver for nonlinear theories over the reals. In *Automated Deduction–CADE-24*, pages 208–214. Springer, 2013.

[63] F. Gerhard, D. Webster, G. van Lenthe, and R. Müller. In silico biology of bone modelling and remodelling: adaptation. *Philosophical Transactions of the Royal Society A: Mathematical, Physical and Engineering Sciences*, 367(1895):2011, 2009.

[64] L. Geris, J. Vander Sloten, and H. Van Oosterwyck. In silico biology of bone modelling and remodelling: regeneration. *Philosophical Transactions of the Royal Society A: Mathematical, Physical and Engineering Sciences*, 367(1895):2031, 2009.

[65] D. Gillespie. Exact stochastic simulation of coupled chemical reactions. *Journal of Physical Chemistry*, 81(25):2340–2361, 1977.

[66] D. Gillespie. The chemical Langevin equation. *The Journal of Chemical Physics*, 113:297, 2000.

[67] R. Grosu, G. Batt, F. Fenton, J. Glimm, C. L. Guernic, S. Smolka, and E. Bartocci. From cardiac cells to genetic regulatory networks. In *Proceedings of the 23rd International Conference on Computer Aided Verification (CAV'11)*, pages 396–411. Springer, 2011.

[68] L. Habets, M. Kloetzer, and C. Belta. Control of rectangular multi-affine hybrid systems. In *Decision and Control, 2006 45th IEEE Conference on*, pages 2619–2624. IEEE, 2006.

[69] E. M. Hahn, A. Hartmanns, H. Hermanns, and J.-P. Katoen. A compositional modelling and analysis framework for stochastic hybrid systems. *Formal Methods in System Design*, pages 1–42, 2012.

[70] A. Harding, T. Tian, E. Westbury, E. Frische, and J. F. Hancock. Subcellular localization determines MAP kinase signal output. *Current biology*, 15(9):869–873, 2005.

[71] Z. He, G. Yang, Z. Chen, B. Li, W. Zhang, and X. Wu. A novel isoform of osteoprotegerin gene: cloning and expression and its hypocalcemic effect in mice. *Protein and Peptide Letters*, 7(4):233–240, 2000.

[72] J. Heath, M. Kwiatkowska, G. Norman, D. Parker, and O. Tymchyshyn. Probabilistic model checking of complex biological pathways. *Theoretical Computer Science*, 391(3):239–257, 2008.

[73] T. Henzinger. The theory of hybrid automata. In *Logic in Computer Science, 1996. LICS'96. Proceedings., Eleventh Annual IEEE Symposium on*, pages 278–292. IEEE, 1996.

[74] M. Herceg, M. Kvasnica, C. Jones, and M. Morari. Multi-Parametric Toolbox 3.0. In *Proc. of the European Control Conference*, pages 502–510, Zürich, Switzerland, July 17–19 2013. http://control.ee.ethz.ch/~mpt.

[75] H. Hermanns, U. Herzog, and J. Katoen. Process algebra for performance evaluation. *Theoretical Computer Science*, 274(1-2):43–87, 2002.

[76] H. Hermanns, U. Herzog, and V. Mertsiotakis. Stochastic process algebras-between LOTOS and Markov chains. *Computer Networks and ISDN systems*, 30(9-10):901–924, 1998.

[77] C. Hernandez, G. Beaupre, and D. Carter. A theoretical analysis of the relative influences of peak bmd, age-related bone loss and menopause on the development of osteoporosis. *Osteoporosis international*, 14(10):843–847, 2003.

[78] J. Hillston. *A compositional approach to performance modelling*. Cambridge Univ Pr, 1996.

[79] C. A. R. Hoare. Communicating sequential processes. *Communications of the ACM*, 21(8):666–677, 1978.

[80] S. Hoops, S. Sahle, R. Gauges, C. Lee, J. Pahle, N. Simus, M. Singhal, L. Xu, P. Mendes, and U. Kummer. Copasi,Äîa complex pathway simulator. *Bioinformatics*, 22(24):3067–3074, 2006.

[81] S. Jabbar, J. Drury, J. Fordham, H. Datta, R. Francis, and S. Tuck. Osteoprotegerin, RANKL and bone turnover in postmenopausal osteoporosis. *Journal of Clinical Pathology*, 64(4):354, 2011.

[82] M. John, R. Ewald, and A. M. Uhrmacher. A spatial extension to the π calculus. *Electronic Notes in Theoretical Computer Science*, 194(3):133–148, 2008.

[83] G. Karsenty and F. Oury. The central regulation of bone mass, the first link between bone remodeling and energy metabolism. *Journal of Clinical Endocrinology & Metabolism*, 95(11):4795, 2010.

[84] W. Kermack and A. McKendrick. Contributions to the mathematical theory of epidemics. *Proceedings of the Royal society A*, 115(772):700–721, 1927.

[85] B. N. Kholodenko. Cell-signalling dynamics in time and space. *Nature reviews Molecular cell biology*, 7(3):165–176, 2006.

[86] S. Komarova, R. Smith, S. Dixon, S. Sims, and L. Wahl. Mathematical model predicts a critical role for osteoclast autocrine regulation in the control of bone remodeling. *Bone*, 33(2):206–215, 2003.

[87] J. Krivine, V. Danos, and A. Benecke. Modelling Epigenetic Information Maintenance: A Kappa Tutorial. In *CAV*, pages 17–32. Springer, 2009.

[88] M. Kwiatkowska, G. Norman, and D. Parker. Stochastic model checking. In *Formal methods for performance evaluation*, pages 220–270. Springer, 2007.

[89] M. Kwiatkowska, G. Norman, and D. Parker. Using probabilistic model checking in Systems Biology. *ACM SIGMETRICS Performance Evaluation Review*, 35(4):14–21, 2008.

[90] M. Kwiatkowska, G. Norman, and D. Parker. PRISM 4.0: Verification of probabilistic real-time systems. In *Proc. 23rd International Conference on Computer Aided Verification (CAV'11)*, volume 6806 of *LNCS*, pages 585–591. Springer, 2011.

[91] M. Kwiatkowska, G. Norman, and D. Parker. Probabilistic model checking for Systems Biology. In *Symbolic Systems Biology: Theory and Methods*. Jones and Bartlett, 2011.

[92] M. R. Lakin, D. Parker, L. Cardelli, M. Kwiatkowska, and A. Phillips. Design and analysis of DNA strand displacement devices using probabilistic model checking. *Journal of the Royal Society Interface*, 9(72):1470–1485, 2012.

[93] M. R. Lakin, S. Youssef, F. Polo, S. Emmott, and A. Phillips. Visual dsd: a design and analysis tool for dna strand displacement systems. *Bioinformatics*, 27(22):3211–3213, 2011.

[94] M. Lapin, L. Mikeev, and V. Wolf. SHAVE: stochastic hybrid analysis of markov population models. In *Proceedings of the 14th international conference on Hybrid systems: computation and control*, pages 311–312. ACM, 2011.

[95] L. Li and H. Yokota. Application of Petri Nets in Bone Remodeling. *Gene Regulation and Systems Biology*, 3:105, 2009.

[96] J. Lin and R. Unbehauen. Canonical piecewise-linear approximations. *IEEE Transactions on Circuits and Systems I: Fundamental Theory and Applications*, 39:697–699, 1992.

[97] P. Liò, E. Merelli, and N. Paoletti. Multiple verification in computational modeling of bone pathologies. In *Third International Workshop on Computational Models for Cell Processes (CompMod)*, volume 67 of *EPTCS*, pages 82–96, 2011.

[98] P. Liò, E. Merelli, and N. Paoletti. Disease processes as hybrid dynamical systems. In *1st International Workshop on Hybrid Systems and Biology (HSB)*, volume 92 of *EPTCS*, pages 152–166, 2012.

[99] P. Liò, E. Merelli, N. Paoletti, and M. Viceconti. A combined process algebraic and stochastic approach to bone remodeling. *Electr. Notes Theor. Comput. Sci.*, 277:41–52, 2011.

[100] P. Liò, N. Paoletti, M. A. Moni, K. Atwell, E. Merelli, and M. Viceconti. Modelling osteomyelitis. *BMC bioinformatics*, 13(Suppl 14):S12, 2012.

[101] A. Looker, H. Wahner, W. Dunn, M. Calvo, T. Harris, S. Heyse, C. Johnston Jr, and R. Lindsay. Updated data on proximal femur bone mineral levels of US adults. *Osteoporosis International*, 8(5):468–490, 1998.

[102] J. Lunze, F. Lamnabhi-Lagarrigue, et al. *Handbook of hybrid systems control: theory, tools, applications*. Cambridge University Press, 2009.

[103] S. Manolagas and A. Parfitt. What old means to bone. *Trends in Endocrinology & Metabolism*, 21(6):369–374, 2010.

[104] E. Merelli, N. Paoletti, and L. Tesei. A multi-level model for self-adaptive systems. In *11th International Workshop on Foundations of Coordination Languages and Self Adaptation (FOCLASA)*, volume 91 of *EPTCS*, pages 112–126, 2012.

[105] E. Merelli, N. Paoletti, and L. Tesei. Adaptability checking in multi-level complex systems. *CoRR*, abs/1404.0698, 2014.

[106] E. Merelli, N. Paoletti, and L. Tesei. Adaptability checking in complex systems. *Science of Computer Programming, In press*, 2015.

[107] R. Meyer, R. A. DeCarlo, P. H. Meckl, C. Doktorcik, and S. Pekarek. Hybrid model predictive power flow control of a fuel cell-battery vehicle. In *American Control Conference (ACC), 2011*, pages 2725–2731. IEEE, 2011.

[108] R. Meyer, M. Žefran, and R. A. DeCarlo. A Comparison of the Embedding Method to Multi-Parametric Programming, Mixed-Integer Programming, Gradient-Descent, and Hybrid Minimum Principle Based Methods. *arXiv preprint arXiv:1203.3341*, 2012.

[109] R. Milner. *A calculus of communicating systems*, volume 92. Springer-Verlag, 1980.

[110] R. Milner. *Communicating and mobile systems: the π calculus*. Cambridge university press, 1999.

[111] N. Morabito and et al. Osteoprotegerin and RANKL in the Pathogenesis of Thalassemia-Induced Osteoporosis: New Pieces of the Puzzle. *Journal of Bone and Mineral Research*, 19(5):722–727, 2004.

[112] R. Norman and C. Shankland. Developing the use of process algebra in the derivation and analysis of mathematical models of infectious disease. *Computer Aided Systems Theory-EUROCAST 2003*, pages 404–414, 2003.

[113] M. North, T. Howe, N. Collier, and J. Vos. A declarative model assembly infrastructure for verification and validation. In *Advancing Social Simulation: The First World Congress*, pages 129–140. Springer Japan, 2007.

[114] E. O. Voit and A. E. Ferreira. *Computational Analysis of Biochemical Systems*. Cambridge University Press, 2000.

[115] L. Olde Loohuis, A. Witzel, and B. Mishra. Towards Cancer Hybrid Automata. *EPTCS*, 92:137–151, 2012.

[116] S. Ott. T and Z scores. http://courses.washington.edu/bonephys/opbmdtz.html, Accessed: 25/12/2013.

[117] G. Pannocchia, M. Laurino, and A. Landi. A model predictive control strategy toward optimal structured treatment interruptions in anti-HIV therapy. *Biomedical Engineering, IEEE Transactions on*, 57(5):1040–1050, 2010.

[118] N. Paoletti, P. Liò, E. Merelli, and M. Viceconti. Osteoporosis: a multiscale modeling viewpoint. In *Computational Methods in Systems Biology, 9th International Conference (CMSB)*, pages 183–193. ACM, 2011.

[119] N. Paoletti, P. Liò, E. Merelli, and M. Viceconti. Multilevel computational modeling and quantitative analysis of bone remodeling. *IEEE/ACM Trans. Comput. Biology Bioinform.*, 9(5):1366–1378, 2012.

[120] N. Paoletti, B. Yordanov, Y. Hamadi, C. M. Wintersteiger, and H. Kugler. Analyzing and synthesizing genomic logic functions. In *26th International Conference on Computer Aided Verification (CAV)*, volume 8559 of *LNCS*, pages 343–357. Springer, 2014.

[121] A. Parfitt. Osteonal and hemi-osteonal remodeling: The spatial and temporal framework for signal traffic in adult human bone. *Journal of cellular biochemistry*, 55(3):273–286, 1994.

[122] M. Parfitt, S. Qiu, S. Palnitkar, and D. Rao. Abnormal bone remodeling in patients with spontaneous painful vertebral fracture. *Journal of Bone and Mineral Research*, 26(3):475–485, 2011.

[123] P. Penna, N. Paoletti, G. Scarcella, L. Tesei, M. Marini, and E. Merelli. Dispas: An agent-based tool for the management of fishing effort. In *Software Engineering and Formal Methods - SEFM 2013 Collocated Workshops: BEAT2, WS-FMDS, FM-RAIL-Bok, MoKMaSD, and OpenCert*, volume 8368 of *Lecture Notes in Computer Science*, pages 362–367. Springer, 2013.

[124] I. S. Peter, E. Faure, and E. H. Davidson. Predictive computation of genomic logic processing functions in embryonic development. *Proceedings of the National Academy of Sciences*, 109(41):16434–16442, 2012.

[125] P. Pivonka and S. Komarova. Mathematical modeling in bone biology: From intracellular signaling to tissue mechanics. *Bone*, 47(2):181–189, 2010.

[126] G. D. Plotkin. A structural approach to operational semantics. *J. Log. Algebr. Program.*, 60-61:17–139, 2004.

[127] A. Pnueli. The temporal logic of programs. In *18th IEEE Annual Symposium on Foundations of Computer Science*, pages 46–57. IEEE, 1977.

[128] C. Priami. Stochastic π-calculus. *Computer journal*, 38(7):578–589, 1995.

[129] C. Priami and P. Quaglia. Beta Binders for biological interactions. In *Computational Methods in Systems Biology*, volume 3082 of *Lecture Notes in Computer Science*, pages 20–33. Springer, 2005.

[130] T. Pronk, E. de Vink, D. Bošnački, and T. Breit. Stochastic modeling of codon bias with PRISM. In *Proceedings of the 3rd International Workshop Methods and Tools for Coordinating Concurrent, Distributed and Mobile Systems (MTCoord 2007)*, 2007.

[131] L. Raggatt and N. Partridge. Cellular and molecular mechanisms of bone remodeling. *Journal of Biological Chemistry*, 285(33):25103, 2010.

[132] R. Raju, L. Balakrishnan, V. Nanjappa, M. Bhattacharjee, D. Getnet, B. Muthusamy, J. K. Thomas, J. Sharma, B. A. Rahiman, H. Harsha, et al. A comprehensive manually curated reaction map of RANKL/RANK-signaling pathway. *Database: the journal of biological databases and curation*, 2011, 2011.

[133] O. Ramilo, W. Allman, W. Chung, A. Mejias, M. Ardura, C. Glaser, K. Wittkowski, B. Piqueras, J. Banchereau, A. Palucka, et al. Gene expression patterns in blood leukocytes discriminate patients with acute infections. *Blood*, 109(5):2066–2077, 2007.

[134] A. Regev, E. M. Panina, W. Silverman, L. Cardelli, and E. Shapiro. Bioambients: an abstraction for biological compartments. *Theoretical Computer Science*, 325(1):141 – 167, 2004.

[135] M. Ryser, N. Nigam, and S. Komarova. Mathematical modeling of spatio-temporal dynamics of a single bone multicellular unit. *Journal of bone and mineral research*, 24(5):860–870, 2009.

[136] K. Soetaert, T. Petzoldt, et al. Inverse modelling, sensitivity and monte carlo analysis in R using package FME. *Journal of Statistical Software*, 33(3):1–28, 2010.

[137] S. A. Stanton and B. G. Marchand. Finite set control transcription for optimal control applications. *Journal of Spacecraft and Rockets*, 47(3):457–471, 2010.

[138] A. Stefanek, M. Vigliotti, and J. T. Bradley. Spatial extension of stochastic π calculus. In *8th Workshop on Process Algebra and Stochastically Timed Activities*, pages 109–117, August 2009.

[139] W. Stewart. *Introduction to the numerical solution of Markov chains*. Princeton University Press NJ, 1994.

[140] T. Suzuki, N. Bruchovsky, and K. Aihara. Piecewise affine systems modelling for optimizing hormone therapy of prostate cancer. *Philosophical Transactions of the Royal Society A: Mathematical, Physical and Engineering Sciences*, 368(1930):5045–5059, 2010.

[141] M. Taffi, N. Paolett, P. Liò, L. Tesei, E. Merelli, and M. Marini. A systems biology and ecology framework for pops bioaccumulation in marine ecosystems. In *11th International Conference on Computational Methods in Systems Biology (CMSB)*, volume 8130 of *LNCS/LNBI*, pages 238–239, 2013.

[142] M. Taffi, N. Paoletti, C. Angione, S. Pucciarelli, M. Marini, and P. Liò. Bioremediation in marine ecosystems: a computational study combining ecological modelling and flux balance analysis. *Frontiers in Genetics*, 5(319), 2014.

[143] M. Taffi, N. Paoletti, P. Liò, L. Tesei, S. Pucciarelli, and M. Marini. Estimation and modelling of pcbs bioaccumulation in the adriatic sea ecosystem. *arXiv preprint arXiv:1405.6384*, 2014.

[144] M. Taffi, N. Paoletti, S. Pucciarelli, M. Marini, and P. Liò. Bioaccumulation modelling and sensitivity analysis for discovering key players in contaminated food webs: the case study of pcbs in the adriatic sea. *Ecological Modelling, in press*, 2014.

[145] K. Takahashi, S. N. V. Arjunan, and M. Tomita. Space in Systems Biology of signaling pathways–towards intracellular molecular crowding in silico. *FEBS letters*, 579(8):1783–1788, 2005.

[146] L. Tesei, E. Merelli, and N. Paoletti. Multiple levels in self-adaptive complex systems: A state-based approach. In *Proceedings of the European Conference on Complex Systems 2012*, pages 1033–1050. Springer International Publishing, 2013.

[147] D. Thakur, B. Marchand, et al. Hybrid optimal control for HIV multi-drug therapies: a finite set control transcription approach. *Mathematical biosciences and engineering: MBE*, 9(4):899–914, 2012.

[148] S. Towers and Z. Feng. Pandemic H1N1 influenza: predicting the course of vaccination programme in the United States, 2009.

[149] M. Češka, F. Dannenberg, M. Kwiatkowska, and N. Paoletti. Precise parameter synthesis for stochastic biochemical systems. In *Computational Methods in Systems Biology, 12th International Conference (CMSB)*, volume 8859 of *LNBI*, pages 86–98, 2014.

[150] M. Viceconti. *Multiscale Modeling of the Skeletal System*. Cambridge University Press, 2011.

[151] M. Viceconti, L. Bellingeri, L. Cristofolini, and A. Toni. A comparative study on different methods of automatic mesh generation of human femurs. *Medical engineering & physics*, 20(1):1–10, 1998.

[152] Y. Wang. Real-time behaviour of asynchronous agents. *CONCUR'90 Theories of Concurrency: Unification and Extension*, pages 502–520, 1990.

[153] J. Whitfield. *Growing bone*. Landes Bioscience, 2007.

[154] WHO Study Group on Assessment of Fracture Risk and its Application to Screening for Postmenopausal Osteoporosis. Assessment of fracture risk and its application to screening for postmenopausal osteoporosis. Technical Report 843, World Health Organization, 1994.

[155] P. Xiao, Y. Chen, H. Jiang, Y. Liu, F. Pan, T. Yang, Z. Tang, J. Larsen, J. Lappe, R. Recker, et al. In Vivo Genome-Wide Expression Study on Human Circulating B Cells Suggests a Novel ESR1 and MAPK3 Network for Postmenopausal Osteoporosis. *Journal*

of Bone and Mineral Research, 23(5):644–654, 2008.

[156] X. Yang and Y. Young. *Handbook of Bioinspired Algorithms and Applications*, chapter Cellular Automata, PDEs, and Pattern Formation. Chapman & Hall/CRC Computer and Information Science, 2005.

A PROOFS

A.1 PROPOSITION 5.3.3

Proof. We prove the proposition, condition by condition, showing the equivalence with the conditions of Def. 5.3.1 applied to D.

1 (5.3.3) $\iff$ 1 (5.3.1) The conditions about the conservation of terms are clearly equivalent:

$$\sum_{Y \in D} M_D[Y, \pi] = \sum_{Y \in D} \#(Y, prod(\pi)) - \#(Y, react(\pi)) = 0$$
$$\iff \#(D, react(\pi)) = \#(D, prod(\pi))$$

2 (5.3.3) $\iff$ 2 (5.3.1) $\#(D, react(\pi)) \leqslant 1$ (i.e. there is at most one term of D among the reactants of π) is equivalent to stating that there is at most one term $Y \in D$ s.t. either Y is consumed and produced by π, or Y is consumed, but not produced by π. If $\#(Y, react(\pi)) = 0$, by conservation, it also holds that $\#(Y, prod(\pi)) = 0$ and the thesis is trivially true ($\sum_{Y \in D} M_D[Y, \pi] = 0$).

Suppose instead that $\#(Y, react(\pi)) = 1$. By conservation, if Y is produced by π, we would have that $\#(Y, react(\pi)) = \#(Y, prod(\pi)) = 1$, and therefore that $\sum_{Y \in D} M_D[Y, \pi] = 0$. On the other hand, if Y is not produced by π, by conservation, there would exist exactly one $Y' \in D$ s.t. $Y' \neq Y$ and $\#(Y', prod(\pi)) = 1$. In other words, $\sum_{Y \in D} M_D[Y, \pi] = (-1)^2 + 1 = 2$.

3 (5.3.3) $\iff$ 3 (5.3.1) We need to prove that

$$\forall Y \in D.\ ((A(Y) \implies B(Y)) \iff (C(Y) \implies F(Y)))$$
$$A(Y) = M_D[Y, \pi] = -1$$
$$B(Y) = \forall X \in E.\ M_E[X, \pi] = 0 \wedge \pi \text{ internal}$$
$$C(Y) = Y \in react(\pi) \wedge \exists Y' \in D.(Y \neq Y' \wedge Y' \in prod(\pi))$$
$$D(Y) = \exists Y' \in D.(Y' \neq Y \wedge react(\pi) = \{Y\} \wedge prod(\pi) = \{Y'\})$$

This is equivalent to showing that the following formulas hold for all $Y \in D$:

$$\begin{aligned} A(Y) \wedge B(Y) &\implies D(Y) \\ \neg A(Y) &\iff \neg C(Y) \\ D(Y) &\implies B(Y) \end{aligned}$$

$A(Y) \wedge B(Y) \implies D(Y)$ This clearly holds because if π is internal and the stoichiometric matrix is such that $M_D[Y, \pi] = -1$, then Y is the only reactant ($react(\pi) = \{Y\}$). Moreover $M_D[Y, \pi] = -1$ implies that Y is consumed and not produced and, by conservation, there exist exactly one $Y' \in D$ such that $prod(\pi) = \{Y'\}$.

$\neg A(Y) \iff \neg C(Y)$ By Corollary 5.3.4, the stoichiometric matrix can take values in the set $\{-1, 0, 1\}$. $\neg A(Y)$ being true additionally implies that $M_D[Y, \pi] \in \{0, 1\}$. $\neg C(Y)$ can be restated as Y is not a reactant of π (1) or it does not exist a $Y' \in D$ such that $Y' \neq Y$ and $Y \in prod(\pi)$ (2). Case (1) implies that the value of the stoichiometric matrix $M_D[Y, \pi]$ cannot be negative, and therefore by Corollary 5.3.4, $M_D[Y, \pi] \in \{0, 1\}$. Then, the bi-implication holds because Case (2) being satisfied implies that, by conservation, $prod(\pi)$ needs to have as many copies of Y as in $react(\pi)$, and thus that $M_D[Y, \pi] = 0$.

$D(Y) \implies B(Y)$ It is immediate to show that if π is given such that $react(\pi) = \{Y\}$ and $prod(\pi) = \{Y'\}$ for some Y', then π is internal and $M_E[X, \pi]$ is zero for any species X.

□

A.2 LEMMA 5.3.6

Proof. We will prove for any action $\pi \in \Pi$ that if the conditions of the Def. 5.3.1 hold for D, then they also hold for any subset D' of D in the partition induced by the SD-graph.

1. Let us remind that, by Corollary 5.3.4, if D is a switching drug, then $M_D[Y, \pi] \in \{-1, 0, 1\}$ for any $Y \in D' \subseteq D$. Let $Y \in D'$ and $M_D[Y, \pi] = -1$ (or $M_D[Y, \pi] = 1$). The conservation of terms in D implies that it exists $Y' \in D$ s.t. $M_D[Y', \pi] = 1$ (or $M_D[Y', \pi] = -1$). Then, by Def. 5.3.5, there must be a directed edge $Y \xrightarrow{\pi, \rho(\pi)} Y'$ (or

$Y' \xrightarrow{\pi,\rho(\pi)} Y$) in the associated SD-graph, implying that Y and Y' belong to the same connected component D'. Therefore, the number of terms in D' is conserved by π.

2. The second condition is trivially true because if $\#(D, \mathtt{react}(\pi)) \leqslant 1$, then $\#(D', \mathtt{react}(\pi)) \leqslant 1$ for any $D' \subseteq D$.

3. Let $Y \in D'$. If $Y \in \mathtt{react}(\pi)$, we know that, by condition 2 of Def. 5.3.1, $\mathtt{react}(\pi) = \{Y\}$ (Y is the only reactant of π). Then, if there exists $Y' \in D'$ such that $Y \neq Y'$ and $Y' \in \mathtt{prod}(\pi)$, by the conservation property on D', it holds that $Y \notin \mathtt{prod}(\pi)$, and thus $M_D[Y, \pi] = -1$. Additionally, it holds that Y' is the only product of π in D'. Note that $\mathtt{prod}(\pi)$ cannot contain additional terms in D because otherwise the conservation property on D would be violated (π has one only reactant in D, Y). Finally, according to the exclusive switch property of Prop. 5.3.3 on D, $M_D[Y, \pi] = -1$ implies that there are no species $X \in E$ participating to the reaction. Therefore $\mathtt{prod}(\pi) = \{Y'\}$.

□

B SIMULATION OF SHAPE CALCULUS-BASED STOCHASTIC AGENTS

In this appendix, we cover some technical details about the implementation of the simulation environment based on Repast Simphony, and used for the Shape Calculus model of bone remodelling (see Chapter 3). In particular, we illustrate how the Repast computation model has been adapted to support also stochastic actions and synchronizations (Section B.1); and how Shape Calculus terms are syntactically translated into Java code (Section B.2).

B.1 SCHEDULING STOCHASTIC ACTIONS IN REPAST

The procedure implemented for scheduling stochastic actions over the discrete - event scheduler of Repast Simphony is shown in Algorithm 1. We keep a set E to store the actions enabled in each agent. An enabled action is described a tuple (A, a, d) where a identifies the action to execute, d is the duration and A is the set of agents associated to a: at this stage, synchronizations are seen as unique actions and thus involve more than one agent. At each tick, the set E is updated with the currently enabled actions for all agents, computed by the $\mathsf{EnabledActions}()$ procedure (Algorithm 2). Since the race condition applies, we process actions $(A, a, d) \in E$ in ascending order with respect to their duration. If the duration d of the current action does not exceed the time-step Δt, it is scheduled for the execution at the current time t ($\mathsf{Schedule}(a, t)$) and all the other actions involving any agent in A are removed from the set E since they cannot fire anymore. When all enabled actions have been processed, E will contain only actions such that $d > \Delta t$, i.e. those that need to be postponed to the next time-step (before that, their duration is set to $d - \Delta t$). Finally, positions and velocities of all agents are updated.

Algorithm 2 illustrates how to retrieve the currently enabled actions at each time step. Three kinds of actions are distinguished::

- *Deterministically timed actions* of the form $(\{\mathcal{A}\}, a, d)$ (agent, action, duration), and computed by the function $\mathsf{enabledDTActions}(\mathcal{A})$.

Algorithm 1 Scheduling of stochastic actions in Repast

$t \leftarrow 0$
$E \leftarrow \emptyset$
while $t \leqslant t_{max}$ **do**
  $E \leftarrow E \cup \mathsf{EnabledActions}()$
  while $\mathsf{hasNext}(E)$ **do**
    $(A, a, d) \leftarrow \mathsf{PickShortest}(E)$
    if $d \leqslant \Delta t$ **then**
      $\mathsf{Schedule}(a, t)$
      $E \leftarrow E \setminus \{(B, a, d) \mid A \cap B \neq \emptyset\}$
    end if
  end while
  $E \leftarrow \{(A, a, d - \Delta t) \mid (A, a, d) \in E\}$
  $\mathsf{UpdateShapes}()$
  $t \leftarrow t + \Delta t$
end while

Algorithm 2 EnabledActions(): compute the enabled actions for all agents

$E \leftarrow \emptyset$
$Act^I \leftarrow \emptyset$
$Act^O \leftarrow \emptyset$
for all $\mathcal{A}$ agent **do**
  $E \leftarrow E \cup \mathsf{enabledDTActions}(\mathcal{A})$
  $Act^I \leftarrow Act^I \cup \mathsf{enabledInActions}(\mathcal{A})$
  $Act^O \leftarrow Act^O \cup \mathsf{enabledOutActions}(\mathcal{A})$
end for
for all $a^O = (\mathcal{A}, (\overline{a}, \lambda)_d) \in Act^O$ **do**
  for all $a^I = (\mathcal{B}, (a, w)) \in Act^I$ **do**
    $rate \leftarrow \beta(a^O, a^I)$
    if $rate > 0$ **then**
      $d \leftarrow \mathsf{Random.Exp}(rate)$
      $E \leftarrow E \cup (\{\mathcal{A}, \mathcal{B}\}, a, d)$
    end if
  end for
end for
return E

Such actions include the Shape Calculus delay term $\epsilon(t)$, and model specific actions used to express resorption and formation by bone cells (see Section 3.4);

- *output actions* and *input actions*, that are computed by the functions enabledOutActions($\mathcal{A}$) and enabledInActions($\mathcal{A}$), respectively.

  For each couple of output and input actions $a^O = (\mathcal{A}, (\overline{a}, \lambda)_d)$ and $a^I = (\mathcal{B}, (a, w))$, their synchronization rate is computed, and the synchronization $(\{\mathcal{A}, \mathcal{B}\}, a, d)$ is added to the result (d is a random duration picked from an exponential distribution with parameter $rate$).

B.2 ENCODING SHAPE CALCULUS INTO JAVA CODE

In this section, we sketch the method used for translating the Shape Calculus terms into Repast agents coded in Java. Firstly, the class diagram of a Shape-based agent is given (Fig. 41). Secondly, we introduce a translation function into Java defined inductively on the syntax of Shape Calculus terms.

CLASS DIAGRAM The class Shape models an agent with physical and geometrical attributes (geometry, mass, position and velocity), and correspond to a *3D Shape* in the calculus. A Shape object can be either a BasicShape or a ComplexShape obtained by composing two or more BasicShape objects. Each BasicShape has associated a Behaviour object, which in turn can be a TerminalBehaviour, that is a concrete action, or a NonTerminalBehaviour, that is an operator for composing one or more Behaviour objects.

Among the non-terminal behaviours we distinguish among alternative composition (Choice), sequential composition (Sequence), repeating behaviours (Iteration), and time-bounded behaviours (Duration).

A terminal behaviour can be either a LocalAction, i.e. an atomic action requiring no interactions among agents such as time delays (Split) and removal of an agent (Thanatos); or a SynchronizingAction that is an atomic action requiring a two-party synchronization (Bind and Split). Finally bind actions have associated a single Channel object, while split actions have associated one or more Channel objects.

TRANSLATION FUNCTION Let $Java$ be the set of Java expressions. In the simulator, we implement a basic shape $\sigma = \langle V, m, \mathbf{p}, \mathbf{v} \rangle \in \mathbb{S}$ as a shape occupying a single unit of volume, e.g. a sphere with radius length $\frac{1}{2}$ or a cube

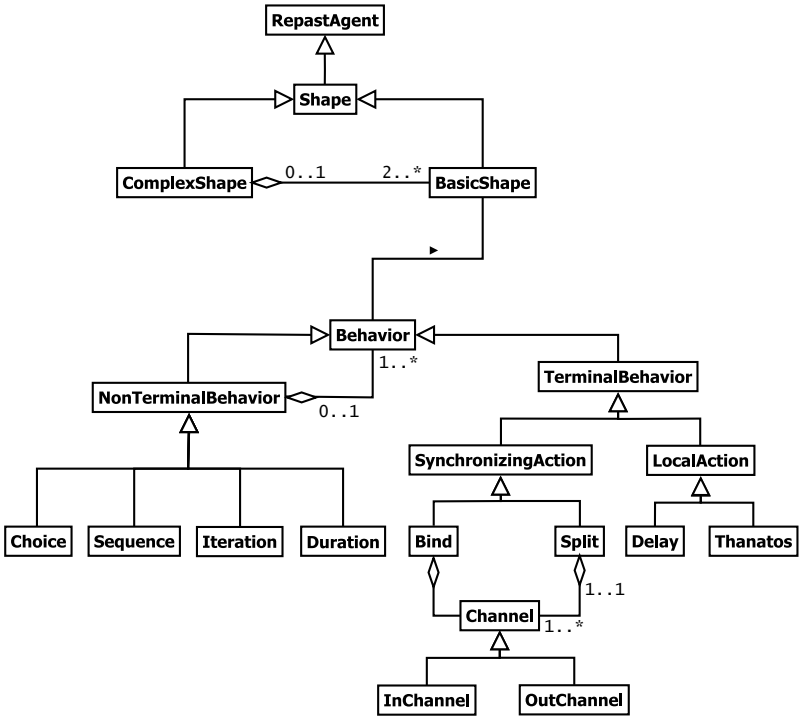

Figure 41: Class diagram of a Shape calculus-based agent.

with edge length 1. Complex shapes can be formed by collision and binding of two or more basic shapes, but cannot be defined directly. We translate basic shapes with a function $f_S : \mathcal{S} \to Java$ defined as:

$$f_S(\langle V, m, \mathbf{p}, \mathbf{v}\rangle) = m, new\ double[]\{p_0, p_1, p_2\}, new\ double[]\{v_0, v_1, v_2\}$$

Another restriction applies consequently to the surfaces X exposed by channels. Let $\sigma = \langle V, m, \mathbf{p}, \mathbf{v}\rangle$ be a basic shape and $X \subseteq V$ a surface of σ. X is not translated as a set of points, but it can take a value among X_x, X_{-x}, X_y, X_{-y}, X_z, X_{-z}, defined as follows.

Let $k \in \{x, y, z\}$, $X_{\pm k} = \{(x, y, z) \in V \mid k = \pm\frac{1}{2}\}$. In other words, X_x (X_y, X_z) is the set of points with the highest x (y, z) coordinate and X_{-x} (X_{-y}, X_{-z}) is the set of points with the lowest x (y, z) coordinate.

Let $\mathcal{C}_{in} = \{\langle \alpha, X \in \mathcal{C} \mid \alpha \in \Lambda\}$ denote the set of input channels and $\mathcal{C}_{out} = \{\langle \alpha, X \in \mathcal{C} \mid \alpha \in \overline{\Lambda}\}$ the set of output channels. Clearly, their union gives the set of all channels: $\mathcal{C} = \mathcal{C}_{in} \cup \mathcal{C}_{out}$. Input channels are translated with a function $f_{\mathcal{C}_{in}} : \mathcal{C}_{in} \times \mathbb{N}^+ \to Java$, s.t.

$$f_{\mathcal{C}_{in}}(\langle a, X\rangle, p) = new\ InChannel(a, X, w)$$

The natural w denotes the weight associated to the action. Output channels are translated with a function $f_{\mathcal{C}_{out}} : \mathcal{C}_{out} \times \mathbb{R}^+ \times \mathbb{R}^+ \to Java$, s.t.

$$f_{\mathcal{C}_{out}}(\langle \overline{a}, X \rangle, \lambda, d) = new\ OutChannel(a, X, \lambda, d)$$

where λ and d denotes respectively the stochastic rate and the sensibility distance of the action. For simplicity of notation in the following functions, we consider a generic function mapping channels $\mathcal{C}$ to Java expressions, $f_{\mathcal{C}} : \mathcal{C} \to Java$, s.t. for some w, λ, d:

$$f_{\mathcal{C}}(c) = \begin{cases} f_{\mathcal{C}_{in}}(c, w) & \text{if } c \in \mathcal{C}_{in} \\ f_{\mathcal{C}_{out}}(c, \lambda, d) & \text{if } c \in \mathcal{C}_{out} \end{cases}$$

Internal behaviours are translated by a function $f_{\mathbb{B}} : \mathbb{B} \to Java$, defined inductively as follows.

$$\begin{aligned}
f_{\mathbb{B}}(\langle \alpha, X \rangle) &= new\ Bind(f_{\mathcal{C}}(\langle \alpha, X \rangle)) \\
f_{\mathbb{B}}(\omega \langle \alpha, X \rangle) &= new\ Split(f_{\mathcal{C}}(\langle \alpha, X \rangle)) \\
f_{\mathbb{B}}(\rho(\{c_1, \ldots, c_n\})) &= new\ Split(f_{\mathcal{C}}(c_1), \ldots, f_{\mathcal{C}}(c_n)) \\
f_{\mathbb{B}}(\sigma(t)) &= new\ Delay(t) \\
f_{\mathbb{B}}(\Theta) &= new\ Thanatos() \\
f_{\mathbb{B}}(B_1. \ \ldots \ .B_n) &= new\ Sequence(f_{\mathbb{B}}(B_1), \ldots, f_{\mathbb{B}}(B_n)) \\
f_{\mathbb{B}}(B_1 + \ldots + B_n) &= new\ Choice(f_{\mathbb{B}}(B_1), \ldots, f_{\mathbb{B}}(B_n)) \\
f_{\mathbb{B}}(B^{\infty}) &= new\ Iteration(f_{\mathbb{B}}(B)) \\
f_{\mathbb{B}}(B^n) &= new\ Iteration(f_{\mathbb{B}}(B), n),\ n \in \mathbb{N} \\
f_{\mathbb{B}}(\delta(t, B)) &= new\ Duration(t, f_{\mathbb{B}}(B))
\end{aligned}$$

Finally a 3D process $P \in 3DP$ is translated into Java by a function $f_{3DP} : 3DP \to Java$, defined by:

$$\begin{aligned}
f_{3DP}(S[B]) &= new\ BasicShape(f_S(S), f_{\mathbb{B}}(B)) \text{ and} \\
f_{3DP}(P_1 \langle a, X \rangle P_2) &= new\ ComplexShape(f_{3DP}(P_1), f_{3DP}(P_2))
\end{aligned}$$

C PRISM MODEL FOR BONE REMODELLING

The PRISM code of the bone remodelling model presented in Chapter 4 is given below.

PRISM module for osteoclasts

```
//formation and death factors
const double alpha1 = 0.5;
const double beta1 = 0.51;

//initial, max and min
const int initX1 = 10;
const int maxX1 = 15;
const int minX1 = 0;

//resorption and formation coefficent
const double k1 = 1.9;
const double k2 = 0.00948;

//autocrine and paracrine regulation factors
const double g11 = 1.1;
const double g21 = -0.5;

//formation and death rates
formula gRateX1 = alpha1*pow(x1,g11)*pow(x2,g21);
formula dRateX1 = beta1*x1;
//formation rate when x2=0 (it avoids +inf valued rate)
formula g1RateX1 = alpha1*pow(x1,g11)*pow(0.1,g21);

//osteoclasts module
module osteoclasts
x1: [minX1..maxX1] init initX1;
[x1Growth] x1<maxX1 & x1>0 & x2>0 -> gRateX1:(x1' = x1+1);
[x1Growth1] x1<maxX1 & x1>0 & x2=0 -> g1RateX1:(x1' = x1+1);
[x1Death] x1>minX1 -> dRateX1:(x1' = x1-1);
[resorb] x1>minX1 -> k1*x1:true;
endmodule
```

```
//Expected value of x1
rewards "expOc"
true:x1;
endrewards

//Expected value of x1^2
rewards "squaredOc"
true:x1*x1;
endrewards
```

PRISM module for osteoblasts

```
//formation and death factors
const double alpha2 = 4;
const double beta2 = 0.02;

//initial, max and min
const int initX2 = 1;
const int maxX2 = 150;
const int minX2 = 0;

//autocrine and paracrine regulation factors
const double g12 = 1;
const double g22 = 0;

//formation and death rates for osteoblasts
formula gRateX2 = alpha2*pow(x1,g12)*pow(x2,g22);
formula dRateX2 = beta2*x1;

//osteoblasts module
module osteoblasts
x2: [minX2..maxX2] init initX2;
[x2Growth] x2<minX2 & x1>0 -> gRateX2:(x2' = x2+1);
[x2Death] x2>minX2 -> dRateX2:(x2' = x2-1);
[form] x2>minX2 -> k2*x2:true;
endmodule

//Expected value of x2
rewards "expOb"
true:x2;
endrewards
```

```
//Expected value of x2^2
rewards "squaredOb"
true:x2*x2;
endrewards
```

PRISM code for bone formed and bone resorbed rewards

```
rewards "boneResorbed"
[resorb] true:1;
endrewards

rewards "boneFormed"
[form] true:1;
endrewards
```

The bone remodelling model follows a *population-based approach* where osteoclast and osteoblast populations are implemented as modules having a state variable that counts the number of osteoclasts (variable `x1`) or osteoblasts (variable `x2`); growth and death transitions (`x1Growth, x2Growth, x1Death, x2Death`); and a transition modelling the resorption (`resorb`) or formation activity (`form`).

Our stochastic model has been derived from the ODE in the following way: the growth rates in the ODE model become the rates of stochastic transitions incrementing the population size of one unit (`gRateX1` and `gRateX2`); analogously, the death rates in the ODE becomes the rates of stochastic transitions decrementing the population size of one unit (`dRateX1` and `dRateX2`). Below, the differential equations for osteoclasts and osteoblasts with the corresponding stochastic rates are given.

$$\dot{x_1} = \underbrace{\boxed{\alpha_1 x_1^{g_{11}} x_2^{g_{21}}}}_{\texttt{gRateX1}} - \underbrace{\boxed{\beta_1 x_1}}_{\texttt{dRateX1}}$$

$$\dot{x_2} = \underbrace{\boxed{\alpha_2 x_1^{g_{12}} x_2^{g_{22}}}}_{\texttt{gRateX2}} - \underbrace{\boxed{\beta_2 x_2}}_{\texttt{dRateX2}}$$

Guards in the stochastic transitions are set in order to avoid out-of-range updates and zero- or infinite-valued transition rates. In particular, we have added in the osteoclasts module a further growth transition (`x1Growth1`) for distinguishing the case when $x_2 = 0$. In this case the stochastic rate would be

$$\alpha_1 x_1^{g_{11}} x_2^{g_{21}} = \infty, \text{ since } g_{21} < 0.$$

maxX1	maxX2	max(E(x1))	max(E(x2))
10	100	10	75.166
15	150	10	84.638
20	200	10	85.458
25	250	10	86.255
30	300	10	85.795
35	350	10	84.488

Table 16: Maximum expected values of x1 (third column) and x2 (fourth column) with different upper bounds for state variables (first and second columns). The quantity $max(E(x1))$ remains constant to 10, because osteoclasts strictly decrease from their initial state initX1=10. On the other hand, the maximum expected value of x2 remains approximately constant for maxX1$\geqslant$ 15 and maxX2 $\geqslant$ 150.

Therefore we set the rate g1RateX1 to $\alpha_1 x_1^{g_{11}}(0.1)^{g_{21}}$.

In order to reduce the state-space of the stochastic model, the relative bone density has not been implemented as a state variable, but as a pair of rewards ("boneResorbed", "boneFormed") on transitions resorb and form, respectively. Such transitions have associated the resorption and formation rates of the ODE model, that are $k_1 x_1$ and $k_2 x_2$, resp. Then, the relative bone density is calculated as the difference between the cumulative "boneFormed" reward and the cumulative "boneResorbed" reward.

Initial values for the random state variables have been adapted from the continuous model (initX1=10 and initX2=1), and ranges for x1 and x2 are determined by the constants minX1=0, minX2=0, maxX1=15 and maxX2=150. While variables are justifiably lower-bounded by 0, their maximum values have been assessed experimentally, by means of the quantitative model checking tool provided by PRISM. We found that even when increasing maxX1 and maxX2, the transient expected values of x1 and x2 remains bounded by 15 and 150, respectively (see Table 16). Moreover the maximum expected values encountered remains approximately constant for maxX1$\geqslant$ 15 and maxX2$\geqslant$ 150. Finally no changes in the dynamics of osteoclasts and osteoblasts have been observed with higher upper-bounds.

[ ]	$0 < O_c < O_{c_{max}} \wedge O_b > 0 \rightarrow$	$\alpha_1 O_c^{g_{11}(1+f_{11}\frac{B}{s})} O_b^{g_{21}(1-f_{21}\frac{B}{s})}$	$: O_c = O_c + 1$
[ ]	$O_c > 0 \rightarrow$	$g_{ageing}\beta_1 O_c$	$: O_c = O_c - 1$
[resorb]	$O_c > 0 \rightarrow$	$k_1 O_c$	$:$ true

(a) Osteoclasts

[ ]	$0 < O_b < O_{b_{max}} \wedge O_c > 0 \rightarrow$	$\alpha_2 O_c^{g_{12}/(1+f_{11}\frac{B}{s})} O_b^{g_{22}-f_{22}\frac{B}{s}}$	$: O_b = O_b + 1$
[ ]	$O_b > 0 \rightarrow$	$g_{ageing}\beta_2 O_b$	$: O_b = O_b - 1$
[form]	$O_b > 0 \rightarrow$	$k_2 O_b$	$:$ true

(b) Osteoblasts

[ ]	$0 < B < B_{max} \wedge treat = 0 \rightarrow$	$\gamma_B B \cdot log(\frac{s}{B})$	$: B = B + 1$
[ ]	$treat = 0 \rightarrow$	$\frac{1}{t_{treat}}$	$: treat = 1$
[ ]	$0 < B < B_{max} \wedge treat = 1 \wedge V < \gamma_B \rightarrow$	$(\gamma_B - V)B \cdot log(\frac{s}{B})$	$: B = B + 1$
[ ]	$B > 0 \wedge treat = 1 \wedge V > \gamma_B \rightarrow$	$(V - \gamma_B)B \cdot log(\frac{s}{B})$	$: B = B - 1$

(c) Bacteria

Table 17: Stochastic model for bone remodelling with osteomyelitis infection. The variable $treat$ is used as a switch for the beginning of treatment firing with rate $1/t_{treat}$, therefore with an exponentially distributed delay having mean $treatTime$. Bacteriocide ($V > \gamma_B$) and non-bacteriocide ($V < \gamma_B$) dynamics is considered separately.

D GENE EXPRESSION IN OSTEOPOROSIS AND OSTEOMYELITIS

Important parameter values of bone remodelling models are based on various authors (see [121] among others); here we also analysed more recent data, particularly available gene expression data. Since that both osteoporosis and osteomyelitis cause loss of bone mass, we decided to cross-compare gene expression datasets of both diseases. We have compared the expression levels of genes involved in osteomyelitis, osteoporosis patients and healthy controls using the box plots and comparison table (Figure 42, 43 and Table 18). We report in Table 18 the significant genes associated with the infection of osteomyelitis and or with the condition of osteoporosis. From the analysis of our data, we observe that few genes, related to TNF, TNF receptor superfamilies and to NF-kB have statistically different levels of expression in healthy controls, osteomyelitis and or osteoporosis. We observe that, with respect to control cases, for the microarray platform GPL96, 22 genes related to RANKL, RANK, OPG, NF-kB proteins, TNF and TNF receptor superfamilies are over expressed and 13 genes are down regulated in osteomyelitis (see Fig 42 and Table 18). There are other 47 genes that are weakly correlated with this infection (not shown). However, in case of GPL97 microarray platform, only 10 genes are highly expressed; 6 genes are down expressed (other 15 genes are weakly correlated in osteomyelitis) (see Figure 43 and Table 18). For the osteoporosis condition, using the platform GPL96, only 10 genes are up regulated and 6 are down regulated (see Table 18). It is notable in the platform GPL96, only 4 genes NFKB2_1, NFKB2_2, REL_2 and RELB are up-regulated in both types of diseases. In contrast, only 3 genes TNFRSF25_2, TRAF3IP3_1 and TRAF5 are down regulated in the both osteomyelitis infection and osteoporosis. However, 5 genes NFKB1, RELA_1, TNFRSF10B_2, TNFSF10_3 and TRAF3IP3_3 are differently regulated in osteomyelitis and osteoporosis.

Interestingly we found that, despite a very small increase of RANKL gene expression in osteoporosis and a larger increase in osteomyelitis, OPG gene expression become more deregulated in both osteomyelitis and osteoporosis. There is the increased expression of different isoforms of OPG which are known to have different binding capability with RANKL and seem to be linked, from mice experiments, to hypocalcemia [71]. Therefore we re-

port that gene expression in osteoporosis and osteomyelitis could generate an unbalance between RANKL and OPG due to the different OPG isoforms, but also other genes, related to TNF,TNF receptor superfamilies and to NF-kB may be involved. Although gene expression and actual protein abundance are only loosely correlated, taking into account the results of gene expression data, we modified the autocrine and paracrine parameters of the existing mathematical model based on Komarova model [86]. We considered more appropriate to incorporate into the model the algebraic relationship of positive and negative regulators (such as RANKL and OPG) than just the RANKL change. On the basis of this consideration we developed new models for reproducing osteoporotic and osteomyelitis conditions.

Data analysis

We found that there are no comprehensive analysis on osteomyelitis; most studies focus on specific conditions. We have collected a large ensemble of gene expression data related to osteomyelitis and osteoporosis. For this reason, we have considered 6 microarray data sets of the same platform GPL96 from the Gene Expression Omnibus [1], accession numbers are GSE16129, GSE6269, GSE11907, GSE11908, GSE13850 and GSE7429 [2, 133, 47, 155]. We observe that RANKL, RANK, OPG and NF-kB proteins impact more on the bone remodelling for osteomyelitis and osteoporosis[133, 2, 47, 50]. For this reason to understand the effect osteomyelitis and osteoporosis on bone remodelling, we have considered the genes related to the proteins RANKL, RANK, OPG, NF-kB proteins, TNF and TNF receptor superfamilies. We observed that there are 82 genes are related with these proteins. So, we filtered the required 82 genes related data. We have selected samples for 48 infected and 27 healthy controls for osteomyelitis and 30 infected and 30 healthy controls for osteoporosis. The datasets contain data from people of different age and sex.

For more evidence about osteomyelitis, we have considered more gene expression data related to osteomyelitis on different platform GPL97. For this reason, we have considered additional 3 microarray data sets from the Gene Expression Omnibus, accession numbers are GSE6269, GSE11907 and GSE11908 [133, 47]. To understand the effect of osteomyelitis on the bone remodelling, we have considered the genes related to the proteins RANKL, RANK, OPG, NF-kB proteins, TNF and TNF receptor superfamilies like previous analysis. We observed that in the platform GPL97, there are 31 genes are related to these proteins and superfamilies. So, we filtered the required

1 http://www.ncbi.nlm.nih.gov/geo/

Regulation for Osteomyelitis (GPL96)	Regulation for Osteomyelitis (GPL97)	Regulation for Osteoporosis (GPL96)
↑ NFKB2_1	↑ NFKB2_1	↑NFKB1
↑ NFKB2_2	↑ NFKBIZ_1	↑ NFKB2_1
↑ NFKBIA	↑ NFKBIZ_2	↑ NFKB2_2
↑ NFKBIE	↑ RELL1	↑ REL_2
↑ REL_2	↑ RELT	↑ RELA_1
↑ RELB	↑ TNFSF13B_1	↑ RELA_2
↑ TNFRSF10B_2	↑ TNFSF13B_2	↑ RELB
↑ TNFRSF10C_2	↑ TRAF7_1	↑ TNFRSF17
↑ TNFRSF10C_3	↑ TRAF7_3	↑ TNFSF10_2
↑ TNFRSF10C_4	↑ TRAFD1_2	↑ TRAF3_1
↑ TNFRSF1A	↓ TNFRSF10A	↓ TNFRSF10B_2
↑ TNFRSF1B	↓ TNFRSF18_2	↓ TNFRSF25_2
↑ TNFSF10_1	↓ TRAF1	↓ TNFSF10_3
↑ TNFSF10_2	↓ TRAF3IP1	↓ TRAF3IP3_1
↑ TNFSF10_3	↓ TRAF3IP3_1	↓ TRAF3IP3_3
↑ TNFSF12 _3	↓ TRAF3IP3_2	↓TRAF5
↑ TNFSF12 _4		
↑ TNFSF12_2		
↑ TNFSF13		
↑ TRAF3IP3_2		
↑ TRAF3IP3_3		
↑ TRAFD1_2		
↓ IKBKG_2		
↓ NFKB1		
↓ RELA_1		
↓ TNFRSF14		
↓ TNFRSF25_1		
↓ TNFRSF25_2		
↓ TNFRSF25_3		
↓ TNFRSF25_4		
↓ TNFRSF25_6		
↓ TRAF1		
↓ TRAF3IP2_2		
↓ TRAF3IP3_1		
↓ TRAF5		

Table 18: Comparative representation of gene expression level for osteomyelitis and osteoporosis. Upregulated genes are marked by ↑, downregulated genes by ↓.

genes related data. We have selected samples for 43 infected and 17 healthy controls. Standard anova and Box plots representation were used to analyse and visualise the expression levels of these genes for the infection of osteomyelitis and osteoporosis condition.

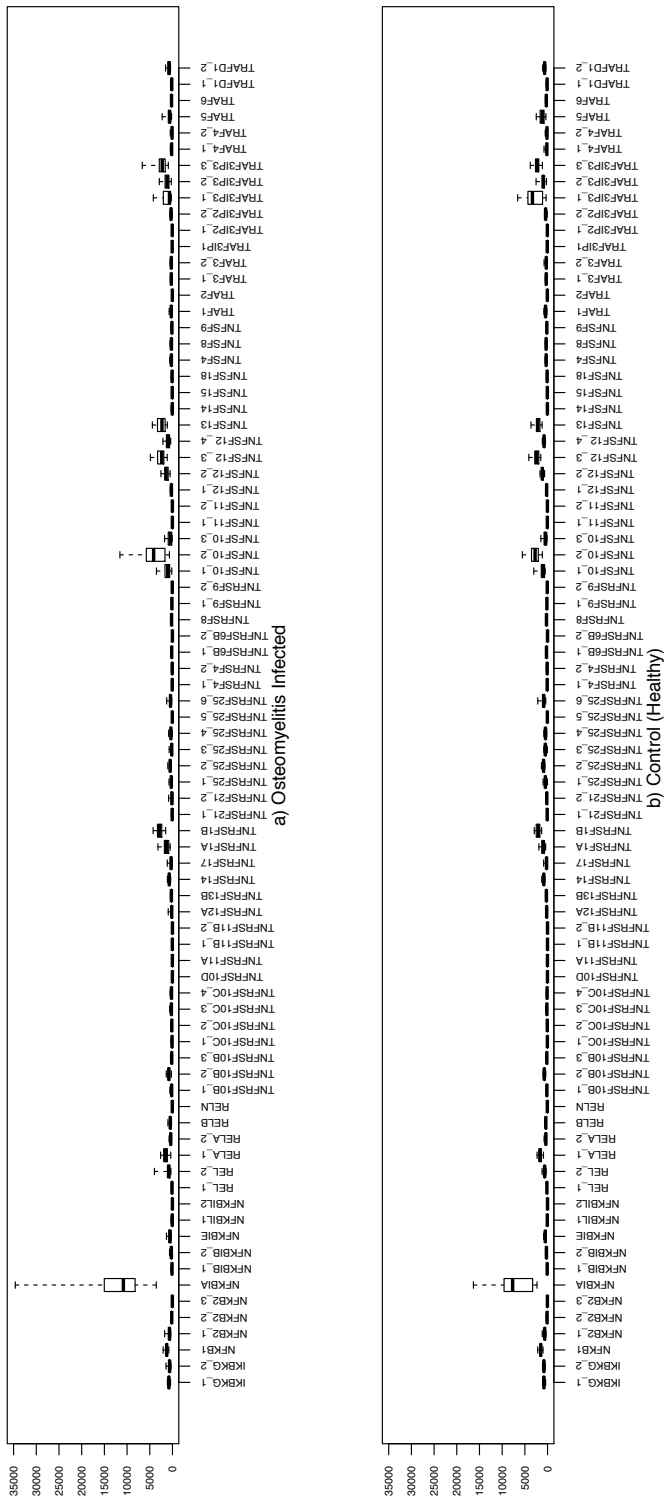

Figure 42: Gene expression of 82 genes corresponding to a) 48 osteomyelitis infected patients and b) 27 healthy controls.

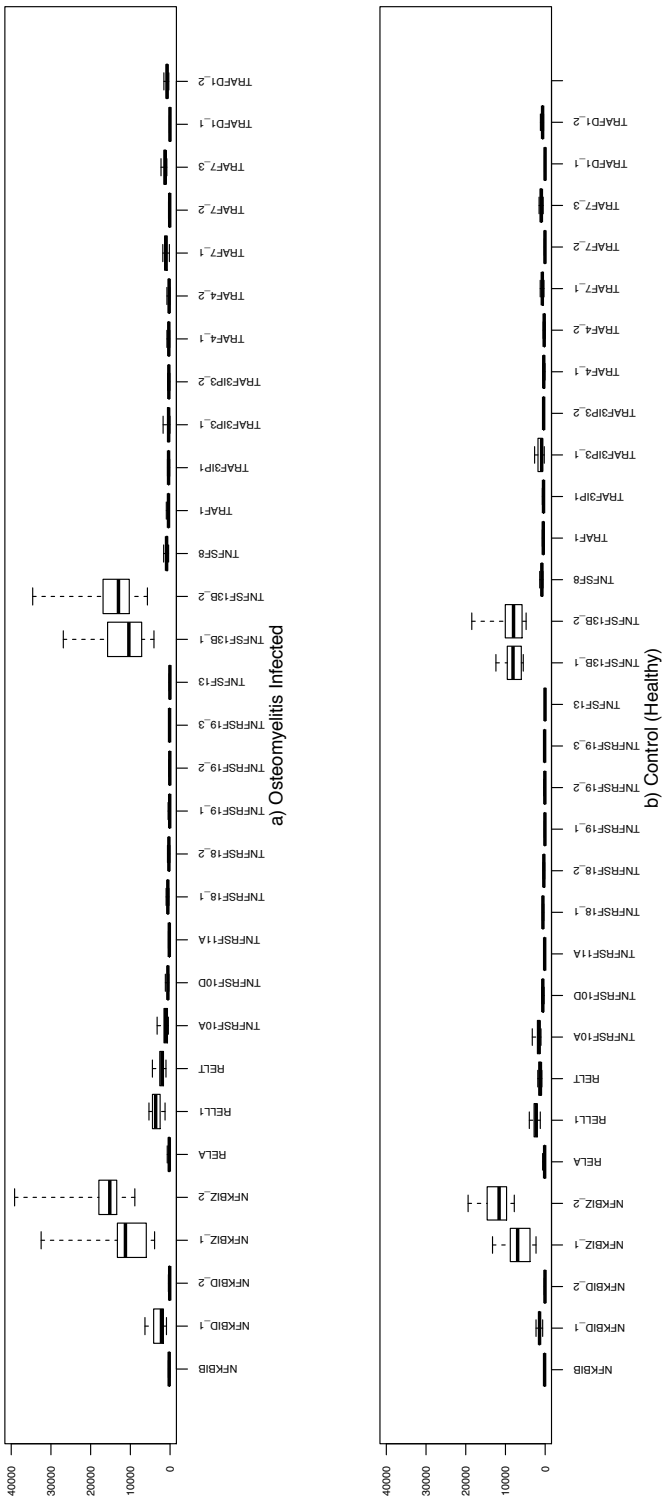

Figure 43: Gene expression of 31 genes corresponding to a) 43 osteomyelitis infected patients and b) 17 healthy controls.